ABSTRACT

Title of Document: THE STRUCTURAL BASIS FOR FUNCTION OF THE *ESCHERICHIA COLI* MECHANOSENSITIVE CHANNEL OF SMALL CONDUCTANCE, MSCS

Bradley Chun-Yee Akitake, Doctor of Philosophy, 2007

Directed By: Professor Sergei I. Sukharev, Department of Biology

The 'small' mechanosensitive channel, MscS, resides in cytoplasmic membranes of most free-living bacteria. MscS is gated directly by membrane tension and functions as an osmolyte release valve in bacterial turgor regulation. In contrast to previously studied MscL, which is a strictly prokaryotic molecule, MscS homologs are found in eukaryotes increasing the value of this channel as a general model for gating by membrane stretch.

Presented here are the results of three studies aimed at characterizing the structural basis for function of *Escherichia coli* MscS. In study one, we provide the first electrophysiological characterization of the wild-type channel in its native membrane free of other mechanosensitive channels. It is, to date, the most complete description the gating cycle specifying the kinetic scheme and dependencies of major rates on tension and voltage. Study two represents a collaborative effort to probe the strength of intersubunit contacts in the homo-heptameric MscS channel. In patch-

clamp experiments we show that the dissociating effects of TFE alter MscS gating in a manner that provides significant insight into the mechanics of channel inactivation. In the final study our research group utilized a novel extrapolated motion technique to explore the conformational pathways of the MscS functional cycle. Guided by these new models, channel mutants were generated to alter helical propensity along the pore lining TM3 helix. Patch-clamp analysis revealed a vivid picture of the functioning MscS in which these TM3 domains provide a structural frame for the open channel. Dynamic collapse of these 'struts' at flexible points along TM3 modulates transitions from the open state to the inactivated and closed states.

My contributions to these studies have allowed for (1) refinement of the MscS functional cycle including identification of a new desensitized state; (2) determination of the physical parameters and spatial scales of channel opening, closing and inactivation; and (3) identification of key hinge elements, residing in TM3, that along with membrane tension serve to modulate the functional cycle of MscS. These findings have led to a better understanding of the biophysical principles that underlie mechanotransduction and provide insights into the larger family of mechanically activated phenomena.

THE STRUCTURAL BASIS FOR FUNCTION IN THE *ESCHERICHIA COLI* MECHANOSENSITIVE CHANNEL OF SMALL CONDUCTANCE, MSCS

By

Bradley Chun-Yee Akitake

Dissertation submitted to the Faculty of the Graduate School of the
University of Maryland, College Park, in partial fulfillment
of the requirements for the degree of
Doctor of Philosophy
2007

Advisory Committee:
Professor Sergei Sukharev, Chair
Professor Jeffery Davis
Professor Marco Colombini
Professor Heven Sze
Professor Stephen Wolniak

Preface

Declaration of author's intent to use own previously published text.

1) Portions of the main text in:

Chapter 1: Introduction to the study of mechanosensitive ion channels

Chapter 5: Conclusions and future research directions

Were adapted from our 2007 book chapter/review of MscS (Sukharev et al., 2007) the full citation is given below.

Sergei Sukharev, **Bradley Akitake** and Andriy Anishkin. "Chapter 9 - The Bacterial Mechanosensitive Channel MscS: Emerging Principles of Gating and Modulation" *Current Topics in Membranes* 2007 Vol.58.

2) The main text and figures and figure legends in their entirety for:

Chapter 2: The "dashpot" mechanism of stretch-dependent gating in MscS

Chapter 3: 2,2,2-trifluoroethanol changes the transition kinetics and subunit interactions in the small bacterial mechanosensitive channel MscS

Chapter 4: Straightening and sequential buckling of the pore-lining helices define the gating cycle of the stretch-activated channel MscS

Were used, and only modified for readability/formatting within the context of this dissertation. Full citations are given below.

Bradley Akitake, Andriy Anishkin and Sergei Sukharev. "The 'dashpot' mechanism of stretch-dependent gating in MscS." *Journal of General Physiology* 2005 125(2):143-54

Bradley Akitake, Robin E.J. Spelbrink, Andriy Anishkin, J. Antoinette Killian, Ben de Kruijff and Sergei Sukharev. "2,2,2-trifluoroethanol changes the transition kinetics and subunit interactions in the small bacterial mechanosensitive channel MscS" *Biophysical Journal 2007* 92(8):2771-84

Bradley Akitake, Andriy Anishkin, Naili Liu and Sergei Sukharev. "Straightening and sequential buckling of the pore-lining helices define the gating cycle of the stretch-activated channel MscS" – *Manuscript submitted*

Dedication

With love to my family and my wife Courtney

Acknowledgements

I would first like to express my most sincere gratitude to Dr. Sergei Sukharev, my research advisor, who has watched over and guided my development as a scientist for the last 5 years. His intellect, patience and generosity are what separate Sergei as a great PI and have truly made this work possible.

Thank you to my closest collaborator Dr. Andriy Anishkin. Andriy's phenomenal insight into the molecular mechanisms of MscS and his great predictions have a countless number of times pointed my experiments in the right directions.

Thank you to the members of my advisory committee: Drs. Marco Colombini, Heven Sze, Steve Wolniak and Jeff Davis for their guidance, teaching and moral support, these not being restricted to my committee meetings.

Dr. Chien-Sung Chiang I am forever indebted to you for teaching me how to patch clamp.

To the members of the Sukharev lab, former and present: Kishore, Naili, Lena, Greg J., Greg M., Andy, Miriam, Mike and Vlad, you have all in some measure touched this research and I thank you.

Table of Contents

List of Tables

List of Figures

Chapter 1: An introduction to mechanosensitive ion channels

Mechanosensory phenomena

The ability for an organism to sense, interpret and subsequently adapt to environmental stimuli is fundamental to its survival. Of the group of physiological inputs that serve to trigger sensory reactions, plain mechanical force is probably one of the most basic. Force transduction plays a critical role in many diverse organismal functions some examples are touch sensation and nociception (detection of pain) (O'Neil and Heller, 2005; Wetzel et al., 2007), hearing (O'Neil and Heller, 2005), cardiovascular regulation (Lammerding et al., 2004), gravity sensing (Haswell and Meyerowitz, 2006) and osmoregulation (Levina et al., 1999; O'Neil and Heller, 2005). In higher organisms, developed sensory systems exist to transmit these mechanical stimuli to the brain where they can be interpreted. However, at a more basic level, all cells must be able to sense and respond to physical alterations that occur as their environment changes. The kinds of cellular components known to mediate the transduction of mechanical force reveals a great deal of diversity (Ingber, 2006).

Receptors of mechanical signals fall into two major groups separated by the rate of their transduction. One group acts to regulate 'fast' mechanosensory responses like touch and pain sensation while the other mediates 'slow' responses, which include taxic behaviors in single cells and tissue remodeling in the course of growth and development (i.e. cell differentiation, migration and guidance) for higher organisms. An example of 'slow' mechanosensory receptors is the integrin family of

cell surface receptors, which have been shown to be critical for lung organogenesis (Virtanen et al., 1996; Coraux et al., 1998). It was recently shown that integrins β_1, α_3 and α_6 are necessary components in the force sensitive differentiation of type II epithelial cells in the developing lung tissues of rats (Sanchez-Esteban et al., 2006). However, the exact mechanisms by which these integrin receptor transmit signals to their associated focal adhesion kinases (FAK) to regulate differentiation is not known (Schober et al., 2007). One of several possible mechanisms may include G-protein coupled receptors (GPRC) as primary mechanoreceptors, a role that was recently discovered for the mechanosensitive angiotensin II type 1 (AT1) receptor of mammalian cardiomyocytes (Zou et al., 2004). This role makes sense as it was previously found that mechanical stretch induces striking levels of kinase activity in cells whereby gene expression is reprogrammed (Komuro and Yazaki, 1993).

For the group of 'fast' mechanosensory responses, it has been established that most if not all are coupled to the activation of mechanically sensitive (mechanosensitive or MS) ion channels. These MS cannels act as transducers of physical force into electrical signals and therefore underlie the quick rate of transmission in more complex control systems (Sukharev and Corey, 2004). Much work in recent years has gone into the molecular identification MS ion channels in a multitude of different organisms from bacteria to mammals. Genetics and biochemistry studies have led to the discovery, isolation and cloning of many different families of MS ion channels starting with the *E. coli* mechanosensitive channels of small and large conductances, MscS and MscL (Sukharev et al., 1993; Sukharev et al., 1994). Study of a group of neuronal degeneration (*deg*) mutants of *C.*

elegans revealed a loss of touch sensitivity and led to the discovery of the MEC family of DEG/ENaC mechanosensitive epithelial sodium channels (Lai et al., 1996; Tavernarakis and Driscoll, 2001). TWIK, which stands for tandem P domain weak inward rectifying potassium (K^+) channels were first identified through BLAST searches of mammalian genomes by its highly conserved P domain, a signature of the potassium channel selectivity filter (Lesage et al., 1996a; Lesage et al., 1996b). Unlike the single P domain K^+ channels, tandem P variants were found to display very distinct phenomenology including, in some members, mechanosensitivity. In particular, the TWIK related channels TREK-1, TREK-2 and the arachidonic acid sensitive channel TRAAK could be gated directly by membrane tension in addition to other traditional stimuli (Fink et al., 1998; Reyes et al., 1998; Maingret et al., 1999; Bang et al., 2000). Most recently it has been demonstrated that a large number of the ubiquitous transient receptor potential (TRP) family of potassium channels display mechanosensitive behaviors (Corey, 2003). TRP channels now appear to be critical for a bevy of mechanosensory tasks including osmotic avoidance and touch response in *C. elegans* (Colbert et al., 1997), defective touch sensation in NOMPC *Drosophila* mutants (Kernan et al., 1994; Walker et al., 2000) and even hearing impairment in TRPV4 knockout mice (Tabuchi et al., 2005). Concomitant with cloning, attempts to observe the localization these mechanosensitive channels using immunohistochemical techniques are now adding to the growing body of information pertaining to the functional role that these channels play (Lai et al., 1996; Suzuki et al., 2003).

Bacterial osmoregulation and the discovery of mechanosensitive channels

Bacteria and other walled cells maintain their volumes and shape by creating positive turgor pressure in the cytoplasm against the confines of their cell wall. This is achieved through a network of solute uptake systems or accompanied by *de novo* synthesis of substances that maintain normal osmotic pressure gradients across the cytoplasmic membrane. It is generally accepted that an intracellular pressure of ~3-4 atm is required for normal proliferation of enteric bacteria such as *Escherichia coli* and much higher pressures (15-25 atm) are typical for gram-positive species (Csonka, 1989; Wood, 1999). Under steady growth conditions, turgor pressure is created collectively by small molecular constituents such as free amino acids, polyols, nucleotides and two major intracellular ions, K^+ and glutamate. If the medium suddenly becomes hypertonic due to increased salinity, bacterial cells initially loose turgor but quickly regain it by accumulating extra K^+ and glutamate (Epstein, 2003) through independent transport systems (McLaggan et al., 1994). Potassium, however, is not the most optimal intracellular osmolyte as its elevation changes the ionic strength inside the cell. Thus, having restored normal turgor, the cells gradually exchange K^+ for more inert substances such as proline, betaine and to some extent trehalose (Csonka and Hanson, 1991). These solutes are called 'compatible' as they minimally affect cellular functions though still aid in the retention of water.

The growth conditions for enteric and soil bacteria are not always steady and periods of proliferation in high-osmolarity environments are often interrupted by low-osmolarity conditions (rain/drainage water). In these instances, previously accumulated solutes put the bacterium at risk for osmotic lysis as the peptidoglycan

cell wall can restrain the volume change but only to a certain extent. It has been shown that peptidoglycan is distensible, and cell swelling results in substantial increases of internal volume (Koch and Woeste, 1992). As the excess slack of the inner membrane is used up, tension in the bilayer starts to build. Amelioration of this tension was found to occur through a drastic permeability increase of the cell membrane followed by the release small solutes to balance the osmotic gradient (Fig. 1-1) (Britten and McClure, 1962; Tsapis and Kepes, 1977). This reversible permeability change, demonstrated to take 1-2 seconds with little effect on cell survival, was initially interpreted as transient membrane 'crack' formation or some sort of reversible membrane breakdown. Later studies (Schleyer et al., 1993) refined the repertoire of released osmolytes and linked the reversible permeability pathways to the activities of bacterial stretch-activated channels first reported by the Kung laboratory (Martinac et al., 1987).

By applying a standard patch-clamp technique (Hamill et al., 1981) to giant spheroplast preparations (Ruthe and Adler, 1985) Martinac and coworkers first documented the presence of 1 nS pressure-activated channels in the *E. coli* cell envelope (Martinac et al., 1987). This channel was more active under depolarizing voltages (cytoplasm positive). Its activity was also found to be dependent on the presence of potassium as the channel was completely inactive in Na^+ buffers.

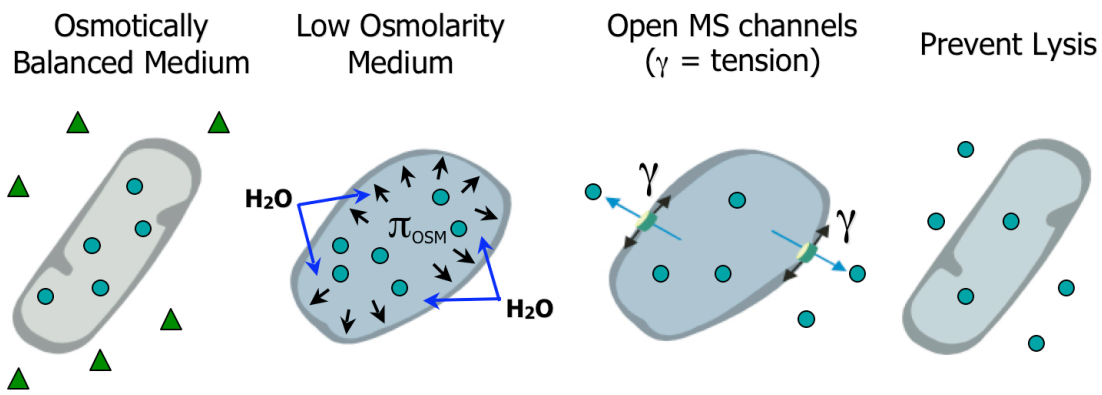

Figure 1-1. The effects of hypotonic shock and the activation of MS channels in bacteria.
This cartoon depicts the effects of transferring a bacterial cell from an osmotically balanced medium into a low osmolarity environment. Higher solute concentration inside of the cell causes an inrush of water through the plasma membrane. MS channels open in response to membrane tension as the cell swells to release osmolytes and ameliorate the osmotic gradient and prevent lysis. Figure illustrates conclusions from the early work of Britten and McClure (Britten and McClure, 1962).

Further studies involving membrane solubilization and reconstitution experiments (Sukharev et al., 1993) revealed that *E. coli* possesses two distinct mechanically-activated channel species, one of smaller (1 nS) conductance, similar to those previously observed by Martinac and designated as MscS, and a channel with three times larger (3.2 nS) conductance and spiky activities named MscL. The MscL protein was subsequently isolated and its gene cloned (Sukharev et al., 1994). Surprisingly, it was found that the *mscL*-null mutant did not exhibit any growth/survival phenotype under a variety of osmotic conditions.

Identification and cloning of MscS and MscK by the Booth laboratory came in 1999 through studies of mutations, which altered potassium exchange with betaine, and genomic analysis of related sequences (Levina et al., 1999). During periods of osmotic up-shock, potassium uptake is mediated by the Trk, Ktr and Kdp pumps that become activated by the resultant low turgor pressure (Epstein, 2003). Subsequent accumulation of proline and betaine is accomplished by the ProU, ProP and BetT active transporters, which also fulfill the roles of osmosensors (Wood et al., 2001). While searching for the K^+ efflux and accompanying proline/betaine uptake pathways, Booth and collaborators studied the *kefA, kefB* and *kefC* loci. The two latter systems were found to be active primarily under toxic or oxidative stresses (Ferguson et al., 2000). A *kefA*-null mutation did not change the course of betaine-for-potassium exchange under high osmolarity either, but a point mutation in *kefA* (called RQ2) exhibited a growth-suppressing phenotype when the cells were grown in a high-osmotic medium in the presence of K^+ and betaine. RQ2 bacteria accumulated betaine normally, but were unable to extrude K^+ efficiently and thus became extremely

sensitive to turgor created by the two osmolytes (McLaggan et al., 2002). From this phenotype, it seemed possible that the product of *kefA* was a stretch-sensitive membrane protein. The *kefA* open reading frame coded for a large (1120 amino acid) multi-domain membrane protein. A search for *E. coli* sequences similar to *kefA* revealed two proteins of the same length (AefA and YjeP) and a smaller protein resembling the C-terminal part of KefA, named YggB. Generation of single and multiple null mutants followed by re-expression of individual genes 'in trans' revealed that *kefA* and *yggB* both code for mechanosensitive channels of similar 1 nS conductance. The KefA channel was characterized by sustained activities under constant pressure gradients. Its activities were also shown to be dependent on the presence of K^+ (Levina et al., 1999; Li et al., 2002), thus it was renamed MscK. The product of *yggB,* which was more abundant and generated transient responses to pressure steps, was renamed MscS. None of the other related ORFs produced measurable channel activities *in situ*.

It was discovered that the generated triple *mscK-, mscS-, mscL-* knock-out strain (MJF465) had increased sensitivity to moderate osmotic downshocks (400-500 mOsm), and that re-expression of either MscL, or MscS, fully restored the osmotic downshift tolerance to WT levels. Expression of MscK alone in the triple knock-out strain did not ameliorate its osmotic fragility (Levina et al., 1999). This ground-breaking work not only identified two new genes for mechanosensitive channels of very similar conductance (previously though to be one), but also unequivocally demonstrated the partially redundant physiological roles for MscS and MscL as turgor-limiting release valves. In addition, the MJF465 strain has become a highly

useful ‘clean’ background system for mechanosensitive channel expression, electrophysiology recording, and testing of the osmotically driven rescuing ability of multiple MscS and MscL mutants.

The E. coli mechanosensitive channels MscS and MscL

MscS and MscL are the primary efflux components in *E. coli* that are responsible for fast osmolyte release to limit turgor pressure during osmotic downshock (Levina et al., 1999). The crystal structures of MscL (homolog from *M. tuberculosis*) and *E. coli* MscS have been solved by Rees and coworkers and are depicted in Fig. 1-2 (Chang et al., 1998; Bass et al., 2002). Both MscS and MscL form large oligomeric channel complexes in the inner membrane that are gated directly by tension developed in the surrounding lipid bilayer (Sukharev et al., 1993; Sukharev, 2002). In patch-clamp recordings, the open state conductance of MscL is ~3.2 nS, roughly two and half times that of MscS (~1.2 nS). MscL currents are characterized by steady, tension-dependent, activities observed near the membrane’s lytic limit (~8-12 dyne/cm) (Sukharev et al., 1997), whereas MscS responds to moderate tensions (4-6 dyne/cm) usually with a transient (decaying) response (Koprowski and Kubalski, 1998; Levina et al., 1999; Akitake et al., 2005). Together MscS and MscL provide the bacterium a graded permeability response to osmotic stress (Berrier et al., 1996; Blount and Moe, 1999; Martinac, 2001; Booth, 2003).

Although it has the larger conductance, MscL is physically a smaller channel than MscS. Its structure reveals a homo-pentamer of 136 amino acids per subunit and two transmembrane domains (TM1 and TM2).

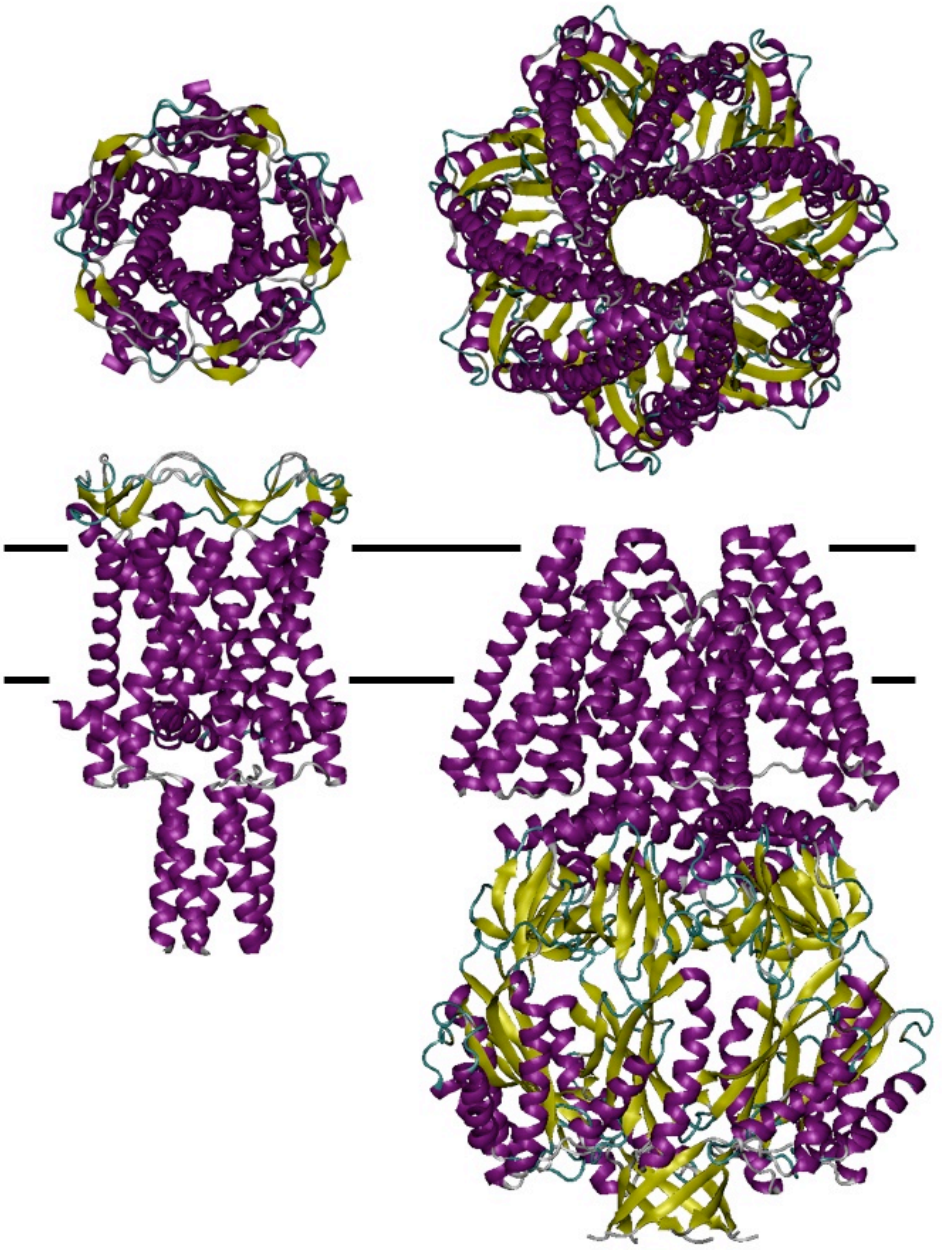

Figure 1-2. Crystal structures of the mechanosensitive channel proteins MscL and MscS. **(Left)** *Mycobacterium tuberculosis* MscL crystal structure at 3.5 Å (2OAR.pdb) (Chang et al., 1998). MscL is a homo-pentameric channel with 136 amino acids per subunit. There are two transmembrane domains with the C-terminal domains coming together to form an alpha helical bundle that acts as a molecular pre-filter. **(Right)** *Escherichia coli* MscS crystal structure at 3.7 Å (2OAU.pdb) (Bass et al., 2002). MscS is a homo-heptameric channel with 286 amino acids per subunit. There are three transmembrane domains with the C-terminal end of each subunit contributing to a large hollow cytoplasmic cage domain. Both channels are shown from the top and side. The lipid bilayer is pictured as black lines. PDB files were visualized and colored using VMD (Humphrey et al., 1996).

MscL has been subjected to a much a longer history of study than MscS, and in 2002 its gating mechanism was demonstrated be an iris like expansion of the transmembrane helices to open its conduction pathway in response to membrane stretch (Betanzos et al., 2002). High-resolution recordings of MscL later revealed a number of subconducting states that were present in both the opening and closing transitions (Chiang et al., 2004; Anishkin et al., 2005). These substates were linked to the presence of a second cytoplasmic gate, the opening of which induced the bulk of MscL conductivity but only a small final fraction of the channel total expansion in the membrane (Chiang et al., 2004; Anishkin et al., 2005). Structurally, MscS is very different from MscL. MscS is a homo-heptameric channel with 286 amino acids per subunit and three transmembrane domains (TM1, TM2 and TM3). TM1 and TM2 appear to associate as a helical pair on the periphery of the channel barrel. The TM3 helices are shown to line the conduction pathway and contribute two rings of leucines at L105 and L109 forming the hydrophobic gate constriction. The c-terminal ends of each subunit come together to form a large hollow cytoplasmic cage domain. While the mechanism of opening has not yet been determined, it has been observed that MscS opening and closing is far more cooperative (Sukharev, 2002; Akitake et al., 2005) than MscL. Recording of MscS opening with 3 μs resolution revealed only one short lived subconducting state (Shapovalov and Lester, 2004). These observations along with the more elaborate structure of MscS and its intricate adaptive physiological behaviors, which include transitions to alternative non-conducting states (inactivated and desensitized), suggest a different and more complex mechanism of gating (Anishkin and Sukharev, 2004; Edwards et al., 2004; Akitake et

al., 2005; Edwards et al., 2005). While MscL is primarily a prokaryotic molecule, with several distant homologs in fungi, MscS-type channels appear to be more widespread increasing the value of MscS as a model system (Pivetti et al., 2003). Multiple homologs have recently been identified in higher plants. Three such homologs in *Arabidopsis thaliana* were found to regulate the volume and division of chloroplasts (Haswell and Meyerowitz, 2006). Knock-down of MSC1 a MscS homologue from *Chlamydomonas* revealed abnormalities in chlorophyll localization and organization of chloroplasts (Nakayama et al., 2007).

Techniques to study mechanosensitive channel physiology

Although the task of identifying MS channels is far from complete, a large number of research groups including ours are already exploring the next logical step, to elucidate the structural mechanisms by which the operations of these sensory molecules are governed. The characterization of ion channel physiology is truly an example of interdisciplinary study, one that has capitalized on the strengths of Genetics, Molecular and Structural Biology, Biochemistry, Biophysics and the Computer Sciences, with each branch providing unique approaches and invaluable clues into how these channels operate.

Crystal structures of MS channels

Our understanding of MS channels has benefited greatly from the various types of structure determination methods most notably X-ray crystallography, which can provide the atomic structures of proteins with angstrom level resolution. However,

many of the crystal structures of membrane proteins available to date have been solved in detergents that completely replace lipids. The organizing role of lipids has been strongly suggested for transmembrane alpha helical proteins (Toyoshima et al., 2000; Long et al., 2005) and therefore every structure obtained in pure detergent should be carefully scrutinized for possible distortions or deviations from their native conformations. In this respect, the first question that arises with a new crystal structure of a channel protein is 'what functional state if any does the structure represent?'

Membrane channels also display an inverted design compared to soluble proteins with their hydrophilic amino acid residues facing towards the core, into the solvated conducting pathway, and hydrophobic residues facing outwards towards the lipid phase (White and Wimley, 1998, 1999; Popot and Engelman, 2000). In the case of mechanosensitive channels the lipid membrane is a critical determinate of tertiary structure, one that acts to modulate the functional domains of the channels. Removal of a mechanosensitive channel from the lipid context may have severe consequence on the final determined structure. There remains much debate on the accuracy of functional mechanisms derived purely from interpretation of crystal structures. Finally, it must be remembered that these structures are merely detailed snapshots that provide a starting point for continued study.

Molecular dynamics simulation and modeling

The explosion of atomic level data from crystal structures has been a boon to molecular modelers in their attempts to elucidate the structural changes that underlie protein function. This data is extremely useful is for molecular dynamics (MD)

simulations which consist of a set of computer-based calculations and utilize complex theoretical and experimentally based algorithms to simulate the explicit interactions between macromolecules in a system over a period of time (Koehl, 2006). In recent years, enhanced computation power has increased the utility of MD for ion channel research and since it is now possible to simulate larger systems (to include the lipid bilayer) for longer periods of time (Tama and Brooks, 2006), the gap between MD and bench experiments has begun to narrow. Recent work in the MscS and MscL channels demonstrated the ability for MD simulations to provide testable hypothesis and suggest targets for molecular manipulation and characterization (Gullingsrud and Schulten, 2003; Anishkin and Sukharev, 2004; Sotomayor and Schulten, 2004).

Electrophysiology: Patch-clamping

The primary method of collecting physiology data from single ion channels including MS channels comes from an electrophysiology technique called patch-clamping. Nobel laureates Edwin Neher and Bert Sakmann pioneered this approach in 1976 as a way to measure the small ionic currents produced by single ion channels (Sakmann and Neher, 1995). The low electrical noise required to observe ion channel currents, typically in the pico-ampere range, was achieved by forming a 'gigaseal' ($> 10^9$ Ω) between the glass recording electrode and the plasma membrane (Sakmann and Neher, 1995).

Patch-clamping can be performed in a variety of configurations to suit the system and channel being studied. Some examples are cell-attached or excised patch in either an inside-out, outside-out or whole cell configuration mode. This allows the researcher a great deal of flexibility to manipulate the recording environment on both

the periplasmic and cytoplasmic sides of the membrane. The activity of channels embedded in the patch may then be modulated through the application of voltage or the addition of numerous external compounds such as neurotransmitters or channel blocking peptides. For MS channels, which are modulated by membrane tension, stretching forces are generated by the application of a pressure gradient across the membrane patch. These gradients generate tension in the attached membranes according to the law of Laplace and provide the driving force for MS channel gating (See Appendix 1). Pressure stimuli are applied to the patches through suction (negative pressure) either manually, by mouth or syringe, or in an automated manner using a pressure-clamp apparatus. The development and application of the pressure-clamp (Besch et al., 2002) to the study of MS channels has proved critical as many MS channels exhibit fast adaptive behaviors, the study of which requires the onset and release of pressure to be rapid (Zhang et al., 2000; Akitake et al., 2005; Honore et al., 2006).

Early study of MscS

Purification and functional reconstitution

After the sequence became available, the *mscS* gene was amplified by PCR and the coding sequence was modified with a 6-His tag on its C-terminus (Okada et al., 2002; Sukharev, 2002; Nomura et al., 2006b). The position of this tag had previously been shown to have minimal effects on channel function under normal ionic conditions (Koprowski and Kubalski, 2003). The *E.coli* expressed protein was purified on a Ni-

NTA column and appeared homogeneous. When subjected to size-exclusion chromatography in the presence of β-octylglucoside and lipids, the protein emerged as a 200 kDa particle, apparently representing a stable complex. In the presence of detergent only, the complexes degraded to 30 kDa monomers. Cross-linking experiments with the bifunctional reagent DSS suggested that at least six identical subunits form the active complex (Sukharev, 2002).

Patch-clamp analysis of pure MscS reconstituted into liposomes revealed fully active channels characterized with a weak anionic preference, slight inward rectification and essentially non-saturable conductance (Sukharev, 2002). Imaging of large liposome patches, along channel recording at different pressures, permitted determination of the radii of patch curvature and in such the magnitude of tension acting on channel population from the law of Laplace. The mid-point tension for MscS activation was found near 5.5 dyne/cm, in good correspondence with previous measurements by Cui and Adler performed in the whole-protoplast recording mode (Cui and Adler, 1996). In the same way that the slope of the conductance versus voltage (G-V) curve for a voltage-gated channel gives an estimation of the gating charge, the slope of Po/Pc on tension estimates the in-plane area change of a mechanosensitive channel. Treatment of dose-response curves in a two-state Boltzmann approximation (Fig. 1-3) (Sachs and Morris, 1998) predicted a protein expansion of $\Delta A = 8.4\ nm^2$ and an energy difference between the closed and open conformations, in the absence of tension, of $\Delta E = 11.4\ kT$. Independently conducted reconstitution experiments by Okada and coworkers (Okada et al., 2002) confirmed that MscS is gated directly by tension in the lipid bilayer.

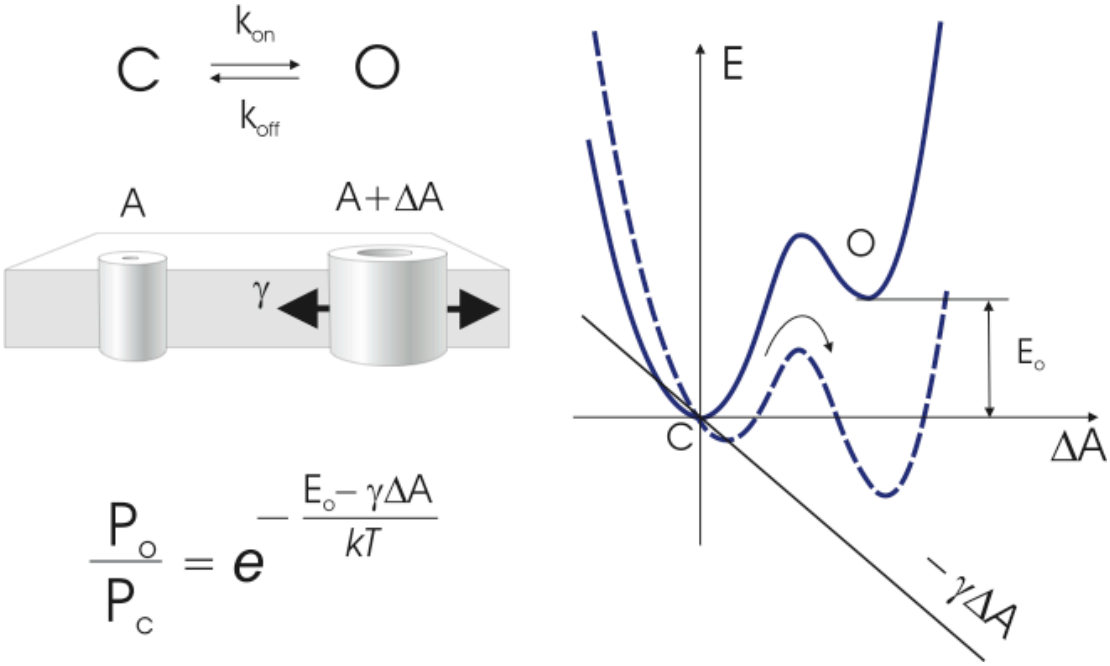

Figure 1-3. Two-state Boltzmann-type model for the gating of a binary MS channel.
Schematic description of the two-state Boltzmann-type model used to fit MscS activation curves. This approximation assumes two states, (C)losed and (O)pen, for which there are equilibrium rate constants. The mechanical energy used to open MscS or other MS channels, is represented by ΔA or the area change of the protein in the plane of membrane scaled by the tension (γ). The ratio of the open probability (P_O) to the closed probability (P_C) thus changes with tension as the stretching force applied to the channel forces a redistribution of the occupancies of the C and O states (Sukharev and Corey, 2004).

MscS versus MscK: how to interpret early functional data?

The earliest functional studies of *MscS-like* mechanosensitive channels in *E.coli* spheroplasts conducted by Martinac *et al*. reported on a population of pressure-sensitive ion channels of ~1 nS conductance (Martinac et al., 1987). Single channel recordings revealed pressure dependence, a strong and sharp increase of channel open probability observed with increasing suction, and voltage dependence. Increasingly depolarizing voltages made the channel population easier to open and shifted the activation curves progressively to the left. Subsequent study of these channels in the whole-protoplast recording mode by Cui and coworkers revealed similar phenomenology (Cui et al., 1995).

Data from these early studies were obviously collected on mixed populations of channels and it is now known that a WT *E. coli* background contains both MscS and MscK with similar activities. Of the two, MscK is a much larger multi-domain protein. From an alignment of the primary sequences, the 286 amino acid long MscS shares 23% identity and 53% similarity to the C-terminal part of MscK. Although these numbers are not quite high enough to conclude structural identity, analysis of the residue patterns, especially those in the transmembrane region, suggested very similar organization, and provides some rationale for their similar gating characteristics (Levina et al., 1999; Miller et al., 2003a). PhoA-fusion experiments concluded that the common parts of MscK and MscS each contain 3 transmembrane domains, with the N-terminal ends of the protein being periplasmic, and the larger soluble C-terminal domains residing in the cytoplasm (Miller et al., 2003a). MscK also has a large N-terminal domain that was predicted to form up to 7 additional

transmembrane spans. In spite of the structural differences, both channels were characterized with similar ~1 nS conductances, a slight anionic preference, and weak inward rectification (Li et al., 2002).

More recent studies of MscS expressed in a clean genetic background (Levina et al., 1999; Vasquez and Perozo, 2004; Akitake et al., 2005) revealed functional characteristics that substantially differed from those originally reported by Martinac and Cui (Martinac et al., 1987; Cui et al., 1995). A detailed comparison revealed that MscK is activated at slightly lower tensions than MscS (Li et al., 2002) however the primary distinction between the two channels lies in their kinetic behavior and regulation. With symmetrical KCl on both sides, MscK exhibits sustained activity in the entire range of activating pressures, whereas under mechanical stimulation below saturating levels, MscS response was transient with characteristic inactivation (Levina et al., 1999; Akitake et al., 2005). Both Martinac and Cui used constant pressure stimuli held for extended durations, conditions at which MscS populations inactivate quickly. MscK was found to be critically dependent on the monovalent cation species present in the recording solution showing activity only when K^+, NH_4^+, Rb^+, or Cs^+ was present in the periplasmic medium and inactive when replaced with Na^+ or Li^+ (Li et al., 2002). In contrast, MscS activity was demonstrated to be the same in both Na^+ and K^+ buffers (Li et al., 2002; Akitake et al., 2005). The channel population studied by Martinac showed marked changes in activity becoming harder to open with faster kinetics in Na^+ buffers. Cui *et al's* also studied the RQ2 strain of *E. coli* and noted that in this mutant *Mscs-like* channel activity displayed a lowered opening threshold. RQ2 was later found to harbor a missense gain-of-function mutation in the

mscK (formerly *kefA*) gene (McLaggan et al., 2002). The position of the RQ2 gain-of-function mutation (G922S) was mapped to the gate region in the most C-terminal transmembrane span of MscK (equivalent to the A106 position in the TM3 helix of MscS). Finally, it has been shown that the opening transition in MscS is not affected by voltage (Vasquez and Perozo, 2004; Akitake et al., 2005; Nomura et al., 2006a). From these comparisons it is now evident that the early phenomenology of *MscS-like* channels in *E. coli* as reported by Martinac and Cui belongs primarily to MscK, not MscS.

Problem statements and questions

Characterization of wild-type MscS

The crystal structure of *E. coli* MscS was solved and published (Bass et al., 2002) shortly after I arrived in the Sukharev lab in the fall of 2002. With a structural starting point, many competing groups raced to mutate the MscS channel in hopes of elucidating its gating mechanism. However, the initial interpretation of the structure as an open state, and the inferred mechanisms of gating both by tension and voltage, presented a picture that to us was not convincing. Little study of the WT MscS channel in its native setting had occurred since Martinac and colleagues observed *MscS-like* activity while working with a mixed population of channels in 1987 (Martinac et al., 1987), and no *in situ* characterization had been conducted except for a brief study by Levina and colleagues, who cloned MscS in 1999 (Levina et al., 1999). It appeared clear to me that a more thorough characterization of WT Mscs was

needed before any well-grounded interpretation pertaining to its gating mechanism could be put forward. At the time I sought to take advantage of new instrumentation, a high-speed pressure clamp (HSPC) apparatus (ALA Scientific Instruments), and newly written data analysis programs from Dr. Anishkin. I therefore focused on the following questions:

- How reproducible is the activation of WT MscS in native *E. coli* membranes now that we can pre-program and exactly reproduce pressure stimuli using the HSPC?
- Is the activation of MscS sensitive to the rate of pressure application?
- Is the activation of MscS sensitive to voltage?
- What are the characteristics of MscS inactivation? Is it also a rate or voltage-dependent process?
- Can we correlate the general behaviors of the WT channel to the new structural information?

The interaction of MscS with small amphiphilic molecules

A large body of experimental and computational data emphasized the role of the phospholipid bilayer for the organization of many membrane proteins providing special anisotropic environment with a complex lateral pressure profile. Work from our collaborators, the de Kruijff laboratory (Univ. of Utrecht, The Netherlands), showed that fluorinated alcohols could distort this pressure profile and hence affect subunit association in membrane bound channels, like KcsA and MscS (Spelbrink et al., 2005). My participation in the study presented in chapter 3 was actually initiated as a small side project to investigate the effects of 2,2,2-trifluoroethanol (TFE) on the

function of MscS in patch-clamp. TFE is broadly used in protein and peptide biochemistry as a co-solvent that stabilizes secondary structure. It seemed however that the inverted design of membrane proteins, with their hydrophilic residues facing towards the solvent in the pore and hydrophobic residues looking outward to the lipid phase, were destabilized by TFE causing oligomeric channel complexes to dissociate into monomers. I initially found that TFE, even in small concentrations, acted to reversibly silence MscS activity. I then sought to address several questions aimed at understanding the mechanisms that underlie TFE-induced silencing:

- Does TFE affect specific functional transitions of MscS? (Closed to Open, Open to Inactivated, Inactivated to Closed)
- Is the TFE-induced silenced state similar to the native inactivated state?
- Are the effects of TFE sided, i.e. application of TFE from the cytoplasm versus the periplasm? Could such a difference be related to the asymmetric position of the MscS gate?
- Does TFE work directly on MscS or are its activities conveyed through the lipid bilayer?

Probing the conformation of MscS during its functional cycle

One of the most salient features of the MscS crystal structure is the sharp kink in the pore-lining TM3 helices at residue G113 (Fig. 1-2, right). From this kink, the nearly parallel helices splay out at 80° relative to the axis of the pore such that the C-terminal (TM3b) segments extend almost parallel to the membrane interface, with their ends separated by about 55 Å, to form the roof of the wider cage. The kink at G113 functionally divides TM3 into two segments (TM3a and TM3b) and appears to

be the only way to pack the TM3a segments as a compact barrel, with L105 and L109 forming the closed hydrophobic gate, while maintaining a connection between the gate and the cage. The cage of MscS is not a rigid structure and various perturbations of this domain have been reported to affect gating (Koprowski and Kubalski, 2003; Miller et al., 2003b; Schumann et al., 2004). The fact that stresses or conformational changes in the cage are transmitted directly to the channel gate points the importance of TM3b as a regulatory joining element.

In the study presented in chapter 4, Dr. Andriy Anishkin used a novel 'extrapolated-motion' technique to envision the conformational pathways that exist to define the gating cycle of MscS. His new models of MscS featured conspicuously different conformations of the TM3 helices in each of the channel's functional states including the formation of an alternative kink in TM3 at G121. Further analysis of the amino acid sequence along TM3a and TM3b prompted us to focus on the flexibility of TM3b. I took on the task of verifying these models by helping to design and conduct patch-clamp experiments to address the following specific questions:

- How does the kinetics of the MscS functional cycle change when the helical propensity of TM3b is either increased or decreased?
- Can we provide verification of the models and unequivocally associate kink formation at either G113 or G121 with specific functional states?
- What role does intrinsic helical stability and its concomitant modulation with membrane tension play in the regulation of the MscS gating cycle?

Chapter 2: The "dashpot" mechanism of stretch-dependent gating in MscS

Bradley Akitake, Andriy Anishkin and Sergei Sukharev

Department of Biology, University of Maryland, College Park, MD 20742

Journal of General Physiology 2005 Feb;125(2):143-54.

Abstract

The crystal structure of MscS has been an invaluable tool in the search for the gating mechanism, however many functional aspects of the channel remain unsettled. Here we characterized the gating of MscS in *E. coli* spheroplasts in a triple mutant (*mscL*$^{-}$, *mscS*$^{-}$, *mscK*$^{-}$) background. We utilized a pressure clamp apparatus along with software developed in-lab to generate dose-response curves directly from two-channel recordings of current and pressure. In contrast to previous publications we found that MscS exhibits essentially voltage-independent activation by tension, but at the same time strong voltage-dependent inactivation under depolarizing conditions. The MscS activation curves obtained under saturating ramps of pressure at different voltages gave estimates for the energy, area, and gating charge for the closed-to-open transition as 24 kT, 18 nm^2, and +0.8 respectively. The character of activation and inactivation was similar in both K^+ and Na^+ buffers. Perhaps the most salient and intriguing property of MscS gating was a strong dependence on the rate of pressure application. Patches subjected to various pressure ramps from 2.7 to 240 mmHg/sec revealed a midpoint of activation almost independent of rate. However, the resultant channel activity was dramatically lower when pressure was applied slowly, especially at depolarizing pipette voltages. It appears that MscS prefers to respond in full to

abrupt stimuli but manages to ignore those applied slowly: as if the gate were connected to the tension-transmitting element via a velocity-sensitive 'dashpot'. With slower ramps, channels inactivate during the passage through a narrow region of pressures below the activation midpoint. This property of 'dumping' a slowly applied force may be important in environmental situations where re-hydration of cells occurs gradually and release of osmolytes is not desirable. MscS often enters the inactivated state through subconducting states favored by depolarizing voltage. The inactivation rate increases exponentially with depolarization. Based on these results we propose a kinetic scheme and gating mechanism to account for the observed phenomenology in the framework of available structural information.

Introduction

MscS is a major component of the turgor regulation system in bacteria that also includes the large channel MscL (Blount and Moe, 1999; Levina et al., 1999). These two osmotic 'valves' activate at different tension thresholds providing a graded permeability response to osmotic down-shifts of varied magnitude. Efflux of osmolytes through these channels reduces the osmotic pressure and effectively protects the bacterial cells against lysis. Each of these molecules, MscS and MscL, forms a gigantic pore in the membrane gated directly by tension in the surrounding lipid bilayer. Despite having no sequence homology or structural similarity, a unique functional convergence and even partial redundancy (Levina et al., 1999) makes these two channels especially interesting for basic studies of mechanotransduction. MscS and MscL represent advanced systems that may reveal how common biophysical

principles of gating are implemented with dissimilar structural designs. In contrast to MscL, which is a strictly prokaryotic molecule, MscS homologs are more abundant having also been found in eukaryotes increasing the value of MscS as a model (Pivetti et al., 2003).

Martinac and coworkers (Martinac et al., 1987), who were the first to apply patch-clamp techniques to giant *Escherichia coli* spheroplasts, reported a pressure-gated bacterial channel of 1 nS conductance. MscS, a mechanosensitive channel with 1-nS conductance was identified later as a product of the orphan *yggB* gene, sharing similarity with the N-terminal half of the potassium efflux protein MscK (formerly KefA) (Levina et al., 1999). MscK was also shown to be a mechanosensitive channel with conducting characteristics similar to that of MscS (Levina et al., 1999). However, while MscS exhibited time-dependent inactivation (Koprowski and Kubalski, 1998; Levina et al., 1999), MscK was characterized by more sustained activities under constant stimulation. MscK gating was also found to be critically dependent on the presence of potassium ions in the external medium (Li et al., 2002).

Crystallographic work by the Rees group recently produced the crystal structure of *E. coli* MscS (Bass et al., 2002) revealing a homo-heptameric complex with three transmembrane helices per subunit and a large cytoplasmic C-terminal domain. Two transmembrane helices M1 and M2 were bundled together resembling the ‘paddle’ of the KvAP voltage sensor (Jiang et al., 2003a; Jiang et al., 2003b). Due to the presence of several arginines, these helices were proposed to serve a similar function as the MscS voltage sensor. The third transmembrane helix (M3) lined a relatively wide but very hydrophobic pore, deemed to represent the open

conformation (Bass et al., 2002). Our computational studies suggested that the MscS pore constriction is dehydrated and likely non-conductive (Anishkin and Sukharev, 2004) thus raising the question of what functional state the crystal structure actually represents. Independent computational studies also confirmed the dehydrated and low-conducting nature of the MscS pore (Sotomayor and Schulten, 2004). Biochemical cross-linking experiments suggested that the native closed conformation of the channel is more compact as compared to the crystal conformation in both the transmembrane and cytoplasmic domains (Miller et al., 2003b).

The availability of molecular information on MscS facilitates tremendously many aspects of functional studies. While cloning and tagging of MscS permitted purification and functional reconstitution of the protein in liposomes (Okada et al., 2002; Sukharev, 2002), generation of the MJF465 triple mutant (*mscL*$^{-}$*, mscS*$^{-}$*, mscK*$^{-}$) *E. coli* strain prepared a 'clean' genetic background on which the channel could be studied it its native setting (Levina et al., 1999). The first brief report of MscS behavior at different voltages measured in a 'clean' system (Vasquez and Perozo, 2004) gave a different picture of gating compared to the previous phenomenology (Martinac et al., 1987; Koprowski and Kubalski, 1998) collected on mixed channel populations.

The present work characterizes the behavior of MscS in the MJF465 triple mutant *E. coli* strain (Levina et al., 1999). Data collection was aided by a high-speed pressure clamp apparatus to deliver reproducible ramps of pressure to patches. Software developed in-lab allowed us to generate dose-response curves directly from the resulting two-channel recordings of current and pressure. The results indicate that

MscS activation is essentially voltage independent, however the net channel activity is strongly influenced by the process of reversible inactivation. MscS inactivation was found to be both tension- and voltage dependent. The interplay of these two processes, activation and inactivation, makes MscS most responsive to abruptly applied mechanical stimuli. We propose a kinetic scheme and gating mechanism in an attempt to reconcile the observed phenomenology with the crystal structure.

Materials and Methods

Strains

Analysis of MscS was performed in giant *Escherichia coli* spheroplasts as described by Martinac *et al.*, 1987. The PB111 construct containing the *mscS* gene under the control of an inducible P_{lacUV5} promoter was generously provided by Dr. P. Blount (University of Texas, Dallas). The expressed channel protein has a C-terminal 6His tag, which was shown previously to have little effect on the character of gating in the absence of His-binding divalent ions (Koprowski and Kubalski, 2003). For electrophysiological analysis the construct was electroporated into the MJF465 (*mscL*$^{-}$*, mscS*$^{-}$*, mscK*$^{-}$) triple knock-out strain, a gift from Dr. I.R. Booth (University of Aberdeen, UK). All analyses were repeated in at least two independent spheroplast preparations.

Electrophysiology

Patch-clamp recordings of MscS were taken in an excised patch, voltage clamp, configuration on an Axon 200B amplifier attached to an Axon DigiData 1320A A/D

converter (Axon Instruments). Electrodes were borosilicate capillaries pulled to a bubble number of 4.5 (resistance 2.8±0.2 MΩ, in a buffer of 39 mS/cm conductivity) on a micropipette puller (Sutter Instruments Company). Recording was carried out in symmetrical potassium (200 mM KCl, 90 mM $MgCl_2$, 10 mM $CaCl_2$, 5 mM HEPES titrated to pH 7.4 with KOH) or sodium (replaces above KCl with 200 mM NaCl) buffers in the pipette. The bath solution differed only in the addition of 300 mM sucrose. Pressure ramps were applied using an HSPC-1 high-speed pressure clamp apparatus (Besch et al., 2002) controlled via analog output from the DigiData1320A. ALA Scientific Instruments' P-V Pump unit was used as the pressure and vacuum source. Vacuum and pressure were calibrated at both the pumps and the headstage using a PM015D pressure monitor (World Precision Instruments). Pressure traces were then recorded directly from the HSPC-1 head stage. Output commands to the HSPC-1 were controlled by Axon pClamp8 software in episodic stimulation mode (Axon Instruments).

Data collection and treatment

Axon pClamp 8 software was used to record the integral current through patches with a bandwidth of 1-5 kHz, digitizing at 1000-25000 samples/sec depending on the duration of the recording. Two-channel (current and pressure vs. time) electrophysiological recordings were converted into Axon Text Format and subsequently analyzed using HISTAN, software custom-written in Matlab. A dose-response curve (P_o/P_c vs. pressure) calculation was implemented using the following protocol. The whole pressure range was divided into bins of 1 mmHg width and all-point current histograms were created for each pressure value. Following baseline

correction an average integral current value I(p) was calculated for every pressure bin. An opening probability for the MscS population was estimated by $P_o(p) = I(p)/I_{max}$, where I_{max} represents the maximal integral current observed in the recording. Under typical conditions (applied pipette voltage range of –30 to 80 mV), where the relative occupancy of subconducting states is very low, this approach gives an adequate estimation of the open probability of MscS. However, out of this range, subconducting states are dominant and this approach provides only an approximation of P_o since it relies on an assumption that the contribution of the substates to integral current, relative to the fully open state, does not change significantly with tension. Proper treatment of MscS traces recorded at high positive and negative voltages will be a focus in future research.

Pressure to tension conversion

The midpoint pressure ($p_{½}^{20}$) at which half of the MscS population was activated under +20 mV during the fastest (1 s) pressure ramp was used as a tension calibration point. $p_{½}^{20}$ was calculated for each patch individually as an average of all traces recorded under a single applied voltage (usually 3 to 10 recordings). This average pressure corresponds to 5.5 dyne/cm, earlier shown to be the tension mid-point for MscS activation in spheroplasts (Cui and Adler, 1996) and liposomes (Sukharev, 2002). $p_{½}^{20}$ was then used in tension calculations for the remaining traces, recorded from the same patch, under different applied voltage. Pressures were converted to tensions using the law of Laplace for spherical surfaces: $\gamma = (p / p_{½}^{20}) \times 5.5$ dyne/cm. This conversion implies that in the range of pressure needed to activate MscS patch geometry does not substantially change (See Appendix 1). Based on video

observations of liposome patches (Sukharev et al., 1999), the membrane was found to be essentially flat at a zero pressure, becoming hemi-spherical under a pressure gradient. The curvature of liposome patches saturated with increasing pressures and remained stable in a range of tensions from 4–5 dyne/cm. These findings are likely true for spheroplast patches as well.

Fitting procedures

Dose-response curves for MscS were fitted with a two-state Boltzmann-type model, $P_o / P_c = \exp[-(\Delta E - \gamma \Delta A)/kT]$, where P_o and P_c are the probabilities for the open and closed states, ΔE is the difference in energy between the states in an unstressed membrane, ΔA is the in-plane protein area change during the gating transition, γ is the membrane tension, and kT has the conventional meaning (Sachs, 1992; Sukharev et al., 1999). Fitting was performed in Microsoft Excel 2000 using a linear least squares method in semi-logarithmic coordinates ($\log(P_o/P_c)$ vs. tension). Only the first linear part of activation curve was fitted (see Results) representing activation of the main population of MscS channels.

To characterize the time course of the MscS inactivation at constant pressure the falling phase of the integral current was fitted with a single standard exponent of the first order ($I(t) = Ae^{-t/\tau} + C$, where I is an integral current, t time, A amplitude, C additive constant, and τ time constant). Fitting was performed in Axon Clampfit 9 using a Levenberg-Marquardt search method and sum of squared errors minimization criterion (Axon Instruments).

Results

Activation curves of MscS measured with reproducible pressure ramps

Membrane patches, excised from giant *E. coli* spheroplasts expressing wild-type MscS, were exposed to 1 s linear ramps of pressure ending with a constant 2 s plateau of saturating pressure. Fig. 2-1A shows seven superimposed traces from one representative patch, recorded under a +20 mV pipette voltage. When the saturating pressure was reached, the current through the open channel population achieved some maximal level. As shown below, various factors such as the rate of pressure application, or pre-activation of the population with non-saturating pressure steps, altered that final level. However, even when the stimulation conditions were kept constant there was still some variability in maximal current under repeated activation (Fig. 2-1A). This base variability, with large channel populations (20 or more channels per patch), was consistently ~10% (Fig. 2-1A, arrows), when provided with a 3 min 'rest' period at 0 mV between pressure applications. Reducing the time between pressure ramps significantly decreased the final current, indicating that prior treatment changes the availability of channels by driving a part of the population to an inactive state.

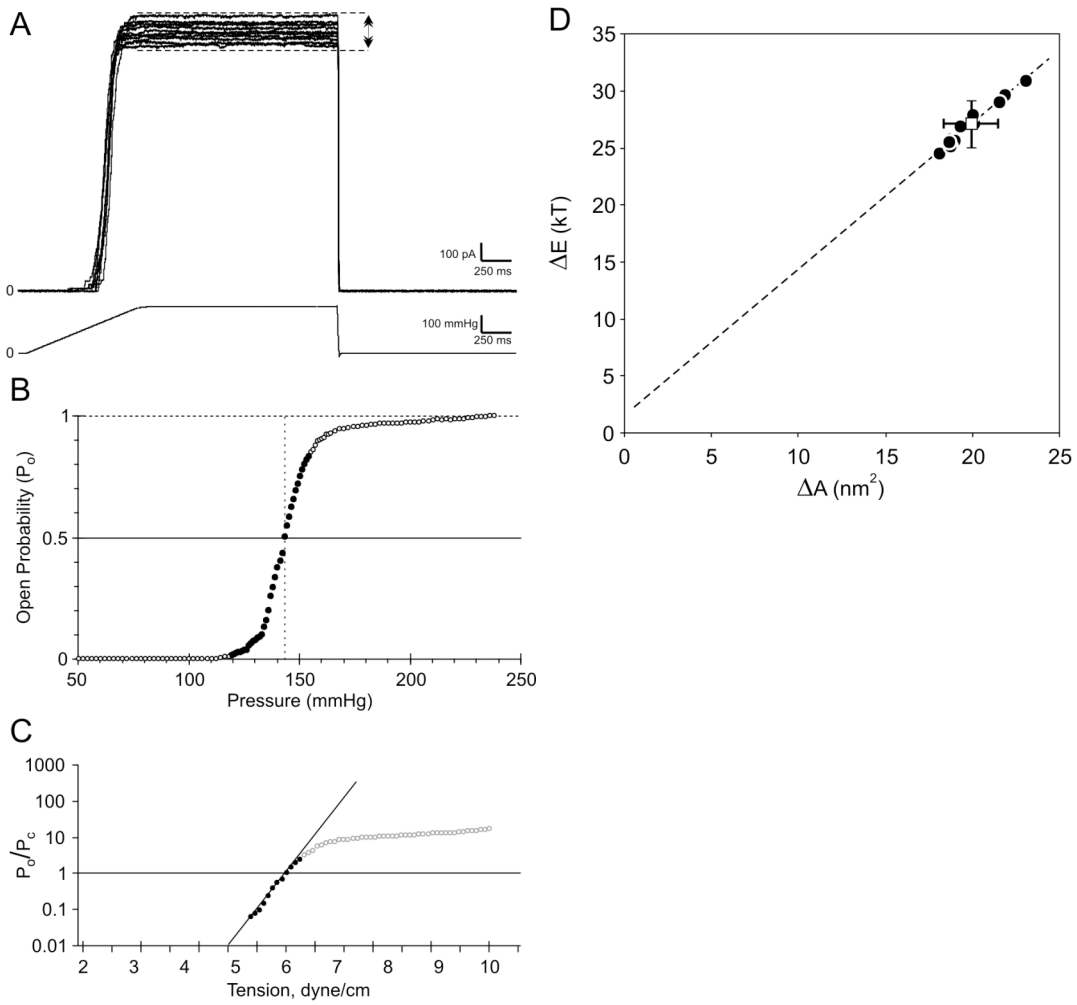

Figure 2-1. Responses of MscS populations to linear pressure ramps.

Ramp duration was 1s followed by a 2s plateau. **(A)** Superimposed raw traces obtained in the same patch at +20 mV pipette voltage. Arrows represent variability in maximal current. **(B)** One trace from the dataset in panel A converted into a dose-response curve by plotting Po = I/Imax vs. pressure. **(C)** The Po/Pc-tension dependence plotted in a semi logarithmic scale. The pressure scale was converted to tensions by equating the tension at the pressure midpoint (mean p1/2 for all traces in panel A) to 5.5 dyne/cm and the linear part of the dependence was fit. **(D)** Correlated distribution of ΔE vs. ΔA parameters extracted from the traces obtained in the same patch (panel A).

The population also showed decreased maximal current if the patch was kept under depolarizing (pipette negative) potentials during the 'rest' period. A 3 min interval between stimuli under positive or zero applied voltage generally allowed the population to fully recover. Despite this variability of maximal current the pressure midpoint (pressure of half maximal activation of MscS, $p_{1/2}$) of MscS channels activated by sequential pressure ramps was more consistent varying within 1.6% of the mean. Among five representative patches studied with standard borosilicate pipettes (see Methods), the average $p_{1/2}$ was 188±31 mmHg, which can be accounted for by differences in pipette size and patch geometry.

Using HISTAN software, dose-response curves of open-probability (P_o) versus pressure were generated using a 2D histogram approach (Chiang et al., 2004) directly from two-channel recordings of current and pressure (Fig. 2-1B). The maximal current (I_{max}) during each pressure application was taken to represent the highest open probability ($P_o = 1$) and all other current points were normalized to it producing $P_o = I/I_{max}$. Maximal current was estimated to be the highest level achieved in each separate pressure application. Assuming a tension midpoint ($\gamma_{1/2}$) for MscS of 5.5 dyne/cm (Sukharev, 2002) at +20 mV, pressure dependencies were converted to $P_o/P_c(\gamma)$ and fit with a two-state Boltzmann equation to extract apparent (ΔE) and area (ΔA) for the opening transition (Fig. 2-1C). Analysis of many patches indicated non-uniformity in the MscS population, with a 'main' population whose P_o/P_c ratio depended strongly on tension and a second, much smaller, 'late' population that activated with a lower slope on pressure. Part of this 'late' population had a delayed behavior activating after the ramp reached its plateau. The contribution of the 'late'

population ranged from 0 to 5% of the total integral current therefore only the linear portion of the activation curve was fitted and used for determination of the overall gating parameters (Fig. 2-1C).

Values of ΔE and ΔA for the MscS gating transition, extracted from sequential ramps applied to the patch shown in Fig. 2-1A, averaged 27±2 kT and 20±1.6 nm^2 respectively (n = 11). The combined values from five different patches taken from independent spheroplast preparations produced ΔE = 24±4 kT and ΔA = 18±3 nm^2 (n = 27). A plot of ΔE versus ΔA from the same patch (Fig. 2-1D) illustrated strong correlation in the variation of these parameters. A previous study of population responses in MscL (Chiang et al., 2004) showed that slightly non-homogenous populations of channels display strong linear correlations of ΔE and ΔA. This appeared to be the case for MscS where variation of the slope of the dose-response curves was substantially larger than variation in the midpoint position. Note that at the tension midpoint ($\gamma_{1/2}$), $P_o = P_c$ and from eqn.1 $\gamma_{1/2} = (\Delta E / \Delta A)$. Statistical simulations of non-homogenous channel populations illustrated that the slope of the dose-response curves should be lower that that of an ideally homogeneous population. Furthermore, this slope reduction increases with the scatter of intrinsic parameters (ΔE and ΔA) characterizing each individual channel. If the source of non-homogeneity is a deviation of the intrinsic parameters, then the values extracted directly from the activation curves represent lower bound estimates for ΔE and ΔA. If however the deviations of the dose-response curves are more related to the stochastic nature of crossing the transition barrier (which can produce variations in P_o under non-equilibrium pressure ramps) during the gating transition then these average

values of ΔE and ΔA may closer reflect the true intrinsic parameters for MscS. Further analysis is required to fully explain the dose-response curve variability in the MscS channel population.

Voltage dependence of MscS activation

The same patch clamp experiments, with linear ramps of saturating pressure, were repeated at different voltages from –100 mV to +100 mV. The midpoint for MscS activation remained essentially constant at both high positive and moderate negative voltages as shown by the raw traces in Fig. 2-2A. A similar character of currents was observed in both symmetrical KCl and NaCl-based buffers. In several independent experiments, the maximal conductance for each individual trace was normalized to that observed at +20 mV and plotted as a function of voltage (Fig. 2-2B). The maximal conductance at high positive pipette voltages (+60, +80, and +100 mV) increases shallowly. At negative pipette voltages, beyond –40 mV, a steep decrease of the integral patch conductance was obvious (Fig. 2-2B). Traces were treated as described in the previous section (Fig. 2-1B and 2-1C) and the effective parameters ΔE and ΔA were obtained for each voltage. The plot of ΔE versus voltage showed MscS activation to be only weakly dependent on applied electric field (Fig. 2-2C). From the slope of the fit, gating charge (q) was determined to be +0.8 per MscS heptamer or about +0.1 per subunit. This small value for q indicates that the charges within the electric field, most of which lie on the lipid facing helices of TM1 and TM2, do not displace significantly during MscS activation.

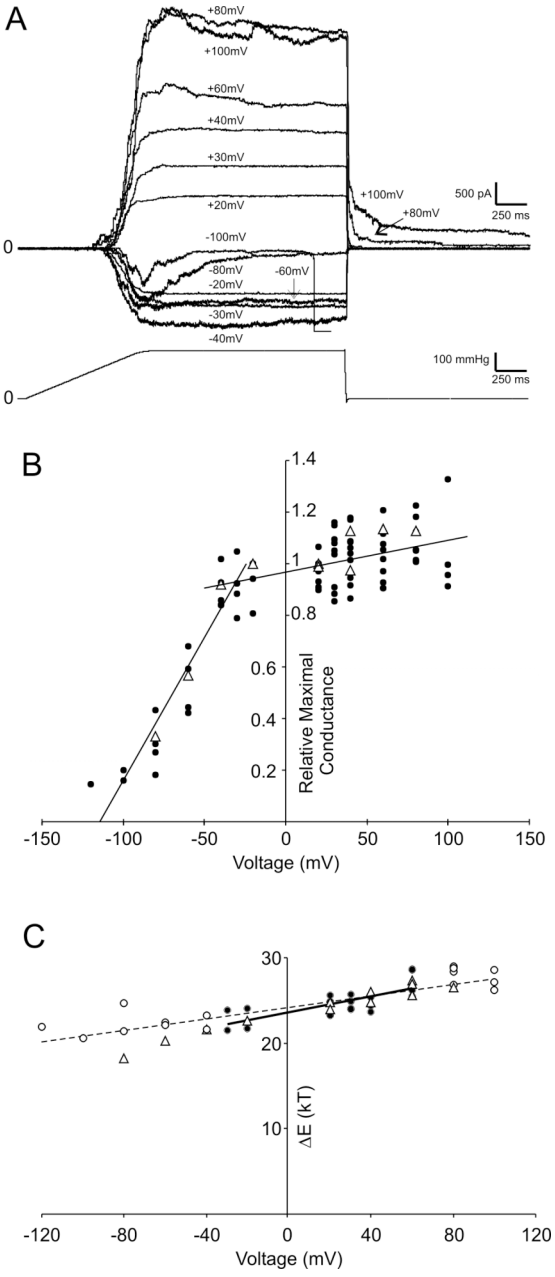

Figure 2-2. Responses of MscS populations to linear pressure ramps under different applied voltages.

(A) Raw traces recorded at pipette voltages ranging from -100 to +100 mV (patch ruptures near the end of the -100 mV trace). Maximal conductance for the MscS population increases linearly with voltage in the range of moderate voltages (–30 mV to +40 mV). At very high positive pipette voltages (> +40 mV) MscS behavior becomes less predictable and a population of channels remains open even after pressure has been released increasing in number with higher voltages (right side, +80 and +100 mV). At very negative pipette voltages (< –40 mV) there is clear break in the modality of the traces as inactivation becomes prominent. **(B)** Maximum relative conductance as a function of voltage for four different patches. The data presented for KCl (closed circles) and NaCl (open triangles) recording buffers. **(C)** The energy of the closed-to-open transition (ΔE, fitted with the fixed $\Delta A = 17\ nm^2$) as a function of voltage, for three independent patches in KCl (circles) and NaCl (triangles).

In an attempt to explain the dramatically decreased integral conductance at negative pipette voltages, MscS activities were recorded from patches expressing a smaller number of channels. An analysis of the most frequently observed MscS single channel amplitudes versus voltage is shown in Fig. 2-3A. The continuous line represents the fit of maximal current amplitudes, reflecting the conducting properties the fully open state of MscS. The plot also reveals a pair of bifurcations (Fig. 2-3A, dashed lines) taking place at +60 and –40 mV, signifying an increased presence of sub-conducting levels. At higher voltages channels exhibited a preference for the lower conducting states. Fig. 2-3B shows a typical trace obtained at a constant moderate pressure with 4-5 channels open. Reversal of the pipette voltage from +40 to –40 mV switched the character of gating. Channels that were fully open at +40 mV showed flickering in and out of substates at –40 mV. The substates display noticeably faster kinetics than the main closed to open transition. All of the MscS channels had inactivated by the end of the shown episode. The same experiment at +60 mV revealed that fully open channels at positive voltages immediately entered stable substates when voltage was reversed to –60 mV and also quickly inactivated (Fig. 2-3C). Substates coincident with inactivation suggest that at negative voltages inactivation proceeds through these lower conducting substates. The increased occupancy of substates and inactivation seen in the single-channel traces explains the decline of the integral current observed in multi-channel patches at high negative voltages (Fig. 2-2B). The small positive slope of the maximal integral conductance observed at positive pipette voltages likely reflects the slightly rectifying nature of the fully open state.

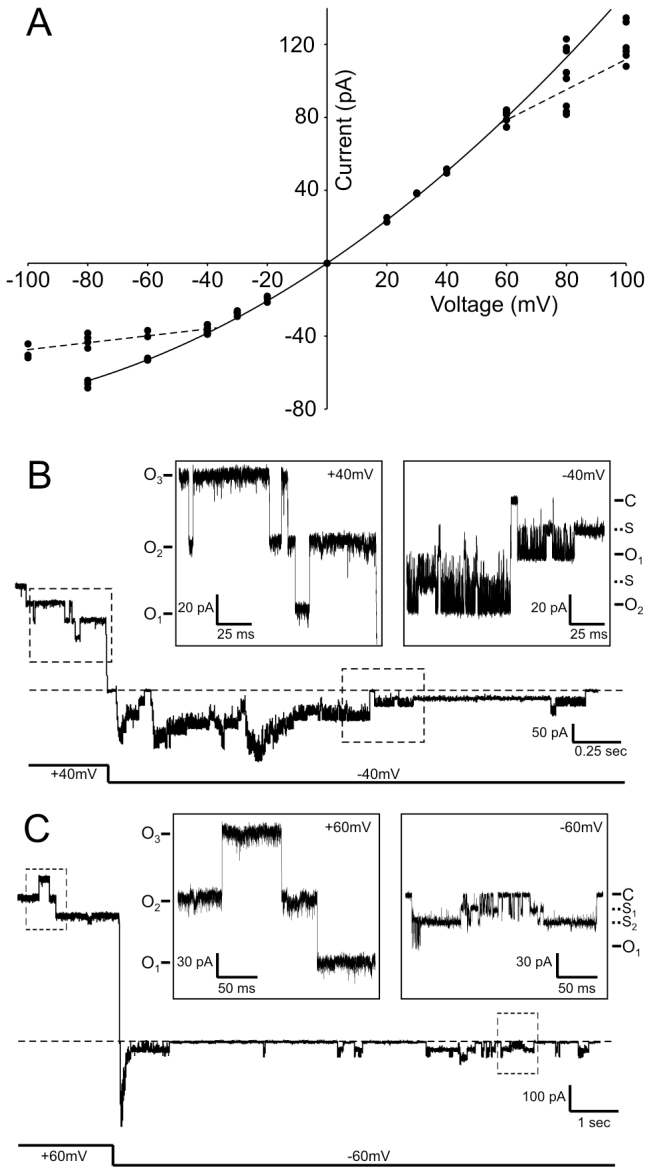

Figure 2-3. Single-channel conductance of MscS as a function of voltage showed the occupancy of substates.

(A) Frequently observed single-channel conductances plotted as a function of pipette voltage. The solid line is the fit of maximal values representing the fully open state of MscS. The 'break' of the curve at –40 and +60 mV mark the points where substates become prominent. **(B and C)** Traces illustrating the changes in MscS gating upon switching pipette voltage from +40 to –40 mV (B) and from +60 to –60 mV (C). The magnified episodes illustrate full transitions at positive pipette voltages and switching to subconducting states and inactivation at negative.

Availability of MscS depends on the rate of pressure application and the amplitude of pre-pulse pressure

In order to investigate the dynamics of MscS responses to stimuli applied with different rates, patches were subjected to various ramps of pressure ranging from 2.7 to 240 mmHg/sec. Raw traces of current aligned with the pressure ramps in Fig. 2-4A show that the resultant channel activity at the end of the ramp was dramatically lower when pressure was applied slowly, especially at negative pipette voltages. Conversion of traces into $P_o(p)$ dependencies (Fig. 2-4B) revealed $p_{1/2}$ of MscS activation to be almost independent of rate. Similarly, a plot of the intrinsic gating parameters ΔE and ΔA revealed no dependence on the rate of pressure application (data not shown). An analysis of P_o, normalized to the fastest ramp, showed a monotonic dependence on the rate of pressure application, with a lower maximal current for a slower ramp (Fig. 2-4B, inset). At the slowest ramp speeds noticeable oscillations appeared in the activation curves suggesting that two competing processes, activation and inactivation, were superimposed. The net result is a reduction in the observed maximal conductance.

To obtain further insight as to why MscS responds in full to abrupt stimuli but tends to 'dump' those applied more slowly, a two-step protocol was adopted. Patches were first exposed to a 20 s pre-pulse of intermediate pressure (non-saturating) and then immediately to a short saturating pulse to sample channel availability (Fig. 2-5A). The range of pre-pulse amplitudes was centered on the activation pressure midpoint ($p_{1/2}$).

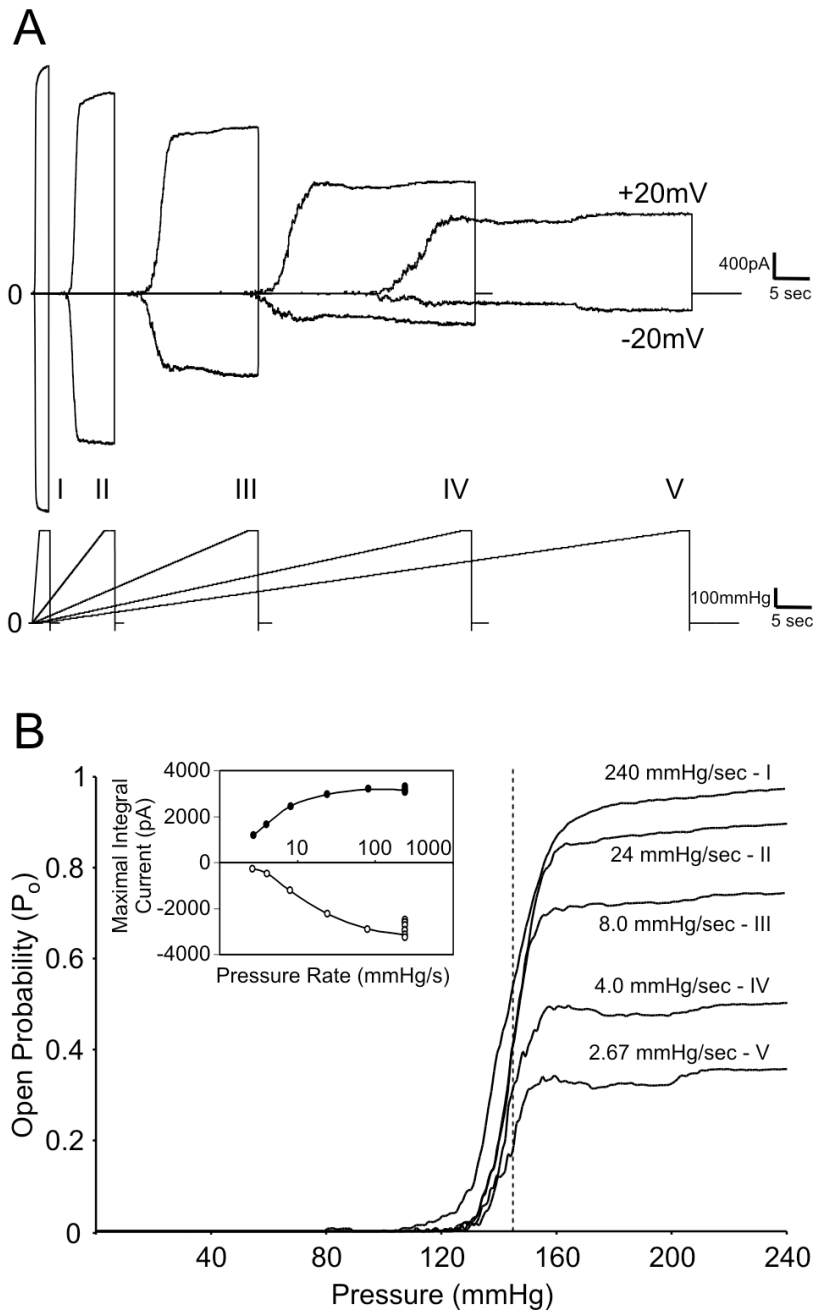

Figure 2-4. MscS responses to pressure ramps applied at different rates.

(A) Raw current traces (top) recorded at pipette voltages of +20 and –20 mV under pressure ramps varying from 2.7 to 240 mmHg/s (bottom). **(B)** Activation curves for different ramps ($P_o = I/I_{max}$, where I_{max} is scored at fastest ramp) presented in one scale as a function of pressure. Inset: maximum current as a function of rate at positive and negative voltages.

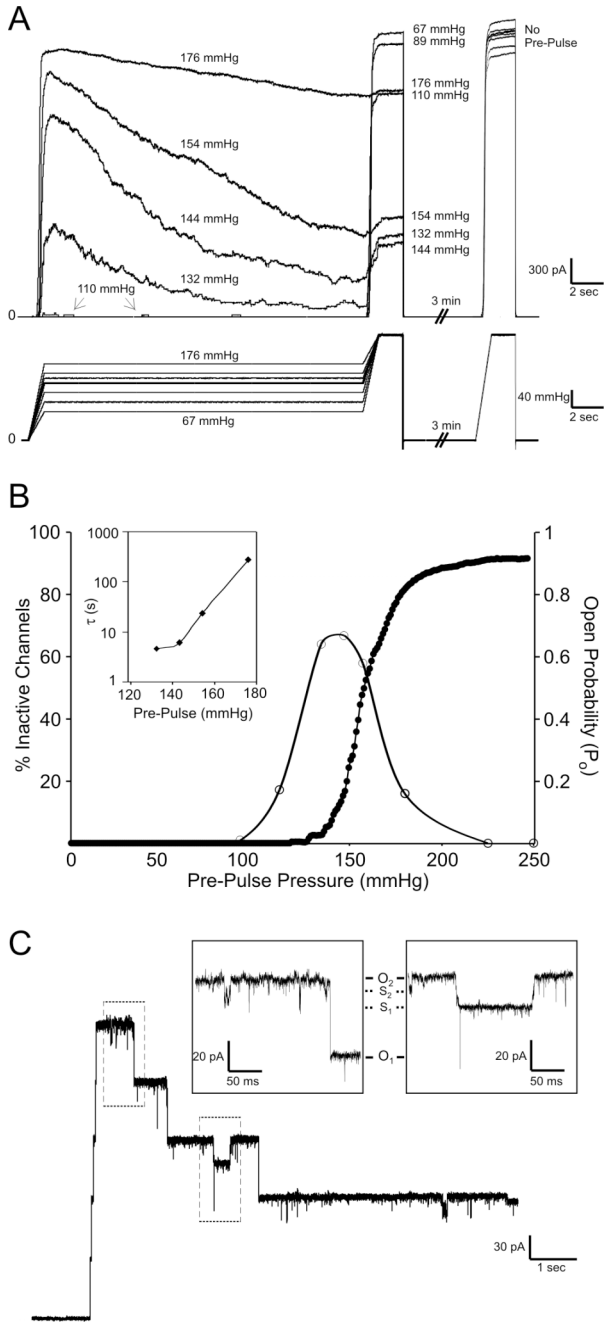

Figure 2-5. Dynamics of MscS responses at intermediate pressures. **(A)** Raw traces obtained with 20 s pressure pre-pulses of different amplitude followed by shorter (2 s) test pulses of saturating pressure. The current kinetics during the pre-pulse reflects the rate of channel inactivation, whereas the response to the test pulse checks for the MscS availability after the pre-pulse. **(B)** The fraction of MscS inactivated during the pre-pulse as a function of pressure (open circles); the activation ($P_o(p)$) curve is presented to show the position of the pressure midpoint for the same patch. Inset: the characteristic time of inactivation as a function of pressure. **(C)** A trace obtained at a pressure near the midpoint from a patch having only five channels. The magnified episodes show the presence of substates at low positive pipette voltages.

The results showed that the majority of channels enter the inactive state at 'pre-pulse' pressures below $p_{1/2}$ (Fig. 2-5B). In addition, raising the 'pre-pulse' pressure significantly decreased the rate of channel inactivation (τ) derived from an exponential fit of the inactivation component (Fig. 2-5B, inset). Saturating pressures or those substantially above $p_{1/2}$ tended to prevent channel inactivation suggesting that the fully open conformation of MscS is stabilized by high membrane tensions. The decrease of inactivation rate signifies an increase of the energy difference between the open state and transition state separating the open from inactivated state. Assuming that the activation midpoint (Fig. 2-5B) is 5.5 dyne/cm, the estimated area change suggests that the footprint of the channel complex decreases by 10.6 nm^2 as it approaches the transition barrier from the open state.

Single-channel inactivation events were resolved in smaller channel populations by preparing spheroplasts with no IPTG induction. Promoter 'leakage' alone results in four to six MscS channels being observed in each patch. Higher resolution (10 kHz) recordings of inactivation at intermediate 'pre-pulse' pressures in these patches showed that MscS visits substates even at positive pipette voltages (Fig. 2-5C). However, a comparison reveals that the total occupancy of substates at positive voltages is substantially lower than its counterpart at negative voltages. At low voltages (both positive and negative) inactivation events appeared as straight transitions from the fully conductive to a non-conductive state without visible intermediates. The resolution of these recording may still be insufficient to reject the possibility of short-lived intermediate states during low-voltage inactivation.

Inactivation is favored by depolarization

Experiments similar to those above, with a 'pre-pulse' pressure slightly higher than $p_{1/2}$, were conducted at different pipette voltages. A comparison of these traces showed a clear increase in the rate of inactivation at negative potentials (Fig. 2-6A). As previously described, the inactivation phase of each trace was fitted with an exponent and characteristic times were determined. A plot of τ versus voltage (Fig. 2-6B) exhibited a shallow increase between –40 and +60 mV, indicating that moderate positive pipette voltages oppose inactivation. A steep decrease of τ below –40 mV revealed the onset of strong MscS inactivation observed under depolarizing conditions. The 'break' point in this dependence corresponds to the voltage (–40 mV) where substates become dominant (compare Fig. 2-6B and 2-3A). This coincidence suggests that the left-most part of the τ(V) dependence likely reflects the rate of transitions between the substates (S) and the inactivated state (I) but not a direct inactivation from the open (O) state. The slope thus reflects the decrease of the activation barrier for the S→I transition on voltage. Estimation shows that this process corresponds to an outward transfer of about 2 positive charges per heptamer across the entire electric field. If one elementary charge per subunit (7 charges total) were moving outward, the effective displacement of charges within the membrane from the S state to the transition state between the S and I states (top of the barrier) would be about 5 Å. This displacement would be less if more charges were engaged.

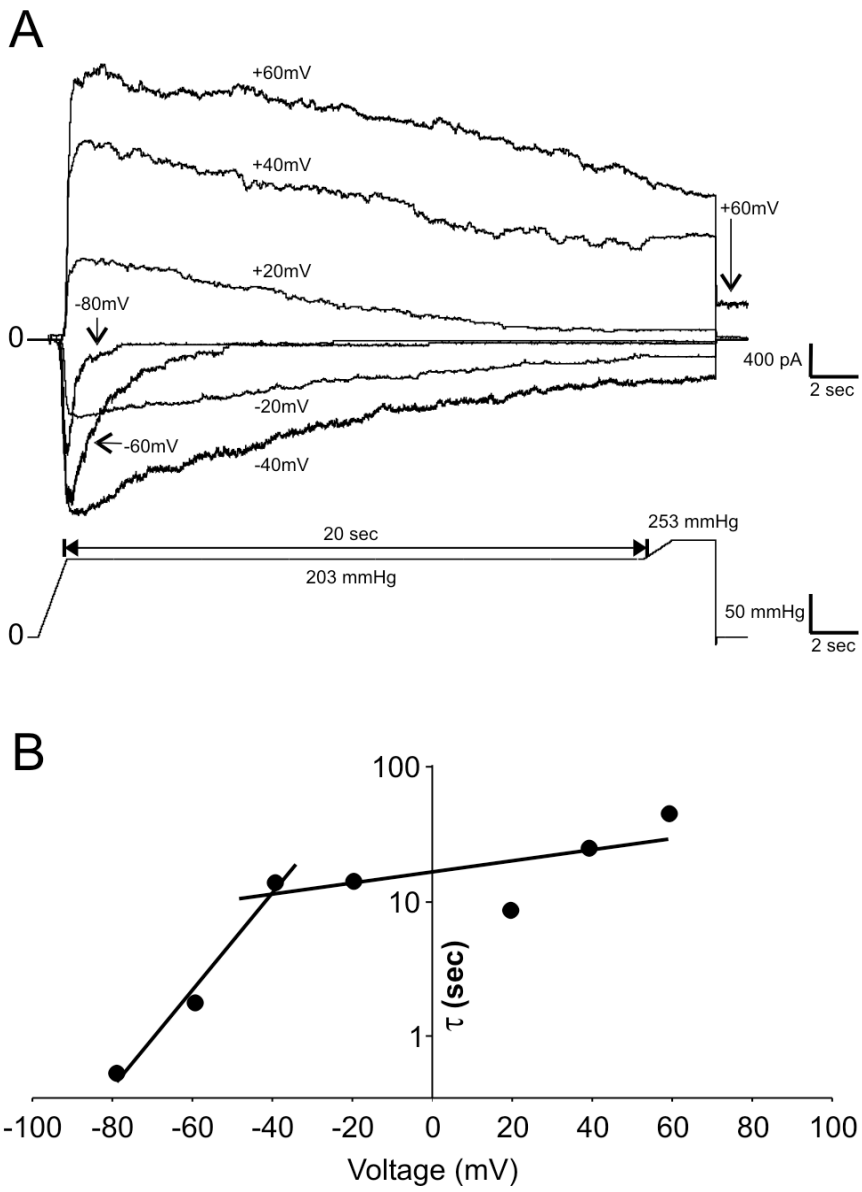

Figure 2-6. MscS inactivation is revealed to be faster at depolarizing voltages.
(A) Traces recorded with the pre-pulse pressure protocol at pipette voltages from -80 to +80 mV. The falling phase was fitted with a single exponent. **(B)** The characteristic time of inactivation as a function of pipette voltage. The high slope of the left part of the dependence corresponds to the barrier reduction equivalent to the energy of two positive charges (q = +2) per complex transferred outwardly across the entire transmembrane field.

Discussion

We presented here electrophysiology recordings and analysis that illustrate the behavior of MscS in its native setting. In some instances the protein was overexpessed 2-4 times compared to its density in wild-type *E. coli* strains via an induction the P_{lacUV5} promoter. Where single channel analysis was desired, a low level of MscS expression, close to wild-type density, was achieved through promoter 'leakage', without induction. The MJF465 triple knock-out (*mscL*$^{-}$*, mscS*$^{-}$*, mscK*$^{-}$) *E. coli* host strain excluded any potential interference from other endogenous mechanosensitive channels. The pressure-clamp apparatus provided a critical advantage in terms of precision and reproducibility of stimulation by ramps of pressure, and the custom-written software HISTAN streamlined generation of multiple dose-response curves.

The major traits of MscS observed *in situ* can be re-iterated as follows. The transition from the closed to fully open state (C→O) displays a steep dependence on membrane tension with an apparent mechanotransduction area of about 18 nm^2. The fully open state is stable at high tensions (and at moderate voltages), however at tensions below the activation midpoint ($\gamma_{1/2}$), the channel tends to inactivate within tens of seconds. Thus, under slow application of pressure, the resultant channel activity is much lower than with an abruptly applied stimulus of the same amplitude. The inactivated state of MscS is non-conductive and long-lived. The complete return from the inactivated (refractory) to the closed state (I→C) takes at least 3 min. The main closed-to-open transition (C→O) is essentially voltage-independent. However,

at negative pipette (depolarizing) voltages lower than –40 mV and strong positive pipette (hyperpolarizing) voltages greater than +80 mV MscS tends to occupy subconducting states (Fig. 2-3A). Depolarizations beyond –40 mV strongly promote transitions to the subconducting states (O→S) followed by inactivation (S→I). While channel activation (C→O) was always observed as an instant conductance increase (at a given recording bandwidth), signifying a fast and concerted conformational change (Shapovalov and Lester, 2004), inactivation broken up into sub-transitions appears to be a less cooperative event. The rate of inactivation exponentially increases with depolarizing voltage and decreases with tension. The gating characteristics of MscS are similar in KCl and NaCl buffers.

The presented phenomenology of MscS gating is different from what was depicted in early studies. The very first report by Martinac and coworkers (Martinac et al., 1987) described a 1 nS channel activated at pipette pressures of 40-60 mmHg, considerably lower than those we used to activate MscS (140-300 mmHg). The open probability for these channels markedly increased at depolarizing voltages, which we do not observe for MscS. The channel was active in KCl, but practically inactive in NaCl, a property later ascribed to MscK (Li et al., 2002). We acknowledge that at the time of the study it was difficult to separate the activities of these two different species, MscS and MscK. The characteristic propensity of MscS to time-dependent inactivation, however, suggests that the quasi-equilibrium traces recorded for minutes presented by Martinac and coworkers belonged mostly to MscK. The inactivation of the small (1 nS) channels taking place specifically at intermediate pressures was well documented by the Kubalski group (Koprowski and Kubalski, 1998), however these

experiments covered only a narrow range of potentials (+30 to –30 mV), which precluded observation of the steep voltage dependence at stronger depolarizations described above.

The presented phenomenology of MscS also helps us to interpret the crystal structure (Bass et al., 2002). The crystal structure of MscS revealed a de-lipidated protein complex with TM1 and TM2 helices splayed at an unusual 30^{o} angle relative to the membrane normal. The protein surface displayed conspicuous gaps between the TM1-TM2 pairs and the pore-forming TM3 helices, which should be either hydrated or filled with lipid (if such a conformation occurs in the native membrane). It is possible that the native resting conformation of MscS packs the TM1-TM2 pairs more tightly against the central pore forming a more compact barrel. Indeed, in the absence of direct interactions between TM1-TM2 and TM3 it is unclear how tension developing in the lipid bilayer could be transmitted from the lipid-facing protein surface to the pore. Our preliminary steered molecular dynamic (SMD) simulations indicated that the swinging motion of the TM1-TM2 bundle about the extracellular hinge (G90 and adjacent residues) is essentially unrestrained and the contacts between TM2 and TM3 can be restored by a gentle pressure constricting the barrel from outside (Anishkin et al., unpublished). Now (Anishkin et al., 2007).

Despite initial conclusion that the crystal structure represents the open state (Bass et al., 2002), our computational analysis suggested that the pore in the crystal structure is largely dehydrated and must be non-conductive (Anishkin and Sukharev, 2004). The estimations showed that the pore constriction with water-accessible lumen of about 7 Å in diameter must be expanded by at least 8 Å to conduct at 1 nS as

measured in experiments. The dehydrated pore and the uncoupled state of the peripheral helices from the pore-forming helices suggest that the channel, in this particular conformation, would not only be non-conductive but also irresponsive to tension applied to its periphery, the functional definition of inactivated state. We believe that the overall structure, represented in the crystal, is a conformation which likely resembles the inactivated state of MscS. Based on these considerations and the phenomenology above we propose the following kinetic scheme and mechanism of MscS gating.

The scheme presented in Fig. 2-7A shows positions of the main states in the area-charge plane. The solid arrows represent transitions observed frequently at either positive or negative pipette voltages. Dashed lines depict possible transitions, which have not been fully characterized. One of these is the direct transition from the fully open (O) to the inactivated (I) state frequently observed in traces at moderate positive voltages. Although we see it as a straight transition (O→I), the path may be a composite (O→S→I) as the frequency response of our recording was not very high. We also cannot exclude the possibility of a slow 'silent' inactivation of MscS directly from the closed state, which may occur at sub-threshold tensions. The rightward transition from the closed (C) to open (O) state is accompanied by a substantial area change but almost no charge transfer as the gating charge associated with the C→O transition was estimated to be only +0.8 per complex or +0.1 per subunit. We presume that in the resting state the barrel has a compact conformation with all transmembrane helices tightly packed around the pore.

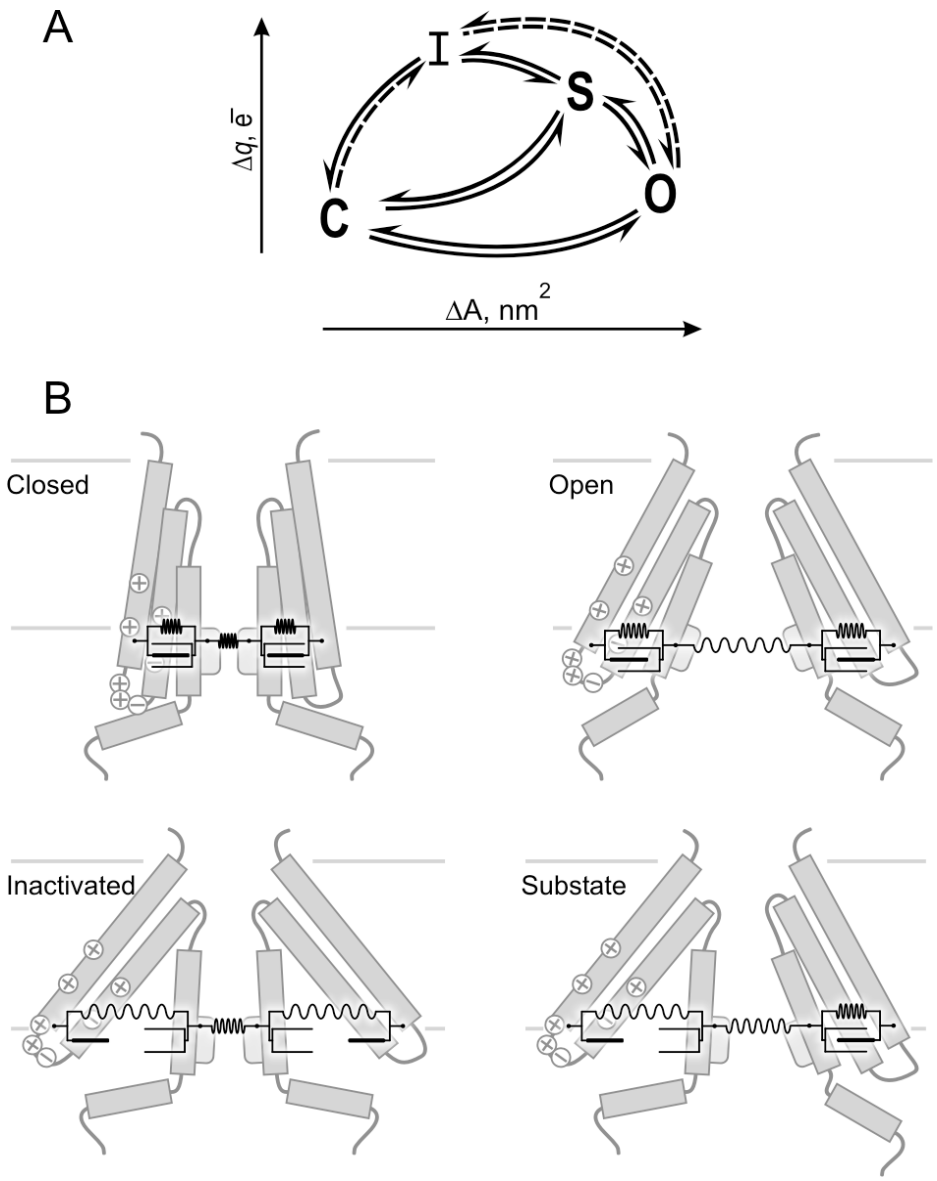

Figure 2-7. Schematic illustration of a hypothetical gating mechanism for MscS.
(A) Kinetic scheme of MscS transitions presented on an area-charge plane. Frequently observed and possible transitions are shown with continuous and dashed lines, respectively. The distances between the main states (closed, C; open, O; substate, S; and inactivated, I) reflect the changes of in-plane area (ΔA) and transmembrane movement of charges (Δq) associated with each transition. **(B)** Cartoon representation of helical positions associated with each state. An effective 'dashpot' between the peripheral TM1-TM2 bundle and the pore forming TM3 allows pore helices disengage and collapse into a closed conformation causing inactivation. A small upward swing of the peripheral helices generates gating charge associated with inactivation.

The opening is achieved through a concerted outward movement of helices, which results in wetting and expansion of the pore constriction. The absence of voltage dependence at this stage signifies that the charges on the outer 'voltage-sensing' helices (R46, R54, R59, K60, R74, as well as D62 and D67) do not experience any net transmembrane movement. TM1 and TM2 likely remain associated with the TM3 helices in the barrel, moving laterally. A cartoon representation of the transition from the closed to the open state is illustrated in Fig. 2-7B.

The data presented in Figs. 2-2, 3 and 6 shows that depolarizing voltages favor transitions to subconducting states followed by the inactivated state. The fact that the channel enters the inactivated state (I) typically through a substate (S) led us to infer that substates are structural intermediates between the open and inactivated states. Therefore we placed these states on the area-charge plane in sequence with increasing q. We presume that under depolarizing conditions the outwardly directed electric field acts on the charged residues residing in TM1 and TM2, pushing the helices toward the extracellular side and thus favoring their detachment from the core TM3 helices. This uncoupling associated with an upward swinging motion generates gating charge and stipulates voltage dependence. At the same time the TM3 helices collapse back to a narrow-pore conformation, which eventually causes dehydration of the constriction and return to a non-conductive state. The substates may represent intermediate states in this pathway with only a few subunits having detached TM1-TM2 pairs and a partially collapsed pore. The fully inactivated state is achieved when the process of helices decoupling comes to a completion and results in formation of the characteristic crevices on the cytoplasmic side of the channel seen in the crystal

structure. Whether these crevices are filled with water or lipid is unclear, but the slow return from the inactivated to the closed state may be limited by slow lipid diffusion out of the confined crevice. The conformations of an 'asymmetric' substate and the inactivated state are schematically illustrated in Fig. 2-7B.

The kinetic data presented in Fig. 2-6 are insufficient to conclude the entire gating charge associated with inactivation because we only measure the increase in rate of the O→I transition on voltage, but not the equilibrium state distribution. However, the data indicates that this increase in the rate of inactivation must be accompanied by a decrease in the transition barrier equivalent to the energy of transferring two positive charges across the entire electric field. If we assume that only one charge per subunit is engaged in inactivation, then all seven charges per complex have to move by about 5 Å across the bilayer. If three charges per subunit are involved (the net charge of each peripheral pair of helices is +3), they then have to travel only about 1.7 Å to reach the transition state leading to inactivation. This estimate seems to be consistent with the expected small scale of the TM1-TM2 helices swing.

Fig. 2-4 illustrates full activation of MscS on a steep application of pressure but strongly attenuated responses to slow ramps. The fact that the midpoint of activation does not change with the speed of ramp suggests that opening is not impeded by channel kinetics within the studied timeframe. The lower total activity observed with slow ramps is apparently due to MscS inactivation at intermediate tensions near the midpoint. It remains unclear why the open state of MscS becomes more stable under high membrane tension. One possible explanation is that the

substates and the inactivated state of MscS have smaller in-plane areas than the fully open state as denoted in the area-charge plane (Fig. 2-7A). Under high tensions the state with the largest in-plane area would be most stable. The decoupling of TM1-TM2 pairs from the core helices and their subsequent spreading creates slits and crevasses critically changing the protein outline in the plane of the membrane. Lipids may penetrate into the slits taking a part of the protein area and thus reducing the effective lipid-excluded area of the protein. In this way, spreading of helical pairs and 'intermixing' with the surrounding lipids may explain the effective decrease of the in-plane area as a result of transitions into the subconducting and inactivated states. With increasing tension, the inactivation rate decreases (Fig. 2-5B, inset) and the slope suggests that the transition state leading to inactivation has 10.6 nm^2 smaller in-plane area than the open state. This implies that the area difference between the end states (O and I) is even larger.

The ability of MscS to reversibly inactivate may be one of the features that allow it to respond differently to various environmental parameter changes. Indeed, the total channel population responds in full when stimulated by a high pressure applied abruptly, but largely inactivates during the slow passage through a narrow region of pressures below the midpoint. The quick reaction to an abrupt stimulus and 'dumping' of a slowly applied force resembles a 'dashpot': a velocity-sensitive viscous element that would connect the gate of the channel to the tension-receiving protein interface (Fig. 2-7B). This 'dashpot' functionality may be ascribed to the postulated contacts between the pore-forming (TM3) and peripheral helices (TM1 and TM2) capable of disengaging and allowing lipid penetration.

This mechanism which makes MscS susceptible to a sudden pressure onset, but allows it to 'ignore' slowly applied stimuli, may be important in environmental situations where re-hydration of cells occurs gradually and release of osmolytes is not desirable. Instead of simply jettisoning the solutes through opening, the channel inactivates giving time to other osmoregulatory systems to release some of the solutes in a more selective manner or exchange them (Wood, 1999). Because the time course of pressure buildup depends on water permeability, there is a possible functional interplay of MscS with aquaporins previously discussed in (Booth and Louis, 1999). It would be interesting to test the osmotic rescuing function of MscS in *aqpZ*$^{-}$ strains. Previously, MscS and MscL have been shown to be redundant in *E. coli* (Levina et al., 1999). However, the evolutionary preservation of the two channel species suggests that they are not interchangeable in certain environmental situations. In fact, after a gradual change of pressure all MscS may be inactivated, and only non-inactivating MscL would be capable of fulfilling the 'safety valve' function. The described kinetics now suggests several enticing possibilities for the study of MscS under different dynamic conditions of osmotic shock.

Acknowledgements

The authors would like to thank Dr. Ian R. Booth (Aberdeen, UK) for the MJF465 strain and Dr. Paul Blount for the MscS clone used in these experiments. This work was supported by NASA and NIH research grants to Dr. Sergei Sukharev.

Chapter 3: 2,2,2-trifluoroethanol changes the transition kinetics and subunit interactions in the small bacterial mechanosensitive channel MscS

Bradley Akitake*[2], Robin E.J. Spelbrink[‡1], Andriy Anishkin*[2], J.Antoinette Killian[‡1], Ben de Kruijff[‡1], and Sergei Sukharev*[2]

[1]Department of Biochemistry of Membranes, Institute of Biomembranes, Utrecht University, Padualaan 8, 3584 CH Utrecht, The Netherlands and [2]Department of Biology, University of Maryland, College Park, MD 20742, USA.

**These authors contributed equally to this work.*

Biophysical Journal 2007 Apr 15;92(8):2771-84

Abstract

2,2,2-trifluoroethanol (TFE), a low-dielectric solvent, has recently been used as a promising tool to probe the strength of intersubunit interactions in membrane proteins. An analysis of inner membrane proteins of *Escherichia coli* has identified several SDS-resistant protein complexes, which separate into subunits upon exposure to TFE. One of these was the homo-heptameric stretch-activated MscS channel, a ubiquitous component of the bacterial turgor-regulation system. Here we show that a substantial fraction of MscS retains its oligomeric state in cold lithium dodecyl sulfate (LDS) gel electrophoresis. Exposure of MscS complexes to 10-15 vol% TFE in native membranes or non-ionic detergent micelles prior to LDS electrophoresis results in a complete dissociation into monomers, suggesting that at these concentrations TFE by itself disrupts or critically compromises intersubunit interactions. Patch-clamp analysis of giant *E. coli* spheroplasts expressing MscS shows that exposure to TFE in lower concentrations (0.5-5%) causes leftward shifts of the dose-response curves

when applied extracellularly, and rightward shifts when added from the cytoplasmic side. In the latter case, TFE increases the rate of tension-dependent inactivation and lengthens the process of recovery to the resting state. MscS responses to pressure ramps of different speeds indicate that in the presence of TFE most channels reside in the resting state and only at tensions near the activation threshold does TFE dramatically speed up inactivation. The effect of TFE is reversible as normal channel activity returns 15-30 min after a TFE washout. We interpret the observed midpoint shifts in terms of asymmetric partitioning of TFE into the membrane and distortion of the bilayer lateral pressure profile. We also relate the increased rate of inactivation and subunit separation with the capacity of TFE to perturb buried interhelical contacts in proteins and discuss these effects in the framework of the proposed gating mechanism of MscS.

Introduction

Since the mid 1960's, halogenated alcohols such as 2,2,2-trifluoroethanol (TFE) have been known to exert strong effects on protein secondary structure. More recently, these solvents have found new applications in the study of membrane proteins. Having a lower dielectric constant than water (Hong et al., 1999), TFE is often chosen as a non-polar medium for spectroscopic determination of peptide conformations (Nelson and Kallenbach, 1986; Sonnichsen et al., 1992; Wienk et al., 1999) and helical propensities (Jasanoff and Fersht, 1994; Luo and Baldwin, 1999). TFE also serves as a non-polar cosolvent in studies of conformational equilibria and protein folding kinetics (Lu et al., 1997; Kumar et al., 2005).

Although TFE is fully miscible with water at any ratio, the molecule forms microscopic clusters in aqueous solutions with the highest propensity for aggregation near 30 vol% (Hong et al., 1999; Chitra and Smith, 2001b). At these concentrations TFE strongly stabilizes the alpha helical and beta sheet structures of many soluble and amphiphilic peptides by reducing solvation of the backbone amide groups thus destabilizing extended coil conformations (Cammers-Goodwin et al., 1996; Kentsis and Sosnick, 1998). TFE has also been proposed to associate with apolar sidechains, providing a non-aqueous matrix for the hydrophobic collapse of polypeptides (Bodkin and Goodfellow, 1996; Rajan and Balaram, 1996; Reiersen and Rees, 2000). TFE was shown to stabilize the secondary and tertiary structures of globular proteins subjected to denaturing agents or elevated temperatures (Banerjee and Kishore, 2005). Finally, TFE has been shown to accelerate protein folding (Lu et al., 1997) and disfavor partially folded intermediates even at low concentrations (Kumar et al., 2005).

In contrast to the stabilizing effects observed in soluble proteins, TFE predominantly destabilizes integral membrane proteins and their complexes. The bacterial potassium channel KcsA has been well studied in this regard. KcsA retains its tetrameric structure in non-ionic detergents and even in SDS (Cortes and Perozo, 1997), however it is completely disrupted into monomers by 20 vol% TFE present in a DDM detergent solution (van den Brink-van der Laan et al., 2004). Further increase of TFE to 35 vol% under such conditions leads to a reversible loss of secondary structure (Barrera et al., 2005). Surrounding phospholipids, especially PE, stabilize the liposome-reconstituted KcsA complex against TFE, despite the fact that TFE

concentrations above 20 vol% severely perturb membranes themselves (van den Brink-van der Laan et al., 2004).

TFE's ability to separate hydrophobic polypeptide chains has been utilized to improve the quality of samples for 2D electrophoresis of membrane protein mixtures (Deshusses et al., 2003; Zuobi-Hasona et al., 2005). More recently, a new proteomic approach to identify partners in stably associated detergent-resistant complexes has been designed. In this procedure a change of protein mobility in gels upon exposure to TFE indicated that the components had altered their oligomeric state (Spelbrink et al., 2005). Such analysis of the *Escherichia coli* inner membrane has identified ~60 oligomeric proteins. One of these proteins is MscS, a ubiquitous component of the bacterial osmoregulation system and a highly convenient model system for mechanistic studies of mechanosensitive channel gating.

MscS, a product of *E. coli mscS* (formerly *yggB*) gene, is a stretch-activated (mechanosensitive) channel which acts as a release valve for small intracellular osmolytes in the event of acute osmotic downshock (Levina et al., 1999). Purification and reconstitution experiments proved that the channel opens in response to membrane tension transmitted directly trough the lipid bilayer (Okada et al., 2002; Sukharev, 2002). Functional patch-clamp analysis of MscS responses to pulses of hydrostatic pressure across the membrane indicate an adaptive multi-state behavior, featuring tension-dependent transitions from the resting to open and then to inactivated states (Koprowski and Kubalski, 1998; Levina et al., 1999; Akitake et al., 2005). The solved 3D structure of MscS (Bass et al., 2002) revealed a heptameric assembly of identical subunits, each comprised of three transmembrane helices

(TM1-TM3). The C-terminal ends of each subunit contribute to a large, hollow, cytoplasmic domain. The third transmembrane helix (TM3) lines the conducting pore and bears a characteristic kink at the cytoplasmic side (Bass et al., 2002). The MscS crystal structure laid the groundwork for several hypotheses about its gating mechanism, with proposed conformational transitions of either smaller (Edwards et al., 2005) or larger scale (Anishkin and Sukharev, 2004; Sotomayor and Schulten, 2004; Akitake et al., 2005). Thermodynamic analysis of dose-response curves, however, strongly suggested that the lateral protein expansion associated with the opening transition is large (~8-18 nm^2) and must involve a substantial rearrangement of interhelical interactions (Sukharev, 2002; Akitake et al., 2005).

In the present work we studied the oligomerization state and functional behavior of MscS in the presence of TFE. We report the conditions at which oligomeric MscS complexes remain stable in the presence of ionic detergents and the range of TFE concentrations at which breakdown into individual subunits occurs. We provide the first evidence that TFE, at concentrations much lower than those required for subunit separation, changes the equilibrium and transition kinetics between the functional states by reversibly driving the channel into the inactivated state. This new data suggests that TFE can be used for controlled perturbations of interhelical interactions in functional studies of membrane proteins.

Materials and methods

Electrophoresis setups were purchased from BioRad Laboratories B.V. (The Netherlands). Lithium dodecyl sulfate (LDS) was purchased from USB Corp. (Ohio,

USA). Octylglucoside was obtained from Labscientific Inc. (New Jersey, USA). Ni^{2+} nitrilotriacetic acid (Ni-NTA) agarose was obtained from Qiagen Benelux N.V. (The Netherlands). Anti-his_6-C-term antibodies were purchased from Invitrogen (The Netherlands). Isopropyl-β-D-thiogalactopyranoside (IPTG) was obtained from Calbiochem (California, USA). 2,2,2-Trifluoroethanol (TFE) was purchased from Merck (Germany). 1,1,1,3,3,3-hexafluoroisopropanol (HFIP) was purchased from Acros Organics (The Netherlands). Coomassie Brilliant Blue G-250 was purchased from ICN Biomedicals Inc (Ohio, USA). LDS-PAGE gradient gels were cast using a Hoefner SG30 gel maker while non-gradient LDS gels were cast on BioRad Protean III casting systems. All other chemicals were of the highest quality commercially available.

Strains and expression constructs

PB111, a plasmid containing MscS with a C-terminal 6His tag, was a gift of Dr. Paul Blount (UT Southwestern, Dallas, TX). MJF465, a triple *E. coli* mutant (*mscL*$^-$*, mscS*$^-$*, mscK*$^-$) (Levina et al., 1999), used in our work as a host strain was kindly provided by Dr. Ian Booth (University of Aberdeen, Scotland). The MscS S95C/I97C double mutant was generated with a single pair of complementary primers using a Quick Change mutagenesis kit (Stratagene, La Jolla, CA) and verified using automated sequencing.

Preparation of membrane vesicles

The PB111 construct containing MscS-his_6, was transformed and expressed in MJF465 cells (Levina et al., 1999). Cells were grown from overnight culture in 800

ml LB medium at 37°C to an OD_{600} of 0.6 and induced with 0.8 mM IPTG for 1 hour. Cells were collected by centrifugation. The cell-pellet was washed with 50 ml of 50 mM potassium phosphate buffer pH 8 containing 5 mM $MgCl_2$ and resuspended in the same buffer. The suspension was passed twice through a French press at 1.1 kbar. Unbroken cells were removed by low-speed centrifugation and membrane vesicles were collected by ultracentrifugation in a Ti60 rotor (45k rpm, 45 min, 4°C), resulting in approximately 0.6 g of cell membranes (wet weight). Membrane pellets were stored at –80^{0}C until either being resuspended in 50 mM phosphate buffer pH 8 or used for the purification of MscS-his_6.

Purification of MscS-his_6

His-tagged MscS was purified essentially as in (Sukharev, 2002). 0.6 g of membrane pellet was dissolved in 8 ml of 50 mM potassium phosphate buffer pH 8, 300 mM NaCl, 20 mM imidazole and 3% (w/v) octylglucoside. This solution was cleared from insoluble particles by ultracentrifugation (45k rpm, 45min, 4°C). The resulting solution was incubated with 0.5 ml Ni-NTA slurry on ice for 1 hour. The slurry was poured into a column and eluted by gravity. The gel bed was washed with 10 volumes of 300 mM NaCl, 50 mM potassium phosphate buffer pH 8, 20 mM imidazol and 1% (w/v) octylglucoside. Elution was performed stepwise with buffers containing 50, 75 and 200 mM imidazol, using 2 gelbed volumes for each step. Aliquots were run on an 11% SDS-PAGE gel and stained with Coomassie G-250. Fractions containing purified MscS were pooled and supplemented with 0.1% (w/v) Triton X-100. The protein solution was stored at 4°C.

TFE-induced dissociation of MscS detected by LDS-PAGE

20 μl samples of either MscS (0.3 mg/ml) or a membrane preparation from MJF465 cells containing roughly 4 mg/ml total protein were added to solutions of TFE in water for a total volume of 30 μl. The samples were incubated at ambient temperature for 1 hour. Samples were cooled on ice before addition of 7.5 μl ice-cold LDS-PAGE gel loading buffer. Samples were run on either 9.5% continuous or 8-18% gradient LDS-PAGE gels. In several experiments TFE-exposed membrane vesicles were spun down and the TFE-containing buffer was carefully removed prior to dissolution in LDS.

To facilitate detection of oligomeric MscS, electrophoresis was performed at low temperature. Precipitation of dodecyl sulfate was prevented by replacing sodium dodecyl sulfate with lithium dodecyl sulfate in the gels and buffers. Otherwise, the gels and buffers were identical to those commonly used in SDS-PAGE. Electrophoresis setups, gels and buffers were chilled prior to use and cooled continuously throughout each run. Gels were run at 120V until the blue dye-front reached the edge of the gel. Gels were stained with Coomassie Brilliant Blue G-250 in the case of purified protein or subjected to western-blotting with anti-his_6-COOH antibodies in the case of inner membrane vesicles. Precision Plus All-Blue protein standards were from BioRad Laboratories N.V. (The Netherlands).

Electrophysiology

Patch-clamp recordings of MscS were performed using bacterial strains, equipment, and general techniques as previously described (Akitake et al., 2005). Briefly, PB111, a plasmid construct containing MscS with a C-terminal his_6 tag, was transformed and

expressed in MJF465 strain (Levina et al., 1999). Voltage clamp recordings were taken at + 30 mV (as measured in the pipette) from excised membrane patches of giant *Escherichia coli* spheroplasts. Patches and MscS activity were stimulated by reproducible ramps of pressure applied with a high-speed pressure clamp apparatus HSPC-1 (ALA Scientific, Westbury, NY, USA). Recording was conducted in symmetrical potassium buffer (200 mM KCl, 90 mM $MgCl_2$, 10 mM $CaCl_2$, 5 mM HEPES titrated to pH 7.4 with KOH) also containing sufficient amount of divalent cations to maintain seal stability under mechanical stimulation. 2,2,2-Trifluorirethanol (TFE) solutions were created by adding 99+ % TFE (Sigma) to the recording buffer for final concentrations of 0.5, 1.0, 2.0, 3.0 and 5.0 vol%. TFE solutions were made fresh before each experiment and solutions older than 3 hrs were discarded.

Membrane patches were exposed to TFE from the cytoplasmic (bath) or periplasmic (pipette) face. Exposure to TFE from the bath occurred after establishment of a gigaohm seal and patch excision. Recording buffer in the bath chamber (~3 ml) was replaced with 4 chamber volumes of TFE solution through perfusion. The total time of perfusion was 3 minutes after which the system was allowed to rest for an additional 3 minutes before stimulation. After cytoplasmic exposure, TFE could be 'washed out' using the same perfusion technique with recording buffer replacing the TFE solution. Exposure to TFE from the pipette was accomplished by filing the electrode with TFE solution (1-5 vol %) behind a 5 mm plug of pipette solution with 300mM sucrose to delay the onset of exposure. This diffusion-limited delay (2-10 min) provided time to take control measurements.

Data collection and analysis

Axon pClamp 9.2 software (Axon Instruments, Foster City, CA) was employed to record integral current with a bandwidth of 5-10 kHz at a sampling rate of 30kHz. The pClamp software was also used to control the pressure application via output commands to the pressure clamp in episodic stimulation mode. Two-channel recordings of current and pressure versus time were then analyzed with Axon Clampfit 9.2. The maximal current (G_{max}) achieved by the MscS population was calculated from traces as the average conductance after the pressure ramp reached its plateau. The midpoint pressure of activation ($p_{1/2}$) was identified as the pressure at which the MscS population reached 1/2 G_{max}. Fitting of the inactivation and recovery kinetics was also performed in Clampfit using built in fit protocols. A standard exponential function with 1 or 2 terms was employed with a Levenberg-Marquardt search method.

Hydrophobicity analysis of MscS surfaces

The crystal structure of MscS (1MXM.pdb) (Bass et al., 2002) was used for mapping the hydrophobic and hydrophilic areas on the solvent-accessible surfaces of the entire protein. Estimations of the atomic solvent-exposed areas were performed using the web-based GETAREA program (Robert Fraczkiewicz, 1998) with a probe radius of 1.4 Å. The hydration energy was computed as the product of the exposed area for each individual atom and the corresponding atomic solvation energy parameter of Eisenberg (Eisenberg et al., 1984). Hydration energies per amino acid residue were introduced into the PDB structure file using the PDBAN program custom written in MatLab. The solvation energy density was mapped on the MscS solvent-accessible

surface and visualized with color-code using VMD (Eisenberg et al., 1984; Humphrey et al., 1996).

Results

TFE induced dissociation of MscS oligomers

To assess the stability of MscS oligomers, the protein, either as a membrane preparation containing MscS-his_6 or in purified, detergent-solubilized form was incubated with varying concentrations of TFE prior to separation by LDS-PAGE. To assign the multimeric state of the gel-separated complexes, we attempted two sets of molecular weight markers. The first set was a commercial Precision Blue set (Bio-Rad) consisting of fully denatured soluble proteins (left side on all gels). As a second set we utilized disulfide-crosslinked subunits of the MscS S95C/I97C double cysteine mutant that formed ladders of products ranging from monomers to heptamers under non-reducing conditions (right side, Fig. 3-1A).

Electrophoresis on *E. coli* membranes overexpressing MscS-his_6 was performed using a gradient-gel to allow for adequate resolution in the high molecular weight region.

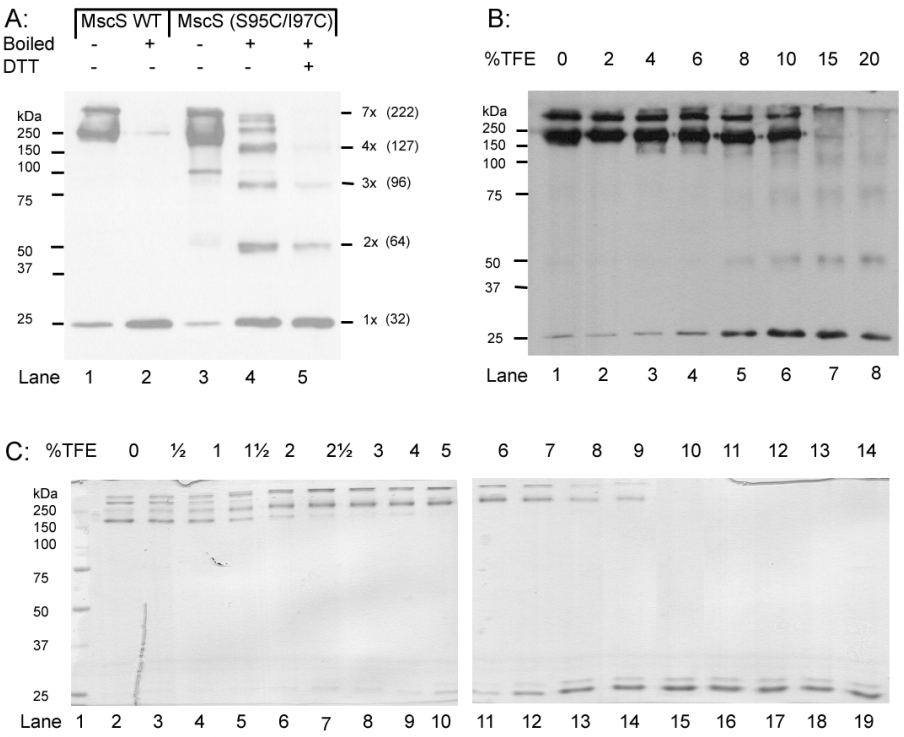

Figure 3-1. *In vitro* effects of TFE exposure on the stability of MscS channel complexes.
(A) Migration of MscS-his$_6$ and MscS-his$_6$ S95C/I97C in *E. coli* membranes as visualized on anti-his6-C-term western-blot of an 8-18% LDS-PAGE gradient gel. Lane 1 contains membrane vesicles of MJF465 overexpressing MscS-his$_6$. The sample was kept on ice after exposure to LDS gel loading buffer. Lane 2 shows the same sample after boiling for 5 minutes upon addition of LDS-PAGE gel loading buffer. Lane 3 was loaded with membranes of MJF465 overexpressing MscS-his$_6$ S95C/I97C. The sample has undergone the same treatment as that in lane 1. Lanes 4 and 5 show MscS-his$_6$ S95C/I97C loaded in membrane vesicles after boiling without and with 14 +mM of DTT respectively. Positions of soluble molecular weight markers indicated on the left are used to provisionally designate the band positions. Marker positions based of disulfide-crosslinked MscS subunits providing better estimations for actual molecular weights are shown on the right with calculated molecular weights in parentheses (kDa). For reasons of legibility the pentamer and hexamer have been omitted. **(B)** TFE-induced dissociation of MscS-6his in *E. coli* membrane vesicles as visualized by anti-his6-C-term western blotting on a continuous 9.5% LDS-PAGE gel. Lanes 1 through 8 were loaded with membrane vesicles of MJF465 overexpressing MscS-his$_6$ that were incubated for 1 hour at room temperature with the indicated percentages of TFE. Densitometry indicated that the total protein intensity in lane 8 is reduced to a third compared to lane 1, presumably due to monomer aggregation. A molecular weight marker is shown on the left. **(C)** TFE-induced dissociation of purified oligomeric MscS-6his in 1% (w:v) octylglucoside and 0.1% w:v TX100 on a continuous 9.5% LDS-PAGE gel. Aliquots of purified MscS-his$_6$ protein solution (0.3 mg/ml) were incubated with the indicated percentages of TFE for 1 hour at room temperature and analyzed by LDS-PAGE.

LDS-PAGE followed by western-blotting with anti-his_6-C-term antibodies revealed three bands (Fig. 3-1A, lane 1). According to the soluble marker scale (left side), the upper band ran at 300 kDa, the second, most intensive band appeared to be close to 250 kDa, and one lightly stained band at 25 kDa. Boiling the sample prior to electrophoresis produced a single band of monomeric MscS at 25 kDa (Fig. 3-1A, lane 2).

Since the mobility of membrane proteins in dodecyl sulfate gels may deviate considerably from that of soluble proteins, electrophoresis standards made of soluble proteins may not provide accurate estimations of molecular weight. Therefore we utilized a double-cysteine mutant of MscS, which spontaneously cross-links under ambient atmospheric oxygen, to compare the migration patterns of known covalent homooligomers of MscS and assess the oligomeric state of the observed high-molecular-weight bands in unboiled MscS samples. Fig. 3-1A, lane 3, shows that the covalent oligomers migrate mainly as two bands at the same location as the regular MscS oligomers. When the double-cysteine mutant was boiled prior to loading, a ladder of denatured, covalent oligomers was observed (Fig. 3-1A, lane 4). The exact sequence-based molecular weights for these bands are presented in parenthesis on the right side of the gel. The difference between the two scales shows that in an 8-18% polyacrylamide gel denatured MscS monomers and dimers run slightly faster than soluble proteins of similar sizes, whereas larger cross-links (4x – 7x) migrate slower. As expected, boiling the double-cysteine mutant in the presence of DTT caused most of the higher MW bands to disappear and the monomer band to increase in intensity (Fig. 3-1A lane 5).

We presume that the positions of covalently cross-linked oligomers of MscS itself (Fig. 3-1A, lane 4) give more reliable estimations of MW than the soluble protein standards. Migration of the bands in this sample suggest that the upper band in lanes 1 and 3 represent intact heptamers, whereas the most intensively stained band near the 250 kDa soluble marker arises from tetramers of MscS subunits that partially retain tertiary structure. Therefore to interpret these data we propose assignment of molecular weights according to the disulfide-cross-linked multimers of MscS (Fig. 3-1A, right). Using this interpretation, heptameric MscS is observed to run at a higher molecular weight than its covalently linked, denatured, heptamer. This result may seem surprising because compactly folded (non-denatured) proteins usually migrate in gels faster than their denatured counterparts. However, native MscS contains a bulky cage-like C-terminal domain, a feature that may cause the native form to migrate slower than the denatured protein.

To test whether MscS oligomers can be dissociated by exposure to TFE, membrane vesicles of a strain overexpressing MscS-his_6 were incubated with TFE for 1 hour at ambient temperature, before being subjected to electrophoresis on continuous LDS-PAGE gels. Fig. 3-1B shows that the upper bands disappear from the gel after exposure to TFE while a monomeric band appears. Both oligomeric forms of the protein disappear at concentrations of TFE larger than 10 vol%, although some signal remains at high molecular weight. This residual signal may be the result of MscS aggregation. Aggregation may also explain the relatively low intensity of the monomeric band since such an effect was observed previously for KcsA upon exposure to high concentrations of TFE (van den Brink-van der Laan et al., 2004). In

order to verify that the observed decomposition of MscS complexes to monomers is specifically due to the presence of TFE, but not a result of the combined action of TFE and LDS, in a separate experiment we pelleted the TFE-exposed membranes and carefully removed the TFE-containing buffer prior to adding the LDS sample buffer. This procedure led to a dilution of the residual TFE by at least 10 times. The resultant pattern of bands in the gel was similar to that in Fig. 3-1B showing a breakdown between 10 and 15 vol% TFE (data not shown). This suggests that TFE present around and inside the membrane is by itself capable of disrupting intersubunit interactions in MscS.

To establish whether the effect of TFE on the MscS-his_6 protein is dependent on the membrane context or whether it is an intrinsic property of the protein, preparations of purified protein in octylglucoside were also subjected to TFE-induced dissociation. The addition of minor amounts of Triton X-100 (0.1% w/v) was found to improve the stability of the purified protein in LDS-PAGE. Under these conditions, purified MscS migrates as a group of four bands with the most dense one, presumably tetrameric, migrating as the lower oligomer band seen in the membrane preparation gel (Fig. 3-1C, lane 1). Exposure of MscS to 2-6 vol% TFE causes some bands to disappear, while simultaneously increasing the intensity of the heptameric and likely pentameric bands (Fig. 3-1C, lanes 6-11). Apparently, even low amounts of TFE are sensed by the protein, causing it to migrate more slowly likely due to the effect of 'swelling' of hydrophobic cavities and voids (Kanjilal et al., 2003).

Increasing the TFE concentration to 10 vol% causes complete dissociation of MscS into monomers (Fig. 3-1C, lane 15). In this case no significant loss of protein

was observed. The concentration of TFE resulting in a complete dissociation of MscS in detergent micelles was slightly lower than that required to achieve the same result in native membranes. Nevertheless, these concentrations are similar, which suggests that TFE induced dissociation is an intrinsic property of the protein, which may be slightly stabilized by the lipid bilayer as compared to detergent micelles. The ability to dissociate MscS is not exclusive to TFE as other alcohols such as HFIP produce the same effect on MscS albeit at lower concentrations (data not shown).

TFE effects on MscS activation by pressure ramps

As was shown previously (Akitake et al., 2005), MscS steeply activates in response to 1 sec duration, linear ramps of negative pressure followed by a plateau (Fig. 3-2). After reaching saturating pressure, MscS stays open for the duration of pressure stimulus. In control experiments with a large number of channels per patch (50 or more), maximal current (G_{max}) of the population reproduced itself within 10%. Using a typical size of patch pipettes, the midpoint pressure of activation ($p_{1/2}$) varied in the range between 120 and 170 mm Hg, however, within each patch sequential sweeps grouped tightly around a single midpoint with <2% deviation around the mean (Akitake et al., 2005).

We tested the effects of TFE on MscS function in a range of concentrations between 0.5 and 5 vol%. Lower concentrations had no observable effect, whereas higher concentrations of TFE mechanically destabilized patches thus precluding reliable measurements. Patches exposed to 1 vol% TFE from the pipette (periplasmic side of the membrane) displayed a slight (~5 mm Hg) leftward shift of the dose-response curves without any significant effect on G_{max}.

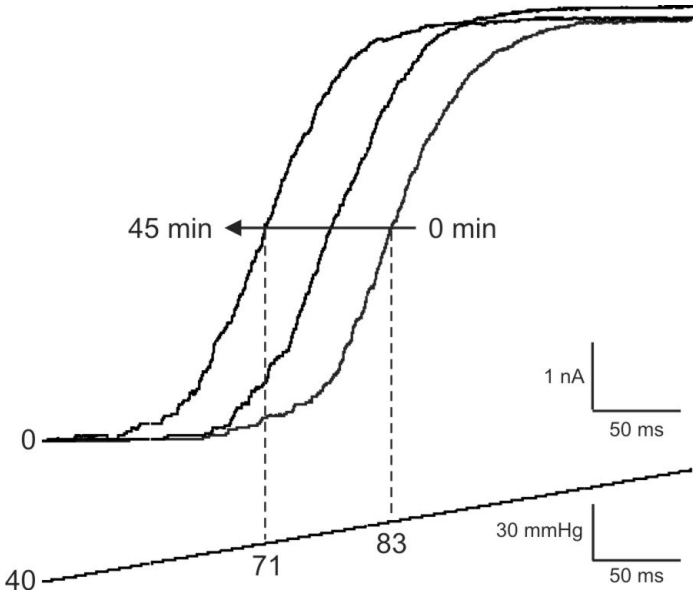

Figure 3-2. Dose-response curves of MscS measured with TFE in the pipette.
The tip of the pipette was first filled ~5 mm with recording solution plus sucrose without TFE. The pipette was then backfilled with recording solution plus 5 vol% TFE. Shown are three traces are taken immediately after patch formation before TFE could diffuse into the tip (right), after 20 (middle) and 45 minutes (left) of incubation. The bottom trace shows the linear ramp of the pressure gradient and the scale of the midpoint shift upon TFE application.

The time for development of the leftward shift at this concentration was long (>1 hr). When the concentration of TFE was increased to 3-5 vol%, larger decreases in $p_{1/2}$ (leftward shifts) of ~20 mm Hg were observed. The ratio of midpoints for 5 vol% TFE in the pipette, as compared to control, was 0.93 ± 0.04 (n=3). These concentration dependent shifts occurred reproducibly in the course of 45 min incubations (Fig. 3-2). During most experiments G_{max}, and the corresponding number of active channels in the population, remained essentially constant falling well within previously established levels of control variability (8-10%).

Perfusion of TFE from the bath (cytoplasmic side of the membrane) even at low concentrations (0.5-2 vol%) invariably shifted p1/2 to the right by ~10-40 mm Hg (Fig. 3-3A-C). The peak ratio of midpoints for 2 vol% TFE in the bath, relative to control, was 1.13 ± 0.08 (n=4). The presence of TFE in the bath appears to make the midpoint less stable from trace to trace when compared to controls. In all bath-perfusion experiments the initial and fastest midpoint movement was always to the right. However, in very long experiments (>2 hrs) $p_{1/2}$ and G_{max} were observed to slowly return to the untreated level. We subsequently found that TFE is very volatile and evaporates from a 35 mm Perti dish filled with 5 vol% TFE at a rate of ~2 μl/min. In the course of 100 min its concentration is thus expected to drop by 80-90%. It was observed that the return of $p_{1/2}$ and G_{max} to control values occurs roughly within this time frame.

TFE presented to the cytoplasmic side reproducibly decreased G_{max} of the MscS population as measured by standard 1 s ramps of pressure.

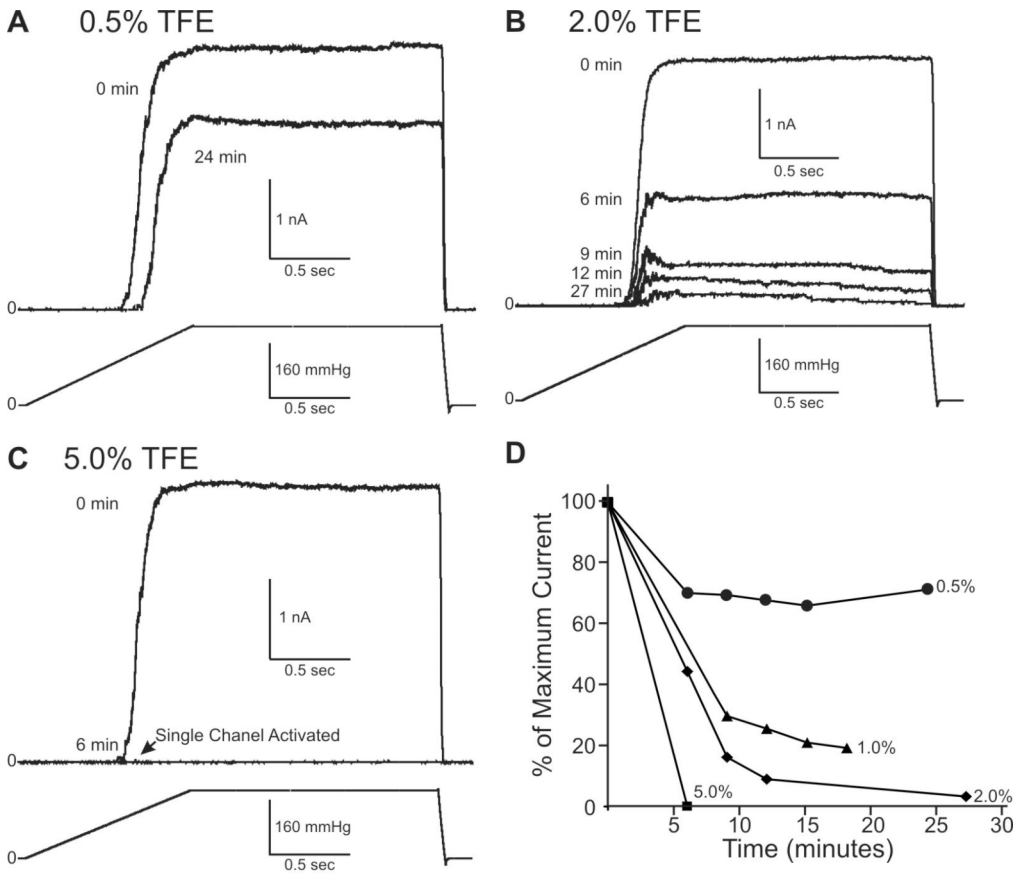

Figure 3-3. Effects of TFE on dose-response curves of MscS when TFE is applied from the cytoplasmic side (bath).

After equilibration, 1 s linear ramps of pressure reaching saturating level followed by a 1.5 s plateau were applied in 3 min intervals. Population responses to 0.5, 2.0 and 5.0 vol% TFE are presented in panel **A**, **B** and **C**, respectively. A right shift of the activation curve (midpoint change from 156 to 180 mm Hg) in the presence of TFE is seen in panel A. Time course of current decline in the traces taken at 6-27 min time points (panel B) indicate MscS inactivation at saturating pressures in the presence of TFE, not observed in controls. The midpoints for these traces are 161 (control), 161 (6 min), 163 (9 min), 166 (12 min) and 179 (27 min) mm Hg. Arrow in panel C points to a single channel transiently activated after exposure to 5 vol% TFE followed by complete inactivation. **(D)** Plot of maximal current achieved by channel population as a percentage of the maximal current before TFE addition. The curves in all panels represent inward currents at +30 mV pipette potential.

A measurable decline (>10%) was observed at 0.5 vol%, with nearly complete silencing of the entire population by a 5 vol% solution (Fig. 3-3C). The concentration of TFE that causes 50% inactivation appears to fall between 0.7 and 1 vol% due to natural variability in patches and spheroplast preparations. This concentration-dependent process of silencing was not instant but developed within the course of 7-20 min (Fig. 3-3D).

In order to verify that the decrease in G_{max} was not due to a drastic change in single-channel conductance we performed measurements of I-V curves in the presence and absence of TFE (Fig 3-4A). The single-channel conductance in the presence of 3 vol% TFE in the bath was essentially the same as in control except for a small deviation at strongly depolarizing voltages (-80 mV pipette) where the open state current becomes noisy due to the increased presence of subconducting states. The pipette electrode potential has been tested independently in the presence of 5 vol% TFE and we observed no systematic deviation larger than ± 1mV.

To further demonstrate that the observed reduction of G_{max} in the presence of TFE was not caused by the right shift of the activation curve, we stimulated the TFE-silenced population with a double-ramp protocol (Fig. 3-4B). Prior to TFE application, the patch was tested with a saturating ramp of pressure followed by a plateau evoking a ~ 4.09 nA current. After exposure to 2% TFE for 15 min, the current stimulated by the same ramp fell to 0.44 nA. Additional pressure applied in the form of a second ramp to a higher plateau did not evoke any extra activity. The inset in Fig. 3-4B shows expanded segments of these traces to illustrate again that the single-channel amplitudes before and after TFE addition are identical.

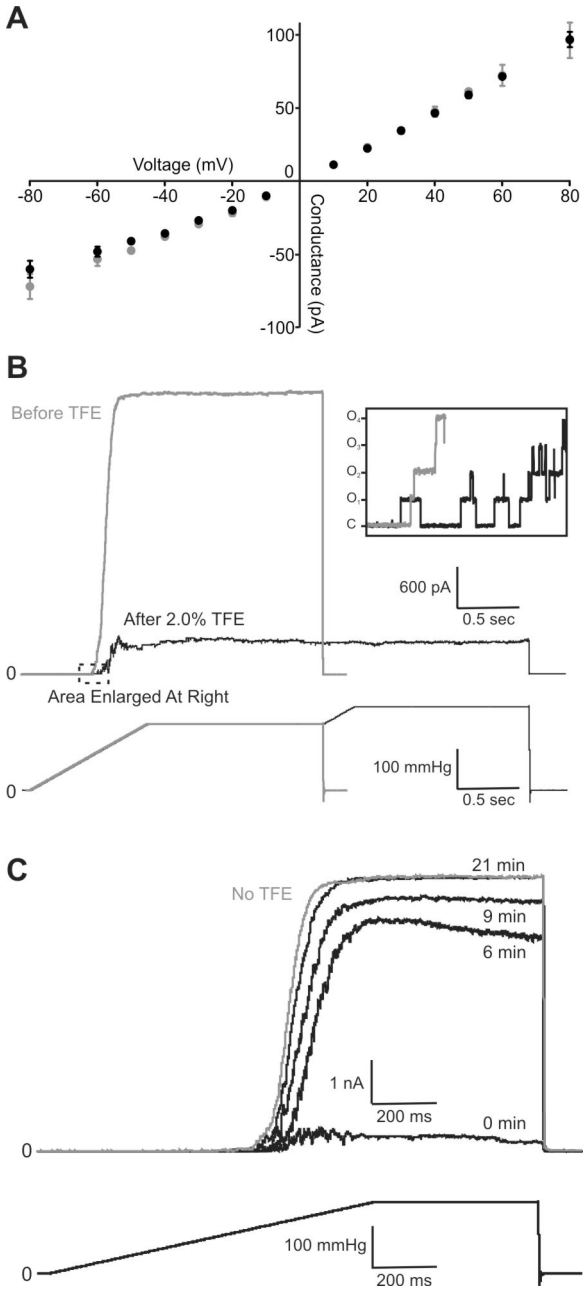

Figure 3-4. Further characterization of G_{max} reduction on exposure to TFE. **(A)** Current-to-voltage relationships for MscS in control (grey circles) and in the presence of 3% TFE (black). **(B)** Effect of additional pressure on a TFE-silenced MscS population. The grey trace represents the 4.09 nA MscS current in response to a 1 s pressure ramp to 160 mm Hg followed by a 1.5 s plateau, recorded before TFE application. The black trace shows the 0.44 nA response of the same patch 15 min after application of 2% TFE in the bath. The pressure protocol was extended by an additional ramp reaching higher pressure (200 mm Hg), which did not produce any additional activity indicating that the active part of channel population is fully saturated by the first stimulus, whereas the rest is in an inactivated state. **(C)** The kinetics of recovery after TFE washout. The gray trace represents the response of a freshly excised patch without TFE, whereas the lower trace (0 min) shows residual current after a 20 min exposure to 3% TFE. A washout resulted in a gradual return of the population current to a pre-TFE level, within approximately 20 min. Shifting of the midpoint to the left occurs concomitantly with the recovery. The midpoints values are 131 (6min), 127 (9min), 122 (21min) and 119 mm Hg in control.

TFE-induced silencing was also found to be reversible. A washout of TFE with recording solution returned 80-100% of the inactivated population back to the active state even after complete silencing with the highest concentration of TFE tested (5 vol%). On washout, $p_{1/2}$ typically shifted back to the left, returning to a pressure close to the control (prior to TFE exposure). A time course for the return of channel activity, after partial silencing with 3 vol% TFE and washout, is shown in Fig. 3-4C. Only after 20 min did G_{max} return to the control level. This reproducible result suggests a slow process of TFE cleansing from some reservoir, possibly the lipid bilayer.

Stimulation by fast ramps and pulses: effects of TFE on inactivation and recovery

To address the nature of the TFE-silenced state of MscS we investigated population responses to pressure ramps applied with different speeds as well as responses to steeply applied stimuli (pulses). Previously published data (Akitake et al., 2005) demonstrated that the MscS population responds fully to fast (< 3 s) ramps of saturating pressure, but with slower ramps (10-90 s), only a fraction of population reaches the conductive state. The part of the population that does not conduct appears to inactivate while the ramp passes slowly through a range of intermediate pressures. Fig. 3-5A depicts MscS responses to short pressure ramps in the presence and absence of TFE. The set of control experiments without TFE (gray) demonstrates that 0.1, 0.5, 1 and 2 s ramps evoke essentially the same maximal current from the MscS population as our fastest (hardware limited) test pressure pulses (10 ms raise time, 250 ms duration). Upon addition of 3 vol% TFE to the same patch (bath perfusion), a 2 s ramp was observed to evoke less than 8% of the original G_{max}.

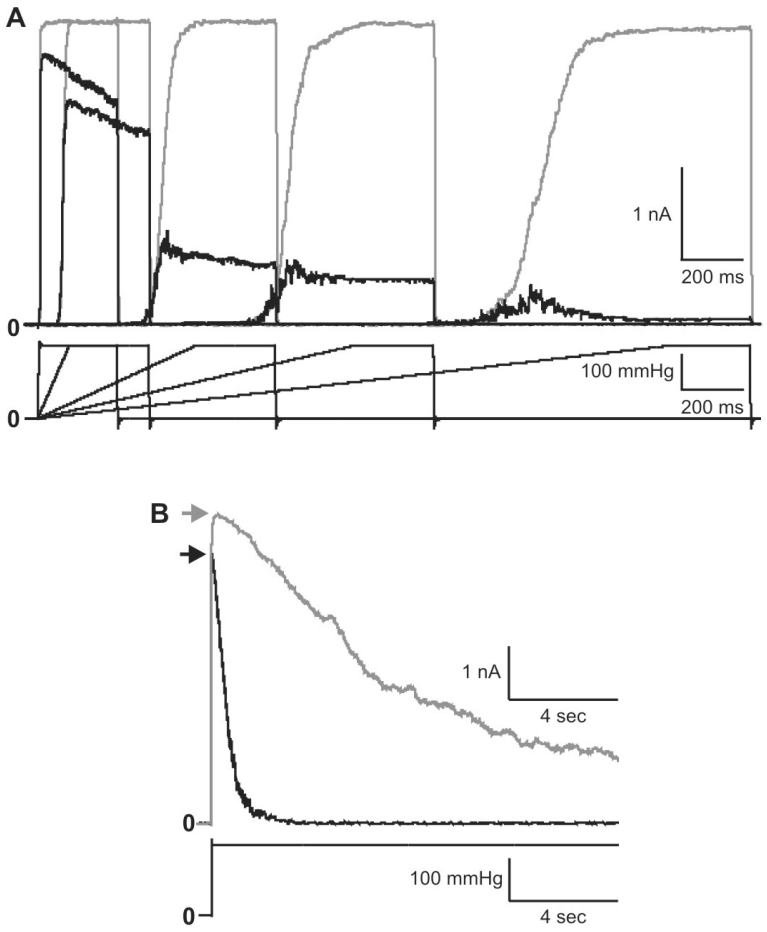

Figure 3-5. MscS responses to ramped and pulsed pressure stimuli with and without TFE present. **(A)** Increasing the speed of linear ramps from zero to a saturating pressure (200 mm Hg) evokes progressively larger current in patches treated with 3 vol% TFE on the cytoplasmic side (black traces). Ramp speed was changed after stabilization of G_{max} under the 1s stimulus, with each subsequent stimulus separated by 3 min. A control set of traces taken prior to TFE perfusion (gray) shows no difference in the maximal current at this range of ramp speeds. **(B)** Responses to a step of sub-saturating pressure (160 mm Hg) recorded on the same patch before (gray) and after TFE perfusion (black). Arrowheads indicate the maximal level of conductance upon application of the pressure stimulus. The current decay time (τ_i) decreased from 2.8 s in control to 0.25 s with TFE illustrating a higher rate of inactivation.

Progressively faster stimuli were found to activate larger fractions of channels population. A declining slope of G_{max} during the pressure plateau at the end of each ramp reveals an increased propensity to inactivation. We know from previous studies (Koprowski and Kubalski, 1998; Levina et al., 1999; Akitake et al., 2005) that MscS displays the tendency to inactivate when subjected to intermediate pressure stimuli (above the threshold and below saturation). In the inactivated state, the channel does not conduct and is no longer responsive to even saturating stimuli. Traces recorded from the same patch with rectangular steps of sub-saturating pressure (Fig. 3-5B) show that indeed, 3 vol% TFE increases the rate of inactivation ~10 times. These data presented in Fig 3-5 reveal that MscS channels do not inactivate spontaneously from their resting state upon exposure to TFE as sharply applied stimuli can elicit activation of the channel population. At sub-saturating pressures, TFE speeds up the process of inactivation which appears to be the reason for the decreased fraction of active channels at slower rates of stimulus application.

Recovery of the MscS population from the inactivated to the resting state was also found to be influenced by TFE. Previous experiments revealed that this process is kinetically complex, with full recovery taking about 3 min under zero applied pressure (Akitake et al., 2005). A typical response of WT MscS to an intermediate stimulus, followed by a series of short saturating stimuli designed to test the kinetics of recovery, is shown in Fig. 3-6A and B. An applied 25 s step of sub-saturating pressure initially opens ~95% of channel population.

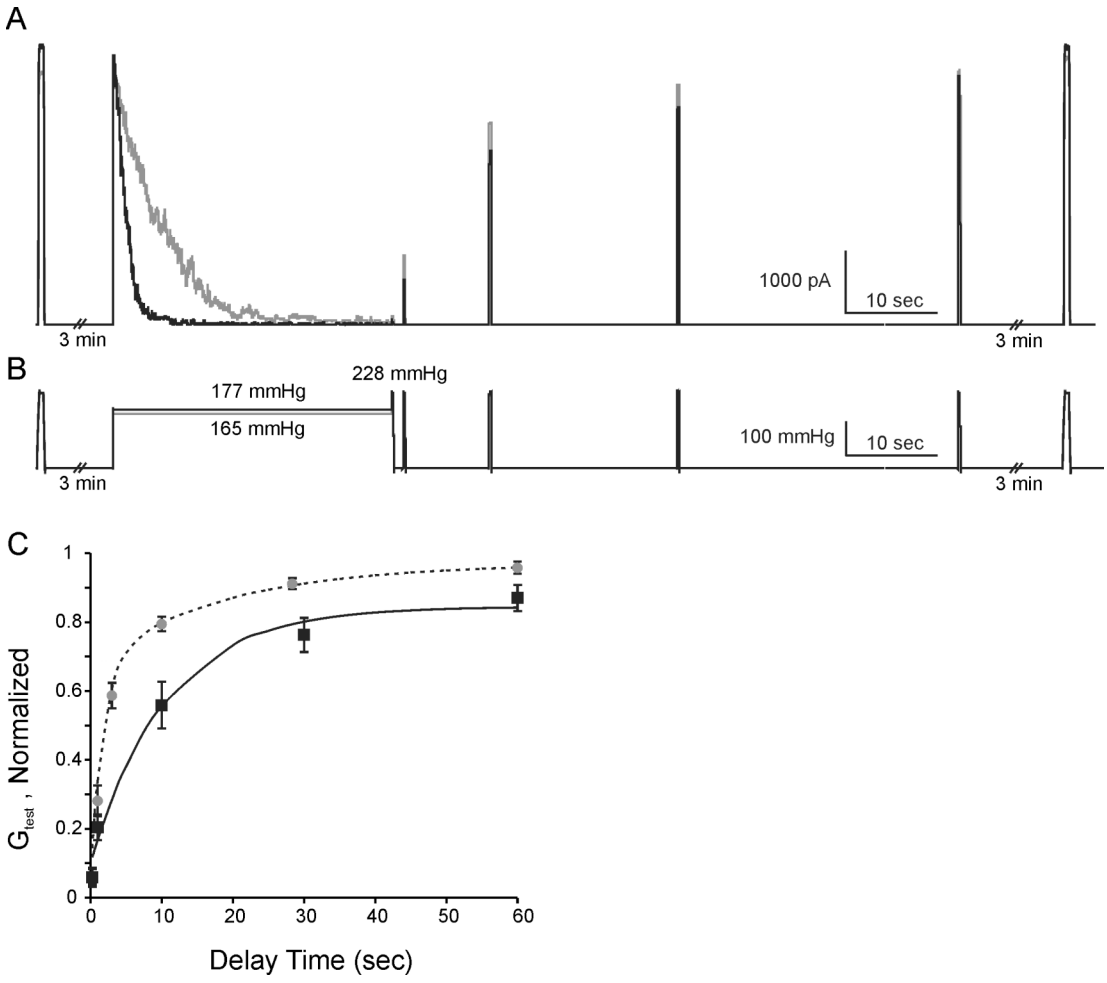

Figure 3-6. Effect of TFE on the rate of MscS inactivation and recovery.

(A and B) Inside-out patches containing ~125 active MscS channels were subjected to a pressure step of 25 s duration, during which the channels transiently open and display inactivation kinetics. The pressure stimulus is followed by a train of 0.25 s test pulses to permit monitoring of the time course of recovery. A single test pulse of saturating pressure (preceding the stimulus by 3 min) indicates the maximal current attainable in the patch (G_{max}). **(A)** Representative current traces recorded before (gray) and after (black) perfusion of 0.5 vol% TFE in the bath. **(C)** The time course of recovery before (gray circles) and after perfusion of 0.5% TFE. The recovery kinetics was fit with one and two exponents, with and without TFE, respectively.

This spike of channel activity decays almost monoexponentially with a characteristic inactivation time (τ_i). The τ_i in MscS is not constant and becomes longer with increasing amplitude of the intermediate pressure stimulus (Akitake et al., 2005). By the end of a 25 s intermediate stimulus, the current approaches the baseline signifying that the entire population is now in a non-conductive state. A short (0.25 s) test pulse of saturating pressure immediately following the 30 s step (Fig. 3-6B) reveals that most of the population is now unresponsive to the stimulus with the exception of a small variable fraction (~0-15%) that still responds to the saturating pressure. A train of test pulses spaced at 1, 10, 30, and 60 s following the intermediate pulse illustrates the kinetics of recovery. Recovery appears to be a multi-exponential process with at least two components ($\tau 1_r$ and $\tau 2_r$). We observed a relatively fast component in the beginning ($\tau 1_r$ = 1.8 s, ~85-90% G_{max}) followed by a much slower recovery to the initial G_{max} ($\tau 2_r$ = 18.9 s). Although the control curve presented here is fit relatively well with two exponents, a third component with a longer characteristic time but smaller contribution may exist.

After perfusion of 0.5 vol% TFE on the cytoplasmic side, G_{max} measured with a 1 s ramp stabilized at 75-90% of its initial level. Experiments were carried out only after stabilization of G_{max}. Even at this low concentration of TFE, inactivation after a stimulus near $p_{1/2}$ was on average 2.6 ± 0.8 times faster (mean ± sd, n=6).

TFE markedly slows down the process of recovery from the inactivated state. Fig. 3-5C shows the normalized conductance of the channel population as a function of time after the intermediate stimulus. The recovery curve from the TFE treated population was fit with a single exponent producing a characteristic τ_r of 10.6 s. The

recovery data for the TFE treated population was fit better with one exponent rather than two. This suggests a delay in the onset of the second, longer recovery component, observed in the control. For comparison, the initial part of the control recovery curve was fit with a single exponent producing characteristic time of τ_r of 2.4 s. The fast stage of recovery of the TFE treated population to 80% G_{max} was therefore 4.2 ± 0.4 times slower than untreated control (n=7) (Fig. 3-6C).

Discussion

The results described above depict two types of events taking place at different concentrations of TFE in the aqueous solution. At lower TFE concentrations (1-5 vol%) we observe a dramatic effect on the kinetics of channel re-distribution between the functional states, whereas at higher concentrations (10-15 vol%) MscS channels dissociate into monomeric form. It appears that the nature of these two effects is qualitatively the same and rests primarily on the capability of TFE to partition into membranes or detergent micelles and to perturb buried interhelical contacts.

Previous work (Spelbrink et al., 2005) identified MscS as part of an oligomeric protein complex that survives solubilization in SDS at room temperature but becomes dissociated by TFE. In this study we showed that MscS forms stable oligomers in cold, ionic-detergent (LDS) gel electrophoresis. Previously, oligomeric MscS could only be visualized by using Blue-Native PAGE (Stenberg et al., 2005).

Exposure of the protein in membrane vesicles to 15 vol% TFE was found to result in dissociation of oligomeric MscS into its monomeric subunits. A similar behavior was observed at 10 vol% for the purified, detergent-stabilized protein. This

effect of TFE on MscS could potentially arise from two mechanisms. First, TFE could act via the lipid-phase by changing the packing properties of the bilayer as was observed for KcsA (van den Brink-van der Laan et al., 2004). Second, TFE may dissociate protein complexes by simply weakening the contacts between the subunits and/or associated lipids. Since we observe dissociation in MscS at approximately the same concentration, both in the context of the *E. coli* inner membrane and in detergent micelles, it seems likely that TFE works mainly by the latter mechanism, although the complexes are slightly more resistant to TFE when surrounded by the native lipid bilayer. Removal of free TFE from the system prior to membrane solubilization in LDS does not change the outcome suggesting that TFE by itself critically compromises intersubunit interactions already in the membrane, and the dissociation of MscS does not appear to be a result of cooperative action between TFE and the detergent.

The existing data indicates a clear difference between TFE's effects on soluble and membrane-embedded proteins. The ability for TFE to stabilize helical conformations in peptides and accelerate protein folding has been explained by aggregation of TFE around the protein backbone, local exclusion of water from the competition for hydrogen bonds, and possibly by lowering the effective dielectric constant of the solvent (Roccatano et al., 2002). This mechanism is consistent with TFE's tendency to form microscopic clusters in aqueous solutions (Hong et al., 1999; Chitra and Smith, 2001b), partition into hydrophobic protein crevices (Kanjilal et al., 2003), and promote desolvation of protein surfaces that normally form buried contacts (Reiersen and Rees, 2000; Roccatano et al., 2002). At the same

concentrations (15-30 vol%) that stabilize soluble proteins, TFE completely disrupts KcsA and MscS as well as many other membrane complexes (van den Brink-van der Laan et al., 2004; Spelbrink et al., 2005).

Soluble proteins are stabilized by the formation of a dehydrated core. They are held together by hydrophobic interactions as well as strong polar interactions in a largely non-aqueous environment. TFE does not interact strongly with hydrophobic sidechains (Banerjee and Kishore, 2005), and thus does not unfold the hydrophobic core of a soluble protein until the concentration in the surrounding aqueous solution exceeds 50%. Membrane proteins, on the other hand, have an 'inverted' design when compared to typical soluble proteins (White and Wimley, 1999; Popot and Engelman, 2000). They have water-filled cavities with hydrocarbon-exposed hydrophobic rims, and are stabilized by interactions with the surrounding lipids. The lipid bilayer could be considered a two-dimensional anisotropic 'solvent' for membrane proteins where the lipids exist in a liquid crystalline state. Lipid tails are relatively large and do not easily intercalate between the helices thus preserving interhelical contacts. In contrast, TFE is small and thus capable of wedging between helices and separating them. Helical separation may be initiated primarily at the membrane boundaries where the TFE concentration is expected to be the highest.

In the transmembrane part of the MscS crystal structure solved by Bass and coworkers (Bass et al., 2002) (Fig. 3-7) only the central helices (TM3) form intersubunit contacts. The peripheral helices TM1 and TM2 do not form a continuous lipid-facing wall, but protrude outward at an angle, forming deep hydrophobic crevices.

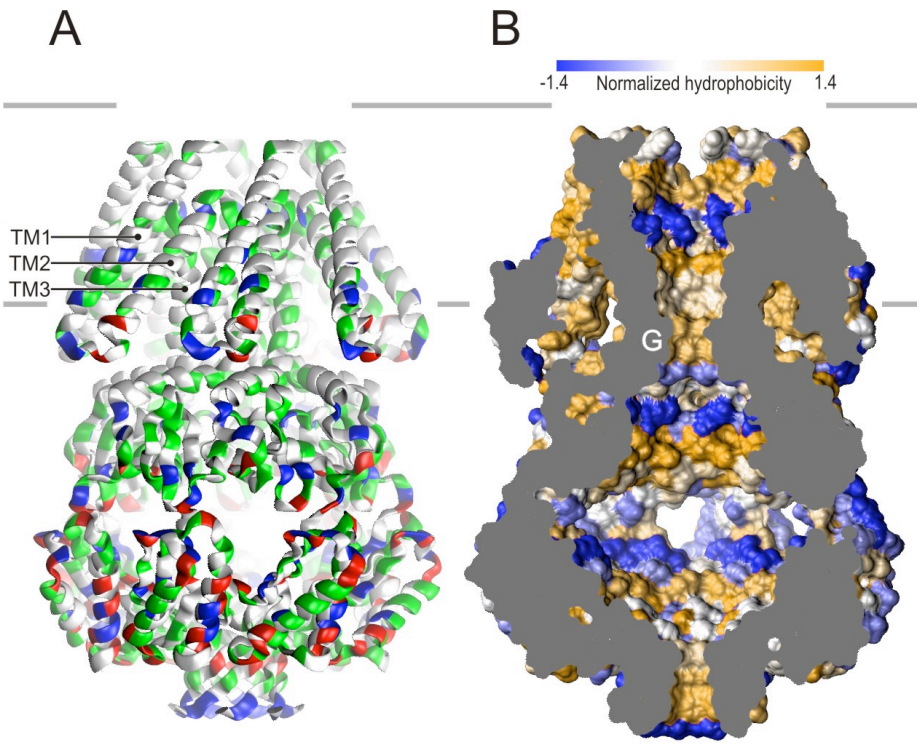

Figure 3-7. Illustration of the MscS crystal structure with calculated hydrophobicity of the protein surfaces superimposed.

(A) (1MXM.pdb) a vertical slice through the channel shown in a space-filled representation **(B)**. The solvent-accessible surfaces were created with the probe of 1.4Å in radius and colored according the normalized consensus hydrophobicity scale (Eisenberg et al., 1984). The most hydrophobic areas (the pore constriction, TM2-TM3 crevices and the distal parts of pore vestibules) are yellow and most hydrophilic regions (rings of charges in the vestibules and the equatorial part of the cytoplasmic cage) are blue. Computation and averaging of solvation parameters was performed using HISTAN. The pore with the hydrophobic gate (denoted as G) is formed by the seven TM3 helices contributed from each subunit. Deep hydrophobic crevices separating the TM3 barrel from the peripheral TM1-TM2 helices might be a result of delipidation. In the crystal structure these crevices are likely filled by the detergent, whereas in our experiments, these spaces can potentially be occupied by TFE. It is thus possible that the peripheral helices in the TFE-induced inactivated state are less tilted than in the crystal structure. The putative positions of membrane boundaries are shown by horizontal lines. The position of the outer boundary implies that 26 N-terminal residues missing from the crystal structure may form a periplasmic extension of the transmembrane domain.

Given that tilting of individual transmembrane helices in the bilayer is energetically unfavorable (Strandberg et al., 2004; Ozdirekcan et al., 2005), the absence of tilt-stabilizing helical contacts between the TM1-TM2 pairs suggests that this unusual angle could be a result of delipidation. Several independent MD simulations showed that when embedded in lipids, without tension, this structure quickly collapses (Sotomayor and Schulten, 2004; Spronk et al., 2006). This suggests that (i) the resting conformation should be more compact, consistent with the hypothesis proposed by Booth and coworkers and supported by cross-linking studies (Miller et al., 2003b; Edwards et al., 2004), and (ii) under certain conditions the peripheral helices can detach from the pore-lining TM3s thus forming crevices. As shown by the color-coded map of the protein surface (Fig. 3-7B), the crevices are largely hydrophobic and could be occupied by an apolar solvent such as TFE. Previous measurements of the adiabatic compressibility demonstrated an increase of protein (lactalbumin) volume in the presence of 10-20 vol% of TFE indicating induction of packing defects and preferential accumulation of the co-solvent in hydrophobic crevices (Kanjilal et al., 2003). For membrane proteins, partitioning of TFE into the lipid would increase the chance of penetration into interhelical gaps and the crystal structure suggests where these gaps may form in MscS.

Based on the above considerations and previous work (Miller et al., 2003b; Akitake et al., 2005), our model of the MscS native resting state is schematically represented as a compact conformation with the TM1-TM2 pairs packed along the TM3s (Fig. 3-8A). In the resting state, the TM1-TM2-TM3 interactions are strong enough to transmit mechanical forces from the lipid bilayer to the gate.

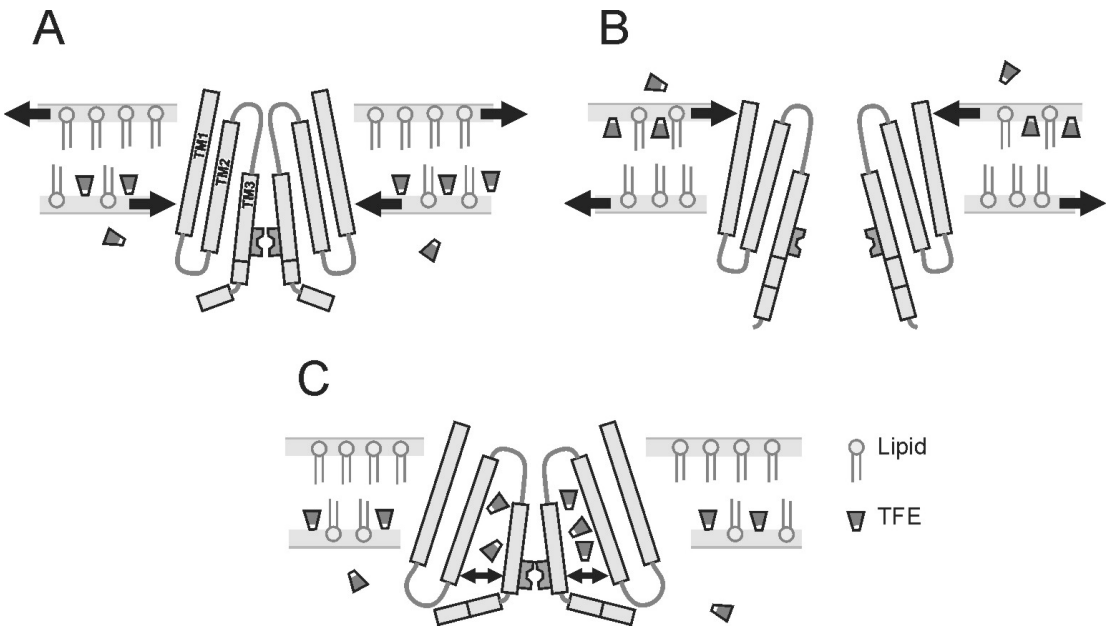

Figure 3-8. Schematic illustration of hypothetical conformations for the transmembrane domains of MscS reveals a possible mechanism for TFE-induced perturbations.

MscS is pictured in the hypothetical **closed (A)**, **open (B)** and **inactivated (C)** states. The gate of MscS is located at the cytoplasmic side and thus the channel is predicted to be more sensitive to increased tension in the inner leaflet. Intercalation of TFE in the inner leaflet (A) would create an extra lateral pressure shifting the equilibrium to the closed state. Addition of TFE to the periplasmic side expands the outer leaflet and produces tension in the inner leaflet, promoting opening (B). When present on the cytoplasmic side in sufficiently high concentration, under membrane tension TFE penetrates the crevices between the TM1-TM2 pair of helices and TM3 facilitating the transition to the inactivated state (C). The black arrows show the locations of TFE-induced tension/pressure components, which superimpose with the externally applied far-field tension used as a stimulus.

Applied tension expands the entire barrel making it conductive (panel B). A subsequent detachment of the pore-lining TM3 helices from the peripheral helices, accompanied by kink formation at glycine 113, leads the channel into a tension-insensitive inactivated state (panel C).

Why are the dose-response curves susceptible to perturbation by low concentrations of TFE, and how does TFE promote inactivation of MscS? It is likely that the membrane acts as an apolar reservoir attracting TFE. Although the exact partitioning coefficient of TFE between membranes and aqueous solutions has not yet been measured, it is known that log P octanol/water is 0.41, indicating ~2.5 times higher preference for the bulk organic phase. Having an OH group with hydrogen-bonding capacity, TFE, like ethanol (Barry and Gawrisch, 1994; Koenig and Gawrisch, 2005), may preferentially accumulate at the polar-apolar interface of the membrane, where its concentration could be higher than that in the bulk. Intercalation of TFE into the interfacial layer may additionally change the dipole and the surface components of the membrane boundary potential thus perturbing lipid-lipid interactions and local interactions with proteins. At concentrations of 10 vol% and above, TFE perturbs phosphatidylcholine liposomes based on permeability tests. Inclusion of phosphatidylethanolamine was found to make the bilayer more resistant to permeabilization by TFE (van den Brink-van der Laan et al., 2004).

The partitioning of TFE is clearly reflected by measurable shifts in the MscS activation dose-response curves. These shifts are dependent on the membrane face (cytoplasmic or periplasmic) to which TFE is applied (Figs 3-2 and 3-3). One possible mechanism for TFE action is illustrated in Fig. 3-8 combined with a

schematic representation of the functional cycle of MscS. When adding TFE to the periplasmic face of the patch (pipette), TFE intercalates into the outer leaflet and increases its area. Because the two leaflets of the membrane are area-coupled by the common midplane, the expansion of the outer leaflet of the membrane must create tension in the inner leaflet (Sheetz and Singer, 1974; Heerklotz, 2001). Since the gate in MscS is located more towards the cytoplasm (Bass et al., 2002), channel activation is likely to be sensitive to tension in the inner leaflet (Fig. 3-8B). Extra tension in the inner leaflet, created by TFE intercalation, should promote early activation of the MscS population. This was indeed the observed result as addition of TFE to the periplasmic face caused a leftward-shift of the dose-response curves (Fig. 3-2). In contrast, when TFE is presented to the cytoplasmic face of the patch (bath perfusion), partitioning of TFE increases lateral pressure in the inner leaflet (Fig. 3-8A) causing a right-shift of the activation curve (Fig. 3-3A and B). Increased pressure caused by TFE intercalation partially negates the applied tension. The fact that the magnitude of the right-shift is not always stable suggests that TFE can, given sufficient time, redistribute between the leaflets thus dissipating the asymmetric area perturbation. This interpretation however needs to be taken with caution, as it has not been demonstrated that excised patches of bacterial membrane lack lipid reservoirs at the edges, which may allow independent area expansion of each of the leaflets, thus uncoupling them. However, because the inner *E. coli* membrane is densely packed with integral proteins (50% by weight) it may be assumed that this greatly impedes slippage of the two leaflets, making this system similar to a closed liposome in terms of its response to amphipath incorporation.

Early data on the modulation of MscS-like channels by chlorpromazine, trinitrophenol and lysophosphatidylcholie (LPC) showed that these substances invariably activate the channels when presented from the cytoplasmic side (Martinac et al., 1990). In this respect, the action of these amphipaths is distinct from the observed inhibitory action of TFE, which lowers the activation threshold only when presented to the periplasmic side. This difference is the focus of further investigation. A strong activating effect of externally applied lysolipids has also been reported for the large mechanosensitive channel MscL. Spontaneous activation was observed in the presence of large concentrations of LPC, an effect which only occurred when LPC is applied asymmetrically (Perozo et al., 2002). In this regard LPC, like TFE, may strongly perturb leaflet area. However, it is not known if TFE causes the same spontaneous positive curvature, a feature characteristic of LPC.

The increased propensity to inactivation in the presence of TFE can be explained by partial separation of TM1-TM2 pairs from the gate-forming TM3 helices and stabilization of this state by intercalating TFE. As illustrated by data in Fig. 3-5, TFE does not drive MscS inactivation at low tension, thus its partitioning into the interhelical crevices (at low concentrations) does not seem to occur spontaneously. Instead, TFE partitioning appears to be critically facilitated by membrane tension that in the framework of our gating hypothesis (Fig. 3-8) normally drives TM2-TM3 separation. TFE occupying voids in the molecule would stabilize the inactivated state preventing fast re-association of the TM1-TM2 pairs with TM3 and thus recovery (Fig. 3-6). Such an effect would also result in a less compact conformation of the MscS channel consistent with a slight up-shift of MscS bands

observed in gel electrophoresis upon addition of TFE (Fig. 3-1C). The sidedness of the inactivating effect of TFE, shown to be active only from the cytoplasmic side (Figs. 3-2 to 3-4), supports the proposed location of the crevices as being accessible only from the cytoplasmic face. TFE added to the pipette does not cause inactivation presumably because after traversing the membrane core it does not substantially accumulate in the cytoplasmic leaflet, as it would quickly partition out into the TFE-free aqueous compartment.

At the present stage we cannot firmly exclude that TFE in some way modifies the cytoplasmic 'cage' domain leading to inactivation. It has been previously shown that the channel propensity to inactivation depends on the state of this cage domain, which can be altered either by truncating mutations (Schumann et al., 2004) or by high-molecular weight cosolvents (Grajkowski et al., 2005). Additionally, it has been demonstrated that concentrations of TFE as low as 3-5 vol% can influence conformational distributions in soluble proteins (Main and Jackson, 1999; Qin and Squier, 2001). Besides the TM2-TM3 crevices, other apolar solvent-accessible areas of MscS, such as the pore vestibules (Fig. 3-7) could potentially act as sites of TFE accumulation. Although possible at higher concentrations, accumulation in the pore does not seem to occur in the tested range of 0.5-5 vol % as TFE was not observed to interfere with the single-channel conductance (Fig. 3-4A and 3-4B inset). The slow onset of TFE action on wash-in (Fig. 3-2 and 3-3) and slow return of channel activity on washout (Fig. 3-4C) are also more consistent with TFE partitioning into and out of a relatively large hydrophobic reservoir, a role more likely to be served by the membrane itself. A detailed comparison of the water-membrane partitioning

coefficients with the concentration dependencies of their membranortopic actions for TFE and similar compounds is a current research focus and may clarify the above issues.

Conclusions and prospects

We have identified two ranges of concentrations for TFE, which cause separable effects on the MscS channel. The lower range (0.5-5 vol%) dramatically affects the kinetics of inactivation under tension with no effect on the oligomeric state of the channel complex. The higher range (10-15 vol%) causes larger perturbations ultimately leading to subunit separation. The data above suggests that TFE can be used not only as a protein-denaturing proteomics tool, but also as a perturbing agent that biases membrane proteins toward specific conformational states or reduces transition barriers. We observed that the effects of TFE are consistent with the existing models of MscS activation and inactivation (Akitake et al., 2005).

Future projects will certainly require a more quantitative analysis of TFE partitioning into cell membranes, liposomes, monolayers and micelles and its effects on lateral pressure. A detailed kinetic analysis of MscS inactivation/recovery in the presence of different concentrations of TFE may suggest the characteristic times, distances and pathways of TFE redistribution between the lipid bilayer and protein. Further understanding of the structural organization of MscS could be obtained by using TFE to probe the strength of intersubunit interactions in mutants with perturbed or stabilized helical contacts, thus the location of crevices filled with TFE in the inactivated state can be further specified. Also, perturbing the tight TM3-TM3 knob-

into-hole packing in the resting state (Bass et al., 2002; Edwards et al., 2005) with mutations may weaken the complex against TFE. If a decrease in stability is not observed in such mutants, we should search for alternative intersubunit contacts, not seen in the delipidated crystal structure.

As more atomic structures of membrane proteins become available and more realistic force fields for molecular simulations are developed, the utilization of non-aqueous co-solvents will become more useful and interpretable. Parameters for MD simulations of proteins in the presence of TFE are already available (Chitra and Smith, 2001a; Roccatano et al., 2002). The merging of computation with experimental research will be a powerful strategy in studies of function-defining conformational transitions in membrane proteins.

Chapter 4: Straightening and sequential buckling of the pore-lining helices define the gating cycle of the stretch-activated channel MscS

Bradley Akitake*, Andriy Anishkin*, Naili Liu and Sergei Sukharev

Department of Biology, University of Maryland College Park, 20742, USA

**These authors contributed equally to this work.*

This chapter relates to the text of submitted manuscript

Abstract

MscS channels are tension-driven osmolyte release valves found in walled cells of bacteria, fungi and plants. Gating of *E. coli* MscS is adaptive involving transitions between at least three functional states, closed, open and inactivated. We describe here a mechanism directly connecting the functional transitions of MscS to the flexibility of the pore-lining helix TM3. Simulated expansion of the crystal structure revealed straightening of a characteristic 'kink' near glycine 113 (G113) in the open state, whereas a return to the closed state produced an alternate kink at G121. Patch-clamp experiments showed that higher helical propensity, introduced by the G113A mutation, prevents MscS inactivation. A similar mutation G121A kinetically impedes both channel closure and inactivation. Increasing the flexibility at each of these sites by duplicating the glycines (Q112G and A120G) produced directly opposite effects. The double G113A/G121A mutation resulted in severely toxic channels that did not inactivate or close with the release of tension. These data suggest that the open state of MscS features straight TM3 helices, whereas closure or entering the newly identified desensitized state is governed by helix buckling at G121. Transitions into

the inactivated state follow desensitization and feature kink formation at G113 with reciprocal straightening at G121 into a conformation that resembles the crystal structure. In our model the TM3 helices act as collapsible 'struts' that define the structure of the conduction pathway. Membrane tension therefore modulates helical buckling at these two weak points in TM3 to orchestrate the functional cycle of MscS.

Introduction

The mechanosensitive channel of small conductance, MscS, plays a key osmoprotective role in most prokaryotes acting as a tension-sensitive release valve that limits the build up of excessive turgor (Levina et al., 1999). MscS is part of a large family of channel proteins with homologues in diverse species from archaea to plants (Pivetti et al., 2003). In higher plants, MscS homologues have recently been shown to regulate the volume and division of chloroplasts (Haswell and Meyerowitz, 2006). The most studied representative of this family, MscS from *Escherichia coli*, opens a large (~1 nS) pore in direct response to tension developed in the lipid bilayer (Sukharev et al., 1993; Sukharev, 2002). Bacteria that lack MscS and its partially redundant counterpart MscL are osmotically fragile (Levina et al., 1999). Opening of this essentially non-selective channel is predicted to reduce osmotic pressure inside the cell by quickly dissipating solute gradients across the cytoplasmic membrane. This 'rescue', however, comes at a metabolic cost as MscS mutants that activate at lower than normal tensions (gain-of-function phenotype) are generally toxic (Okada et al., 2002; Miller et al., 2003b). It was previously demonstrated that the gating of

E.coli MscS is highly adaptive as the channel readily responds to abrupt changes of membrane tension, but displays a tendency to inactivate when the mechanical stimulus is applied slowly or does not reach a saturating amplitude (Akitake et al., 2005). This intriguing feature may restrict channel opening to true "emergency" situations, protecting the bacterium from the unnecessary collapse of energy-coupling gradients. The adaptive behaviors of MscS are achieved through transitions between at least three functional states, closed (resting), open and inactivated (Koprowski and Kubalski, 1998; Levina et al., 1999; Akitake et al., 2005). The characteristics of these states have been the focus of intense experimental research and modeling (Edwards et al., 2004; Edwards et al., 2005) since Rees and coworkers published the crystal structure of MscS in 2002 (Bass et al., 2002).

MscS is a homoheptameric channel with a subunit structure of three N-terminal transmembrane domains (TM1, TM2 and TM3) and a C-terminal, which contributes to a large hollow cytoplasmic domain (cage) (Fig. 4-1A) (Bass et al., 2002). A nearly parallel arrangement of the N-terminal (TM3a) segments of TM3 lines the conduction pathway along which two rings of leucines, 105 and 109, form a hydrophobic constriction recognized as the channel gate. Although originally reported as the open conformation, recent work from several groups supports a non-conducting, largely dehydrated state of the gate in the crystal structure (Anishkin and Sukharev, 2004; Sotomayor and Schulten, 2004; Sotomayor et al., 2006b; Spronk et al., 2006).

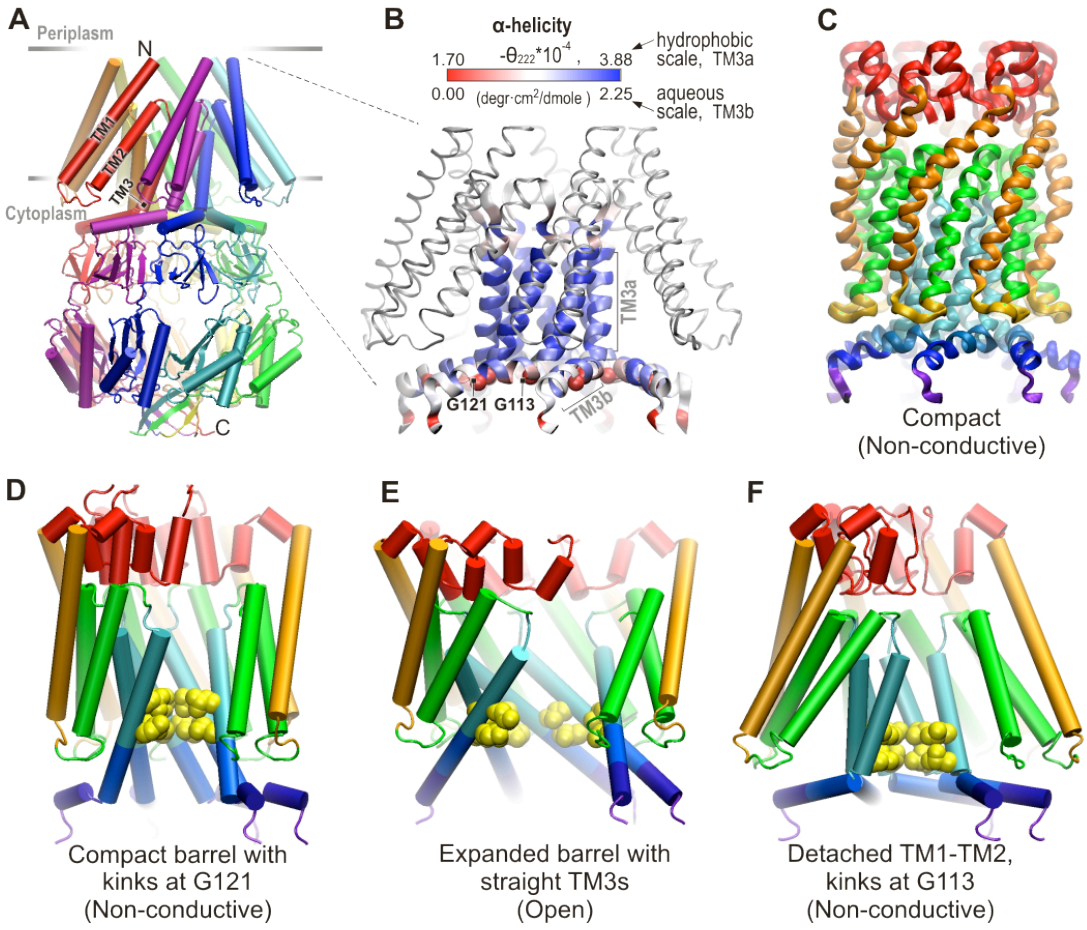

Figure 4-1. Analysis of the MscS crystal structure and modeling of its different functional states. **(A)** The crystal structure of MscS (1mxm.pdb) (Bass et al., 2002). **(B)** Magnified view of the transmembrane domain with TM3 colored according to helical propensity. An apolar environment (n-butanol) scale developed for peptides was used for the largely dehydrated TM3a, and an aqueous medium scale (Liu and Deber, 1998) was used for the water-exposed TM3b. **(C)** Compacted conformation obtained in steered MD simulations featuring reduced splay of the TM1 and TM2 peripheral helices. A Robetta-predicted N-terminus (red) was added as a continuation of TM1. **(E)** Gradual expansion of this compact structure using extrapolated motion/energy minimization cycles produced a conformation with straight TM3s satisfying the criteria of the open state. **(D)** Repeated inwardly directed transitions from the open state produced compact states with a closed gate (yellow) and kinks at the alternative G121 site. The models in D and E are not the original extrapolated frames, but structures obtained after extended all-atom MD simulations to test for stability in the lipid bilayer. **(F)** Conformation with helical buckling at G113 in which steric clashes between the TM1-TM2 loops and TM3b were resolved by relaxation of the lipid-facing helices towards the conformation found in crystal structure. Experimental data presented in the following figures allows us to relate the two principal non-conductive models to the closed resting (D) and inactivated (F) states.

A salient feature of the MscS crystal structure is a sharp 'kink' in TM3 near glycine 113 (G113). From this kink, the nearly parallel helices splay out at 80° relative to the axis of the pore such that the C-terminal (TM3b) segments extend almost parallel to the membrane interface to form the roof of the wider cage (Fig. 4-1A). This peculiar arrangement of TM3b appears to be the only way to pack the TM3a segments as a compact barrel, with L105 and L109 forming the closed hydrophobic gate, while maintaining its connection between the gate and the cage. The cage of MscS is not a rigid structure and various perturbations of this domain have been reported to affect gating (Koprowski and Kubalski, 2003; Miller et al., 2003b; Schumann et al., 2004). The fact that stresses or conformational changes in the cage are transmitted directly to the channel gate points to a possible regulatory role for TM3b.

In this work we utilized a novel 'extrapolated motion' technique to explore the pathway for conformational transitions in MscS. We observed complete straightening of TM3b in the expanded (open) state and buckling of the helix at two different sites (G113 and G121) on return to compact non-conductive (closed or inactivated) conformations. Based on these simulated trajectories, we performed patch-clamp analysis of MscS mutants with altered flexibilities at either or both of these sites. The data below provide evidence for a functional cycle of MscS that involves transitions to four states, closed-resting (C), open (O), desensitized (D) and inactivated (I). We show that the processes of activation, desensitization and inactivation are critically controlled by the flexibility of the C-terminal part of TM3 near glycines 113 and 121.

Materials and methods

Modeling and simulations

All of the employed modeling techniques were variations of Molecular Dynamics (MD) or energy minimization and are detailed in the supplement. Briefly, MD simulations were performed using NAMD (Phillips et al., 2005) with a CHARMM27 forcefield (MacKerell et al., 1998). VMD (Humphrey et al., 1996) was used for molecular modification, visualization and analyses using custom-written Tcl scripts for the determination of in-plane area changes, assessment of conductance and measurements of kink angles. The initial compacted conformation was obtained from the crystal structure using targeted energy minimization followed by a symmetry-driven simulated annealing. These steps produced a compact symmetric homoheptamer (Fig. 4-1C).

A path for barrel expansion was predicted using the *extrapolated motion* protocol. 50-cycle extrapolations typically produced a 5-15 Å radial displacement of all transmembrane domains. The structure of the 26-residue N-terminal domain was predicted *de-novo* using the Rosetta algorithm (Simons et al., 1997). Extrapolation of trajectories for opening and closure were repeated 50 times with the complete model. The putative open state conformation was selected to satisfy the experimentally estimated protein expansion area and conductivity. Previous measurements estimated an in-plane expansion of between 8.4 and 18 nm^2 (Sukharev, 2002; Akitake et al., 2005). A more recent estimate of 11.8 nm^2 was obtained on the 'fast' A98S mutant that permitted measurements under a more equilibrium regime (Akitake et al, unpublished). The resting and open states best satisfied these parameters were each

MD simulated in a fully hydrated POPC bilayer with TIP3P water (Jorgensen et al., 1983) as NPT ensemble at 310 K and membrane tension of 10 dyne/cm for 12 ns.

Generation of mutants and patch-clamping

Site directed mutagenesis was conducted on the *mscS* gene in a pB10b vector (Okada et al., 2002) using a Quick Change (Qiagen – Valencia, CA) kit and verified with automated sequencing. Mutants were expressed in the MJF465 triple knockout *E.coli* strain (*mscS*$^{-}$*, mscL*$^{-}$*, mscK*$^{-}$) (Miller et al., 2003b), from which giant spheroplasts were generated as previously described (Martinac et al., 1987; Cui et al., 1995). Recording of MscS from excised membrane patches was carried out at –30 mV using potassium buffers and borosilicate patch pipettes in a manner previously described (Akitake et al., 2005). Programmed pressure stimuli were applied using a 2nd generation high-speed pressure clamp apparatus (HSPC-1, ALA Scientific - Westbury, NY) with a valve-limited slope of ~30000 mmHg/s (~10 ms rise time). Data acquisition and analysis were performed using the PClamp 10 software suite (Molecular Devices – Sunnyvale, CA).

Modeling and extrapolated motion analysis of transitions in MscS

Molecular dynamics (MD) simulations provide valuable insights into channel mechanisms however they typically represent events shorter than the timescales necessary to observe gating. To overcome this limitation we developed a novel 'extrapolated motion' technique for the prediction of conformational transitions in proteins. This technique, which involves cycles of extrapolated atomic displacements,

followed by symmetry-constrained minimizations, and short relaxing MD simulations was used to generate pseudo-continuous low energy trajectories for conformational transitions in MscS (Anishkin et al., unpublished). Experimentally determined spatial parameters for MscS conductance (Sukharev et al., 1993; Levina et al., 1999; Sukharev, 2002) and in-plane expansion (Sukharev, 2002; Akitake et al., 2005) served as the basis for selection of plausible end-state conformations. From these simulations we generated two new structures representing the resting and open states of the channel (Fig. 4-1D,E). These structures were tested for stability, water occupancy and conductance in the lipid bilayer under extended all-atom MD simulations.

Generation of the resting conformation from the crystal structure started with packing of the peripheral TM1 and TM2 helices closer to the central TM3 shaft using targeted energy minimizations. The result was a reduction in the splay of the TM1-TM2 helical pairs, which critically improved packing with the surrounding bilayer (Fig. 4-1C). In previous attempts to simulate MscS in the bilayer, packing conflicts with tilted helices were observed and the TM3 barrel collapsed asymmetrically (Sotomayor and Schulten, 2004; Spronk et al., 2006). Tighter packing also re-established contact between the peripheral helices and the gate region, additionally stabilizing the symmetric barrel assembly and the 'vapor-locked' state of the gate (Fig. 4-1C). The N-terminal domain (26 residues), missing in the MscS crystal structure, was reconstructed using the Rosetta structure prediction algorithm (Fig. 4-1C, red helices) (Simons et al., 1997; Simons et al., 1999; Simons et al., 2001). The barrel was slightly expanded with steered MD to provide space for insertion and then

re-packed. Adding the N-termini filled nicks in the outer rim of the barrel and adjusted the hydrophobic thickness of the transmembrane domain (Lomize et al., 2006) making it more compatible with the lipid bilayer.

From the compact conformation, the transmembrane barrel was expanded using extrapolated motion until the radius of the pore satisfied the experimentally determined pore conductance and in-plane expansion. It was observed during barrel expansion that the TM3 helices gradually straightened and once the inner pore diameter reached 18 Å, corresponding to ~1.6 nS conductance, the kink at G113 had completely disappeared (Fig. 4-1E). It should be noted that after adding the resistance of the cage domain, the conductance of the channel complex is estimated to be 1.2 nS, close to the experimentally determined value (Sukharev et al., 1993; Levina et al., 1999; Sukharev, 2002). Analysis of pore electrostatics and all-atom MD simulations revealed that this open conformation produces very low anionic selectivity, consistent with experimental data (Sukharev et al., 1993; Levina et al., 1999). Upon opening, the effective radius of the outer boundary of the transmembrane domain increased from 26 Å to 32 Å producing an in-plane area change of ~1200$Å^2$, comparable to the values estimated from the slopes of MscS dose-response curves on tension (Sukharev, 2002; Akitake et al., 2005). Straightening of the G113 kink was not an artifact of the modeling protocol since the same tendency was previously observed in all-atom MD simulations of a pre-expanded MscS barrel (Sotomayor and Schulten, 2004; Sotomayor et al., 2006b; Spronk et al., 2006).

From our hypothetical open state we attempted to construct a smooth transition back to the closed (resting) state. Motions of the cage domain during these

transitions were slight. Repeated cycles of expansion and contraction were conducted 50 times in which the opening transitions consistently showed full straightening of the G113 kink. The closing transitions, however, revealed several different outcomes with ~60% of simulations showing helical buckling at an alternate site near G121 (Fig. 4-1D). In the initial steered compaction of the barrel visible bending of the TM1-TM2 loops (Fig. 4-1C, yellow) was observed due to steric clashes with the TM3b helices. Formation of the G121 kink two helical turns below G113 appears to alleviate these conflicts permitting a more compact packing of the TM1-TM2 pairs around the TM3 barrel. In another set of extrapolated closures the kink at G113 was observed to reform, resulting in a state of the TM3 helices that resembled the crystal conformation. The model in Fig. 4-1F is an example of such a conformation featuring partially detached peripheral helices. Detachment of TM1-TM2 from the TM3 barrel appears to be the only way to avoid major distortions of the helices and loops while still maintaining the kinks at G113. Other outcomes of extrapolated closure produced less pronounced helical buckling at both G113 and G121 that may suggest a possible intermediate state.

Bending of the pore-lining helices has been shown as a critical component in the gating mechanisms of many ion channels (Jiang et al., 2002a; Long et al., 2005) and the functional role of conserved glycines as hinges has been assumed (Kellenberger et al., 1997; Shealy et al., 2003; Magidovich and Yifrach, 2004; Ding et al., 2005). Fig. 4-1B shows the crystal conformation of the MscS transmembrane domain with the helices colored according to helical propensity. Coloring of the largely dehydrated TM3a segment (Anishkin and Sukharev, 2004) reflects the helical

propensity in apolar environment, whereas an aqueous helicity scale was used for the more water-exposed TM3b (Liu and Deber, 1998). The coloring reveals that regions in the vicinity of G113 and G121 are weak points in TM3b and may be prone to buckling.

Based on these new structural models, we hypothesized that the unique gating characteristics of MscS could depend on straightening and sequential buckling of the TM3b helices at G113 or G121. Structural differences at these sites could potentially correspond to different functional states of the channel (Fig. 4-1 D-F).

Functional analysis of TM3 helical flexibility

To study experimentally the role of helical flexibility at residues G113 and G121 we engineered either alanine or glycine mutations to respectively increase or decrease helical propensity at these sites. Although both are small amino acids, alanine favors the formation of α-helical protein conformations by ~0.4-2 kcal/mol over glycine (Serrano et al., 1992). Mutant channels were then expressed in a clean genetic background (*mscS*$^{-}$*, mscK*$^{-}$*, mscL*$^{-}$) in *E.coli* spheroplasts and characterized through patch-clamp recording under computer-controlled mechanical stimulation. Control experiments indicated that the MscS mutants (except the toxic G113A/G121A mutant) expressed at a similar level (Fig. 4-S1). All mutants displayed single-channel conductances similar to WT.

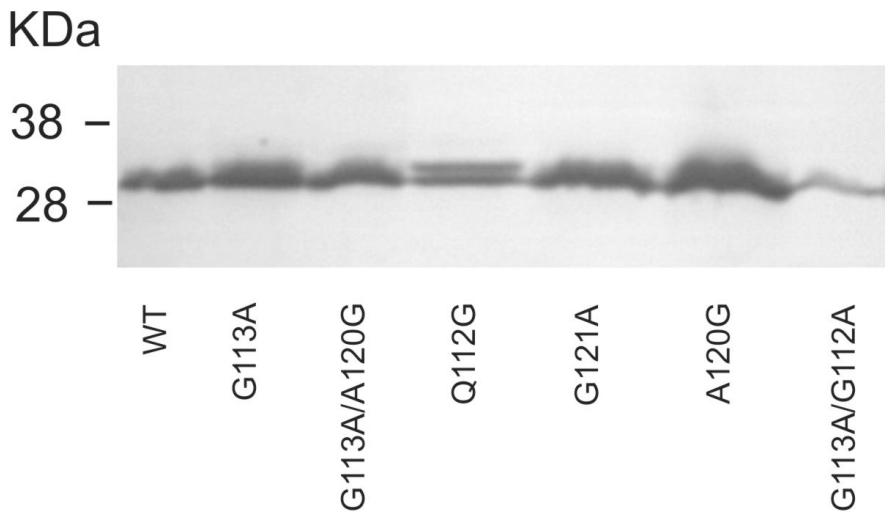

Figure 4-S1. Western blot analysis of MscS mutants showing the relative expression levels of channel protein in the membrane.

Membranes were isolated by French press from IPTG induced *E. coli* cultures. Fractions were run on a 4-15% polyacrylamide gel (Bio Rad – Hercules, CA). Bio Rad broad range pre-stained SDS-PAGE standards were used. Gel was blotted onto an Immobilion PVDF membrane (Millipore – Bedford, MA). MscS protein was then labeled with anti-6His antibody conjugated to AP (Invitrogen) and visualized with Western Blue stabilized substrate (Promega – Madison, WI). Expression levels of most mutants were even with the exception of the G113A/G121A double mutant, which is severely toxic to the bacteria. This double alanine mutant and the Q112G and G121A mutants that predispose the channel to inactivation showed poor rescuing ability under a 400 mOsm osmotic downshock. Other mutants were fully functional *in vivo* showing osmotic rescuing capacity comparable to WT.

Adaptive behavior of WT MscS

Wild-type (WT) MscS channels have been shown to respond most readily to steeply applied stimuli, whereas pressures applied slowly invoke lower population currents (Akitake et al., 2005). Fig. 4-2A depicts typical traces from a patch containing ~100 WT channels recorded with 1, 10 and 30 s ramps to saturating pressure. There is a marked reduction in the current response of this WT population at the end of the longest ramp due to adaptation. This type of protocol tests the dynamic response of the channels and simulates variable environmental conditions in which swelling or osmotic change can occur slowly or abruptly. As a result, the most effective stimulus to activate WT channels is a 'test-pulse' protocol consisting of a machine-limited step of saturating pressure (10 ms rise time, 0.25 s duration). Test-pulses are used to observe maximal conductance (G_{max}), a reference measurement that indicates the number of channels available to activate within a given patch.

Adaptation of WT MscS was most clearly shown in channel responses to prolonged steps of sub-saturating pressure. Under these conditions MscS initially opens, but the elicited current gradually declines with a rate that depends on the amplitude of the stimulus (Figs. 4-2E and 4-3A). This rate of current decay was previously demonstrated to increase as the pressure step became smaller (Akitake et al., 2005). At the end of the sub-saturating step a test-pulse (Figs. 4-2E and 4-3A, red asterisk) was applied to sample the channel population for availability. We observed that with a long enough sub-saturating step (20-60 s) the test-pulse activates only a fraction of the channels, revealing a population that is no longer responsive to stimulus, i.e. inactivated (Akitake et al., 2005).

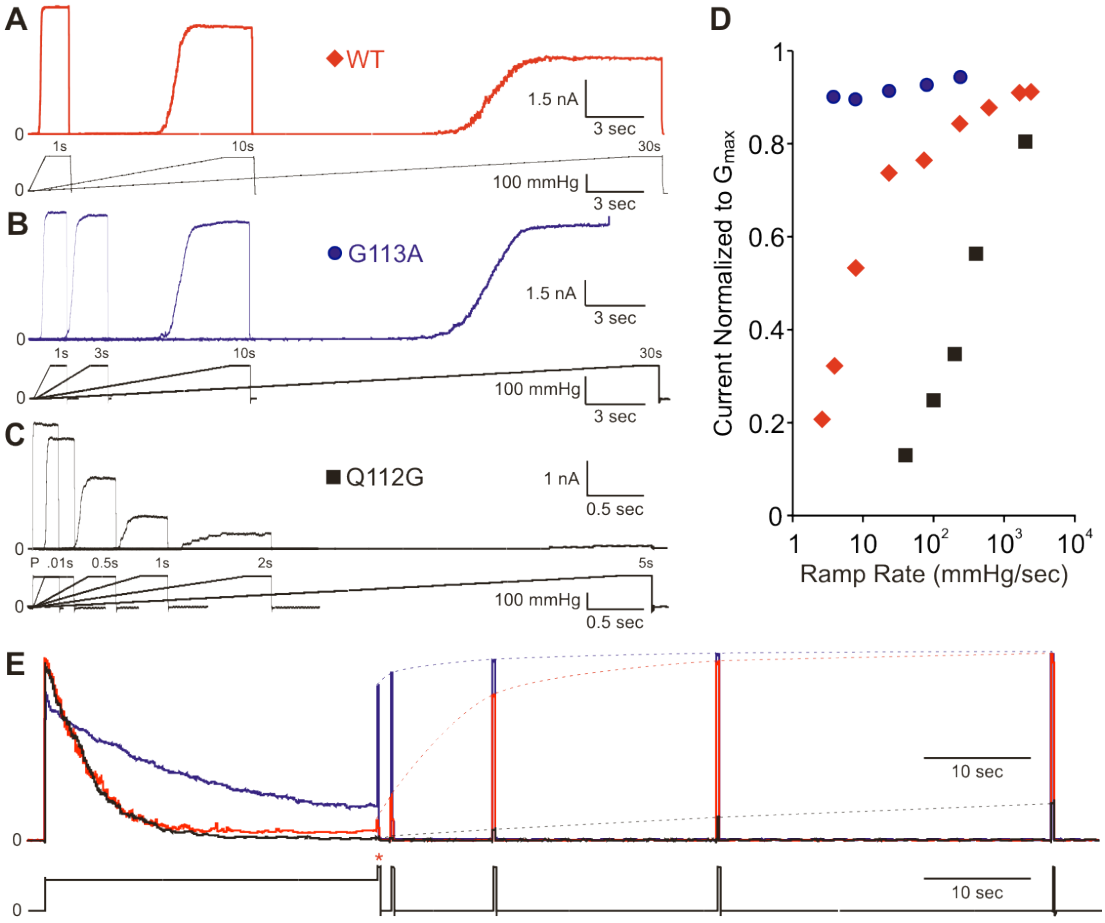

Figure 4-2. Characterization of the adaptive behaviors of WT MscS and two mutants with altered TM3b flexibility near G113.

(A-C) Current responses to linear ramps of pressure recorded in isolated patches at -30 mV. (A) In WT, slow ramps of pressure mimic conditions of gradual swelling and produce lower end currents compared to fast ramps. **(B)** Non-inactivating G113A shows negligible current decline. **(C)** Q112G, which is prone to inactivation, shows an abrupt current decline. **(D)** Plot of the end currents normalized to G_{max} as a function of the pressure ramp rate. **(E)** Responses to 30 s steps of sub-saturating pressure reveal the kinetics of adaptive current decline. A series of short saturating test-pulses (10 ms rise time, 0.25 s duration) applied at the end of the step reveal the extent of inactivation and the process of recovery. The WT response is shown in red. G113A channels (blue) display slower current decay attributable to reversible desensitization. At any time almost all G113A channels are available showing a non-inactivating phenotype. The Q112G mutant (black) inactivates more completely than WT and also displays slowed recovery (see Fig 4-3E,F for time courses).

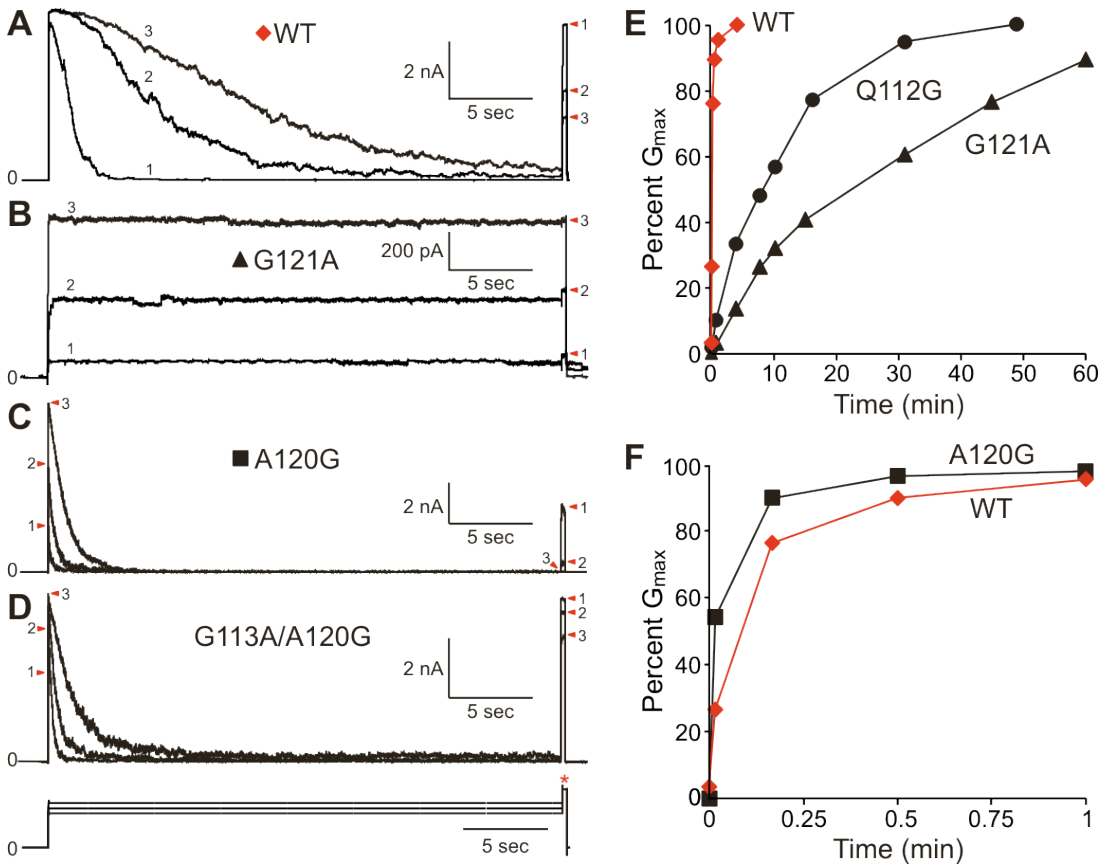

Figure 4-3. Mutations in TM3b at G121 strongly affect channel responses to pressure. **(A-D)** Characteristic responses of channel populations to a series of three different sub-saturating pressure steps. Step amplitude was chosen to sample a range of pressures near the midpoint of activation (both above and below) for each channel population. **(A)** Increasing step amplitude slows down visible current decay in WT but increases the fraction of inactivated channels as revealed by a test-pulse at the end of the step (red asterisk). **(B)** G121A shows fractional activation and no current decline in response to the sub-saturating steps. Test-pulses reveal negligible additional activation at the end of the step. **(C)** A120G exhibits extremely fast current decay with high degree of inactivation at the end of the step. **(D)** The double G113A/A120G mutant shows fast current decline similar to A120G but with essentially no inactivation. **(E-F)** Time courses of recovery for WT MscS and mutants were determined with a series of test-pulses as shown previously in Fig. 4-2E. Data for recovery from the inactivated state cannot be shown for G113A and G113A/A120G as only a fraction of these channels inactivate.

Upon the release of pressure, a series of test-pulses were used to observe recovery of the population from the inactivated to the closed state at multiple time points (Fig. 4-2E). Control experiments show that these short pulses do not change the kinetics of recovery. The return of MscS activity to G_{max} was observed to be a kinetically complex process that requires the release of tension. The fastest component of recovery, which accounts for ~80% G_{max}, occurs immediately after the cessation of tension with a characteristic time ($\tau_{recovery}$) of 7.13 ± 0.14 s (n=3) (Figs. 4-2E and 4-3F). A complete return of activity to G_{max} takes ~3 min (Akitake et al., 2005).

Application of test-pulses during the sub-saturating step revealed that in the course of current decline not all closing channels go to the inactivated state as previously thought. In Fig. 4-4A, the sub-saturating step initially invokes ~97% of the channel population and within 10 s the current drops by about 50%. However, a test-pulse at this moment reveals that a majority of the closed channels are still available for activation having mode shifted to open with a higher pressure threshold. Non-responsive (inactivated) channels only account for about 20% of the population. By the end of the pressure step only ~12% of the population is still conducting with ~25% still able to open with the test-pulse. The grey trace in Fig. 4-4A shows the response of the same population to an uninterrupted step of pressure illustrating that test-pulses do not perturb the kinetics of adaptation. The data show that current decline at sub-saturating pressures is a combination of two processes; inactivation, and a new process we term desensitization, which results in channels that can be reactivated by a higher stimulus.

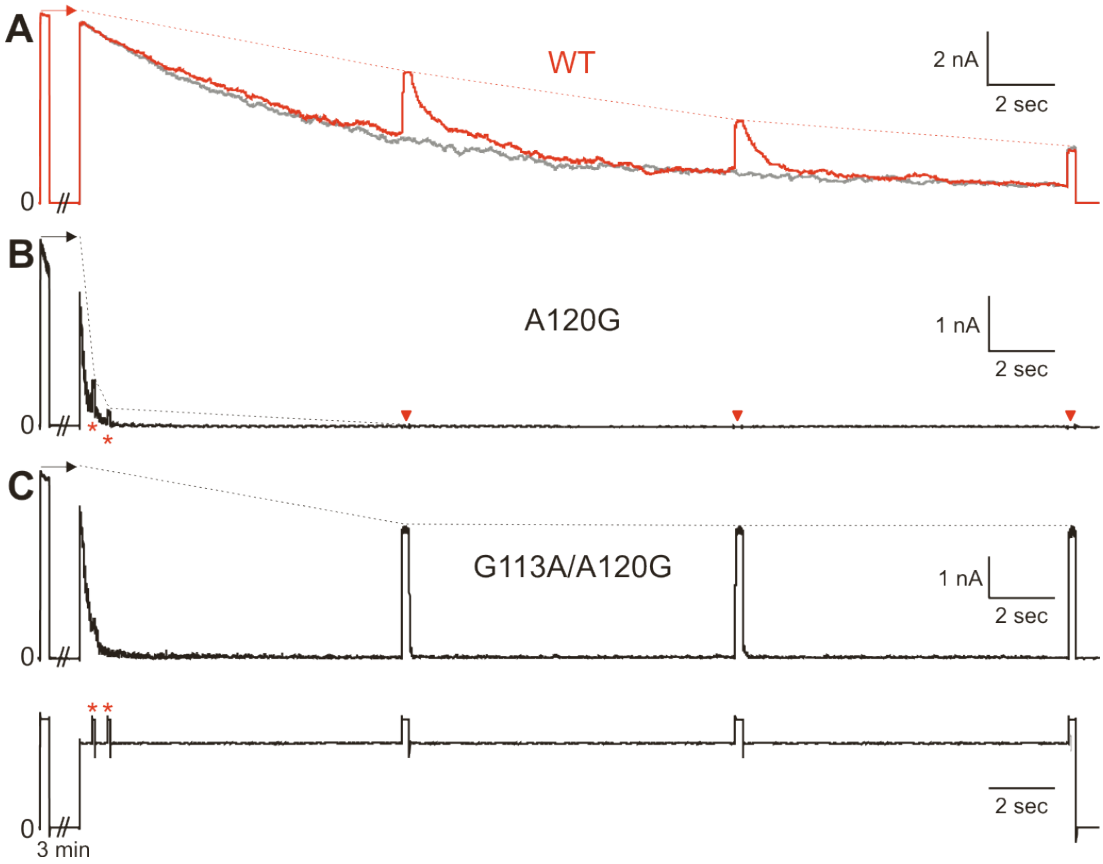

Figure 4-4. Adaptive current decline is a result of two processes, desensitization and inactivation. **(A-C)** The maximal conductance of the population was measured by a test-pulse applied 3 min prior to 30s sub-saturating step. Step amplitude was chosen to activate >80% of the channel population. The 30s step was intervened by a series of three test pulses during and at the very end of the step. **(A)** The response of WT MscS reveals that a substantial portion of channels that closed in the course visible current decay can be reactivated if a higher pressure stimulus is applied. These channels are in the desensitized state. The other part of the population that closes is unable to open with test-pulses. These channels have entered the inactivated state. In WT there is a significant difference between the rate of desensitization (visible current decay) and the rate of channel inactivation (red dotted line). Test-pulses during the sub-saturating step do not affect the kinetics of current decline (grey trace). **(B)** Current decay in A120G is extremely fast so two extra 0.1 s test-pulses (red asterisks) were delivered during the first seconds of stimulation to visualize the components of current decline. A120G displays extremely fast desensitization immediately followed by inactivation. **(C)** The double G113A/A120G mutant displays fast desensitization and essentially no inactivation.

In WT MscS, the process of desensitization initially proceeds faster (with a shorter τ) than inactivation. Our analysis of mutants will show that desensitization and inactivation are sequential processes.

To test this scheme further and answer the question of whether the processes of activation and inactivation are interdependent, we measured inactivation in a range of tensions above and below the activation threshold, a stimulus invoking just the first channels. A test-pulse to measure G_{max} was followed by a 30 s sub-saturating step of varying amplitude with a second test-pulse applied at the end of the step indicating the fraction of channels remaining active (Fig. 4-5A). In WT, no significant inactivation occurs with sub-threshold stimuli and there is usually a rough correspondence between the fraction of channels activated at beginning of the step and the fraction of channels inactivated at the end. The fraction of active channels plotted in Fig. 4-5E indicates that MscS has to open in order to proceed to either the desensitized or inactivated states. The data suggest that there is no native path directly from the closed to the inactivated state ($C \rightarrow I$), although at rest the reverse transition $I \rightarrow C$ provides a path for recovery (Fig. 4-5F).

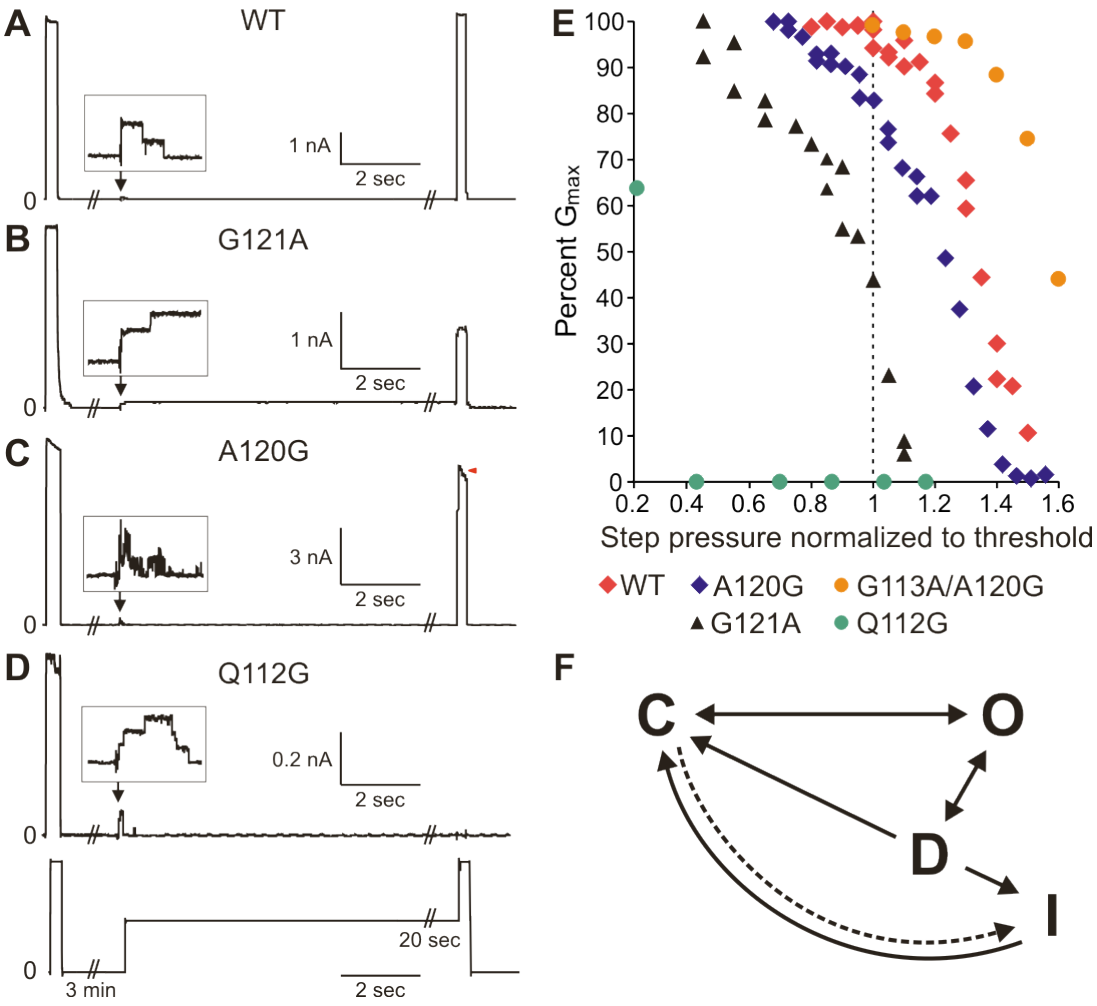

Figure 4-5. Tension-dependence of inactivation for WT MscS and mutants.

(A-D) A 30 s sub-saturating steps protocol was applied to WT and each MscS mutant in a large range of amplitudes. These traces show the response of the channel population to steps near the activation threshold. **(A and C)** In WT and A120G there is virtually no inactivation at these pressures. **(B and D)** In G121A and especially in Q112G massive inactivation occurs during a prolonged pressure stimulus at sub-threshold pressures. **(E)** A plot of the end currents as a percent of G_{max} versus the amplitude of the sub-saturating step normalized to the activation threshold pressure. **(F)** Kinetic scheme for functional transitions in MscS. The closed, **C**, to open, **O**, transition was not strongly effected by any of the mutations. Exit from the **O** to the desensitized, **D**, state was impeded by the G121A mutation, which also opened a direct pathway from the closed to the inactivated, **I**, state (dashed arrow). The **D** to **I** transition was abolished by the G113A mutation, whereas the Q112G mutation stabilized **I**.

Altered helical propensity at G113

Substitution of G113 by alanine (G113A) to increase helical propensity does not affect channel opening as the activation pressures for this mutant were found to be comparable to WT. However, when G113A was subjected to ramps of pressure of varying durations (1 to 30 s), it was observed that the adaptive behaviors, characteristic of WT, were totally abolished. The dynamic responses of G113A to both fast and slow stimuli, shown in Fig. 4-2B, reveal population currents that were nearly indistinguishable from G_{max}. Consistent with these findings, G113A was observed to impede current decay at sub-saturating pressures (Fig. 4-2E) with rates of the current decline an order of magnitude slower than WT (Fig. 4-S2). A test-pulse at the end of the sub-saturating step revealed that nearly all of the G113A population was still available to open indicating that the observed decay of the current was due primarily to desensitization. Since only a small fraction of the channels was found to be inactive at the end of the step, test-pulses for recovery showed a correspondingly fast return to G_{max} (Fig. 4-2E). The dynamic responses of G113A show that a straighter helix at G113 prevents inactivation making the channel population available for activation regardless of stimulation pre-history (Fig. 4-2E).

Increased flexibility at G113 was achieved by introducing a second glycine at Q112 (Q112G). This mutant displayed opposite gating characteristics to G113A. Significant Q112G activation was only observed with fast stimuli (< 1 s rise time) with the mutant being nearly irresponsive to slower ramps of pressure (Fig. 4-2C,D), suggesting faster inactivation at intermediate pressures.

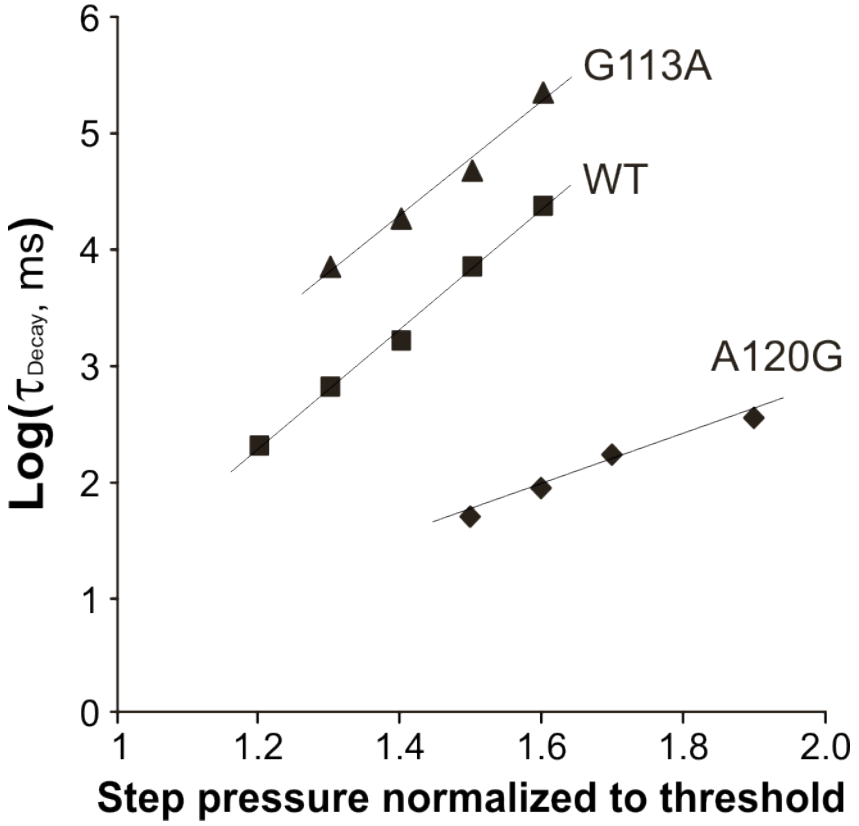

Figure 4-S2. Analysis of the kinetics of current decline under prolonged pressure steps.
The characteristic time of current decay (τ_{Decay}) was obtained by a single exponential fit of the falling phase of the current recording using a Levenberg-Marquardt method in the Clampfit program a part of the PClamp software suite (Molecular Devices – Sunnyvale, CA). The non-inactivating G113A mutants show a reduction in the rate of current decline at all pressure levels relative to WT. The fast inactivating and fast recovering A120G mutant shows rates of current decay that are at least two orders of magnitude faster than WT.

The dynamic response of Q112G to a sub-saturating step showed inactivation rates comparable to that of WT (Fig. 4-2E). However, a test-pulse at the end of the step revealed complete inactivation. The recovery of Q112G from inactivation was also slower than WT by two orders of magnitude ($\tau_{recovery}$ = 437 ± 233 s, n=3) requiring ~50 min for completion (Fig. 4-2E). The data show that higher flexibility at the G113 site markedly stabilizes the inactivated state and strongly support the notion that helical buckling at G113 is a structural characteristic of the inactivated state. However, it appears that the rate-limiting step for the inactivation process lies elsewhere as Q112G did not strongly affect the overall rate of inactivation.

Altered helical propensity at G121

Substitutions of G121 by alanine (G121A) to increase helical propensity or insertion of an extra glycine in the adjacent position (A120G) to increase flexibility did not appear to affect activation of the channels, but had dramatic effects on the kinetics of closing, inactivation and recovery. It was observed that successive stimulations of G121A by ramps or steps applied with the standard 3 min resting interval gradually reduced G_{max} indicating a predisposition to inactivation and incomplete recovery. The use of test-pulses and extended periods of patch "rest" at zero pressure (~15-30 min) was the only way to keep the number of active channels from declining through each series of trials.

In sharp contrast to WT, G121A mutant channels displayed no visible current decline under prolonged pressure steps of different amplitude (Fig. 4-3B). A test-pulse at the end of each step revealed that very few additional channels (above those already activated) were available to open (Fig. 4-3B, red asterisk and arrows). This

type of response suggests that under moderate tension G121A is unable to exit from the open state into the desensitized or inactivated states. However, those channels that did not open during the prolonged stimulus appear to inactivate 'silently' without prior activation. The most effective way to inactivate G121A was with a slow pressure ramp (> 30s) enabling the observation of recovery with a series of test-pulses. The return of G121A to the closed state was severely retarded, even more so than for Q112G (Fig. 4-3E). These findings reveal that although both G121A and Q112G drive the channel to the inactivated state, recovery back to the resting state is more difficult for G121A.

Like the Q112G mutation, the A120G substitution adds a second glycine and is predicted to increase the flexibility at this site. Similar to Q112G, A120G could only be effectively activated with test-pulses. Ramped stimuli (> 1 s) produced only a fraction of the test-pulse elicited G_{max} suggesting massive inactivation at sub-saturating pressures. In the entire range of accessible pressures, including saturating (for WT), rectangular 30 s steps produced sharply declining currents with rates of decay at least 100 times faster than WT (Fig. 4-3C and 4-S2). Sampling of the A120G population at the end of the step indicated that a larger fraction of channels was inactivated compared to WT. In contrast to G121A, inactivated A120G channels recovered very quickly ($\tau_{recovery}$ = 5.23 ± 0.32 s, n=4), ~1.36 times faster than WT (Fig. 4-3F). Test-pulses applied during current decay (Fig. 4-4B) vividly show that most of the A120G population easily finds the inactivated state with very few desensitized channels. It appears that higher flexibility near G121 correlates with

faster kinetics of exiting the open state and channels that do not remain desensitized but quickly inactivate.

To address the question of which non-conductive state is associated with kink formation specifically at G121 we generated the G113A/A120G double mutation. This mutant has higher flexibility at the G121, which was shown to facilitate exit from the open state, and increased helical propensity at G113 shown to disfavor inactivation. Fig. 4-3D shows that under a sub-saturating step, G113A/A120G does indeed easily exit from the open state, but gets trapped in the desensitized state. Fig. 4-4 A-C illustrates the differences in desensitization and inactivation kinetics between WT, A120G and G113A/A120G. As expected, G113A/A120G desensitizes much faster than WT, with a rate comparable to A120G, but does not readily inactivate. These results taken together with the inability of the open G121A to both desensitize and inactivate (Fig. 4-3B), suggest that helix buckling occurs sequentially, first at G121 leading to the desensitized state and then at G113, to stabilize the inactivated state.

G121A and Q112G mutations favor inactivation by lowering its tension dependence

To observe the tension-dependence of inactivation each mutant was subjected to the same 30 s sub-saturating step protocol in a range of pressures. These cumulative data are presented in Fig. 4-5. As previously mentioned, WT MscS does not inactivate until the pressure reaches the activation threshold (Fig. 4-5A,E). A120G displays a similar dependence, though with an earlier onset of current decline (Fig. 4-5C,E). G113A/A120G did the opposite, delaying the onset of inactivation (Fig 4-5E). Fig. 4-5B shows that under a step of near- threshold pressure, ~50% of G121A channels are

active while the other half of the channel population has inactivated silently without opening. The tension-dependence for inactivation in G121A is therefore shifted strongly to the left versus WT (Fig. 4-5E). Q112G displayed an even more severe tendency towards silent inactivation as pressure steps as low as 20-40 mmHg were observed to completely eliminate channel activity (Fig. 4-5D,E). Remarkably, the mutation straightening TM3b at G121 produces a similar phenotype as the one conferring higher flexibility at G113. It appears that both mutations stabilize the inactivated state and open pathways for silent inactivation that correlate with extremely slow recovery. The main difference lies in G121A precluding the native path towards inactivation from the open state by kinetically hindering transition to the desensitized state.

Helicity at both G113 and G121 impairs MscS closure and inactivation.

Based on the data presented above it appears that flexibility of TM3b near G121 is required for MscS desensitization. It therefore stands to reason that increased helical propensity at G121 should alter the mutant channel's ability to close. In WT, closing transitions in response to test-pulses are essentially square ($\tau_{closure}$ = 0.89± 0.17 ms, n=10) (Fig. 4-6A and inset) with similar behavior observed for G113A ($\tau_{closure}$ = 1.37± 0.29 ms, n=7) (Fig. 4-6B and inset). However, G121A currents were observed to linger for hundreds of milliseconds after cessation of the pressure stimulus (Fig. 4-6C and inset). Exponential fits of these residual currents show relaxation with 64 ± 24 ms (n=7) kinetics, 70 times slower than WT.

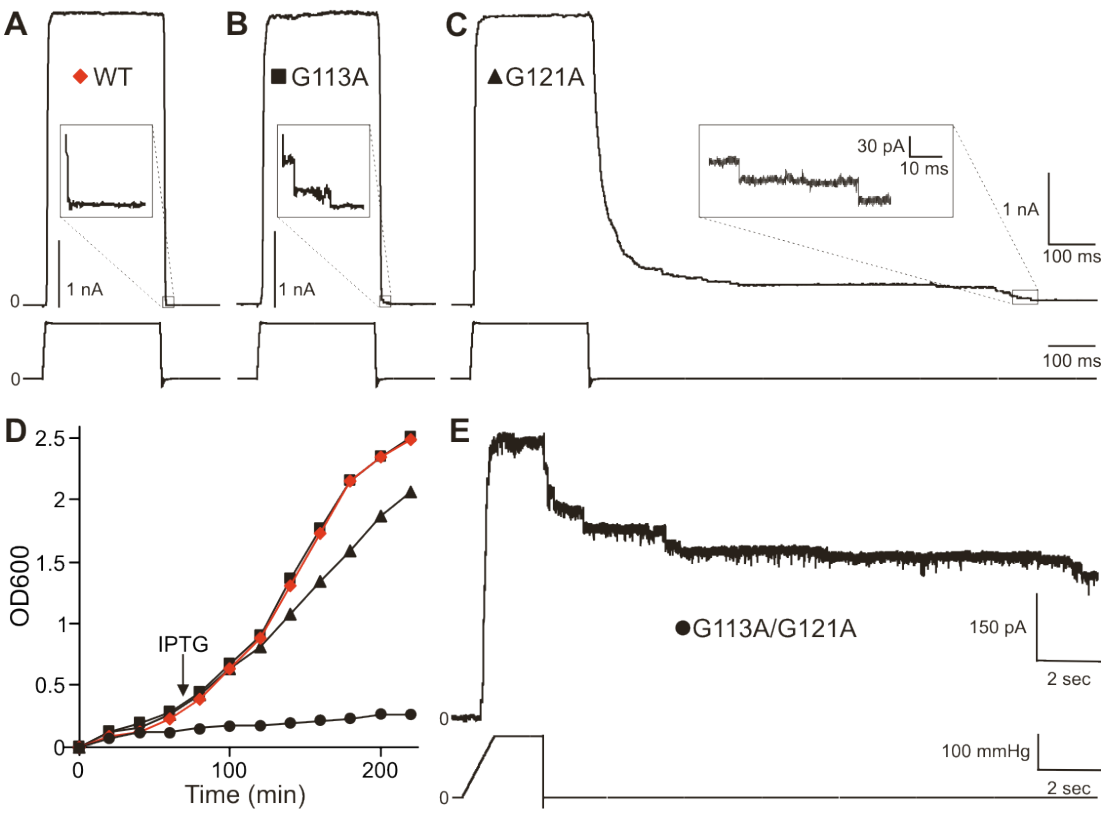

Figure 4-6. High helical propensity in TM3b impairs closure of MscS.
(A-C) WT, G113A and G121A MscS responses to a test-pulse with a prolonged recording at zero pressure. **(A and B)** Opening and closing of WT and G113A is essentially square with the pressure stimulus. **(C)** G121A mutation prolongs the closing process and slightly slows down bacterial growth kinetics *in vivo* **(D)**. **(E)** The double G113A/G121A mutant prevents both MscS closure and inactivation resulting in channels that do not close upon cessation of the pressure stimulus. After induction with IPTG (arrow) the double mutant expressing bacteria stop growing and form no colonies on IPTG plates.

While G121A showed impaired closing, increased helical propensity at both G113 and G121 conferred by the G113A/G121A mutation produced channels that refused to close. The response of G113A/G121A to a 1 s ramp of saturating pressure with continued recording at zero pressure is shown in Fig. 4-6E. As pressure increased, G113A/G121A opens normally, however upon a drop in pressure a majority of the channels remained open. G113A/G121A current does eventually return to the baseline within 3 min. Expression of this mutant produced a strong toxic (gain-of-function) phenotype (Ou et al., 1998) as illustrated by the growth curves in Fig. 4-6D. Bacterial cultures were started under non-induced conditions and by addition of 1 mM IPTG were allowed to continue growth under induced channel expression. G113A did not produce any visible gain-of-function effect, whereas full expression of G121A slightly retarded bacterial growth. Expression of the G113A/G121A double mutant caused most severe retardation (Fig. 4-6D). These results clearly illustrate the *in vivo* effect of the inability of G113A/G121A to properly close or inactivate. Higher helical propensity at both flexible sites appears to dramatically stabilize the open state, thus confirming modeling predictions of an open channel with completely straightened TM3s (Fig. 4-1E).

Discussion

Kinked conformations of pore-lining helices in the crystal structures of open Kv1.2 (Long et al., 2005) and MthK (Jiang et al., 2002a) channels clearly illustrate the importance of conserved glycines as hinges (Kellenberger et al., 1997; Shealy et al., 2003; Magidovich and Yifrach, 2004; Ding et al., 2005). In MscS, multiple helical

propensity scales (Liu and Deber, 1998) predict that the stretch from L111 to G121, must be the most flexible region in TM3. Glycines 101, 104 and 108 above the gate may also contribute to flexibility, however tighter helical packing in this less water-accessible region should render these sites less prone to buckling.

In the present study, steered simulations and cycles of extrapolated motions, although simplified and performed in vacuum with adjusted charges, provided testable predictions to the character of transitions in MscS. Our predicted opening pathway, associated with complete straightening of TM3, was consistent with tendencies previously observed in simulated expansions of channel (Liu and Deber, 1998; Sotomayor and Schulten, 2004; Sotomayor et al., 2006a; Sotomayor et al., 2006b; Spronk et al., 2006). However, unlike these previous attempts, we were able to successfully incorporate into the models experimentally determined spatial parameters for the opening transition (Sukharev, 2002; Akitake et al., 2005). Our modeled closed and open states predicted a ~4 Å outward displacement of the TM3 helices on opening associated with a 12 nm^2 in-plane expansion of the barrel, which is considerably larger than proposed previously (Edwards et al., 2005). Simulated closing transitions provided plausible representations of two alternative non-conductive states of MscS. Experimental patch-clamp analysis also confirmed the presence of a novel, previously unidentified desensitized state, which kinetically precedes inactivation (Fig. 4-5).

We found that increased helicity at both flexible sites in TM3b (G113A/G121A) dramatically stabilized the open state indicating that in the open conformation TM3 must be straight (Fig. 4-1E). Higher helical propensity at G121

was also shown to kinetically trap the open state, while greater flexibility at this site strongly facilitated exit from the open conformation to the closed, desensitized or inactivated states. A model of the compact state with TM3b buckled at G121 allowed the most conflict-free packing of the peripheral TM1-TM2 helices restoring contact of these lipid-facing pairs with the gate region. The conformation shown in Fig. 4-1D well approximates this resting (closed) state of the channel.

While G121 is one of the most conserved glycines in the MscS family of bacterial channels (Pivetti et al., 2003), G113 is not well conserved, notably being replaced by the more 'helical' glutamate in MscK (Fig. 4-S3). MscK has a non-inactivating phenotype (Levina et al., 1999; Li et al., 2002) that the G113A mutation in MscS appears to mimic. In contrast, Q112G, which provided higher flexibility in this region, was found to strongly promote inactivation. According to our simulations, buckling of TM3b so close to the gate causes steric clashes between the ends of TM1-TM2 and TM3b, which may lead to detachment of these helices and a structure that must be non-responsive to membrane stretch. Our experimental evidence gives strong impetus for attributing helical buckling at G113 (Fig. 4-1F) to the inactivated state. Since this kink and the splayed state of the TM1-TM2 pairs are prominent features of the solved structure of MscS (Bass et al., 2002) we conclude that the crystal conformation must resemble the inactivated state. The observations that the rate of desensitization is slowed down, whereas inactivation is promoted by tension (Fig. 4-3A) suggests that the inactivated state has a conformation different from that of the desensitized state, and is likely to be characterized by a larger in-plane area.

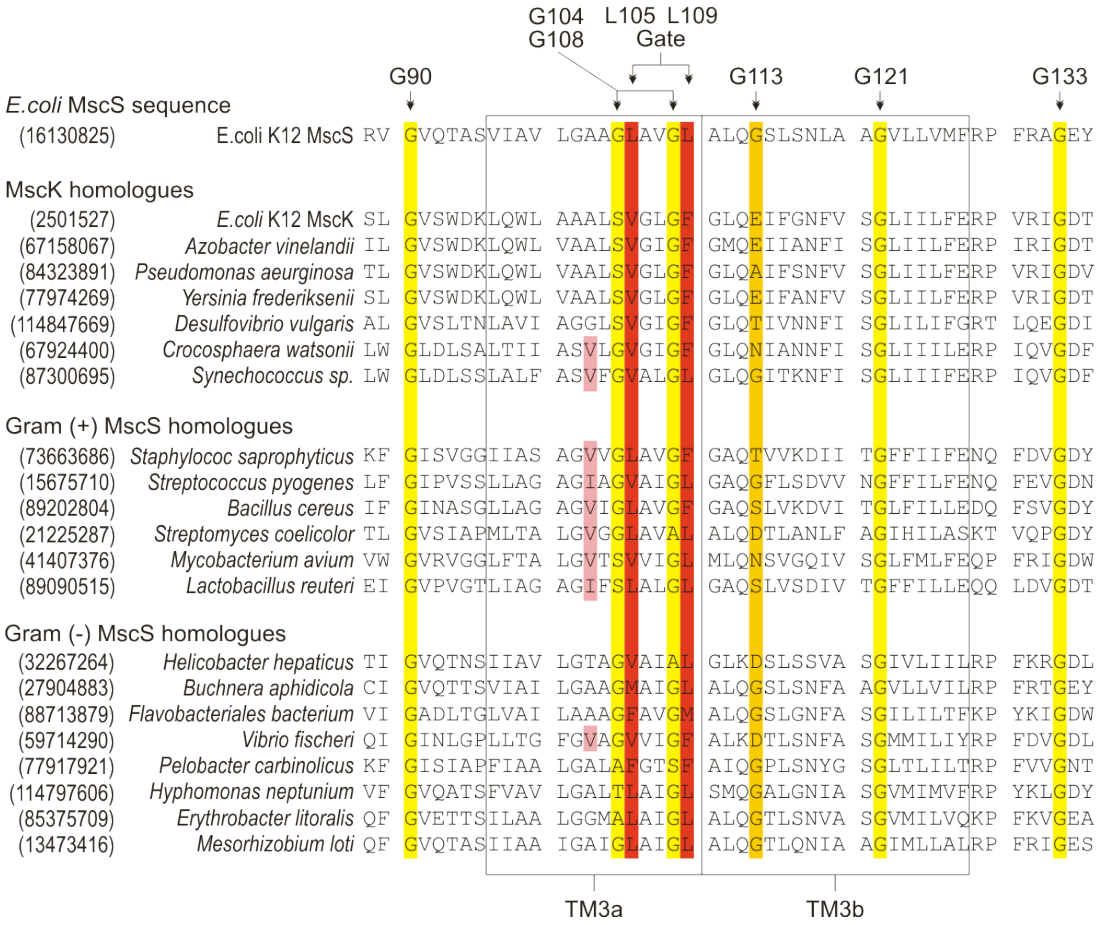

Figure 4-S3. Selected multiple sequence alignments of MscS and MscK bacterial homologues. MscS family members were obtained from protein BLAST searches of the GenBank database using the membrane embedded portion of MscS including the gate region and TM3b as a seed. Close matches were then aligned using the Clustal W algorithm in the Align X module of Vector NTI (Invitrogen – Carlsbad, CA). Sequence analysis of TM3 shows that MscS family members share a large degree of conservation in the hydrophobic gate region L105 and L109 (red) with some having not a two-fold, but a three-fold constriction (large hydrophobic sidechain in position 102, pink). Glycines (yellow) in TM3a, especially G104 and G108 that provide 'holes' for tight interhelical packing, are conserved. In TM3b, G121 is absolutely conserved whereas G113 (gold) is not. In the sequences of the non-inactivating MscK channels, G113 is largely absent and suggest helices that are not prone to buckling at this site.

While some mechanistic details remain to be clarified, we can depict the emerging picture of MscS gating in the following way (Fig. 4-S4). Membrane tension conveyed through the peripheral TM1-TM2 helices and TM2-TM3 linkers expands the outer vestibule and promotes hydration of the entire pore. The TM3 helices straighten and slightly rotate making the pore wider and more hydrophilic (L105 and L109 swing out while G101 and G104 become exposed) thus stabilizing the aqueous pathway. In this conformation, the C-terminal ends fixed on the roof of the cage domain will define the relative positions and tilts of the TM3 helices and hence the dimensions of the pore. The straightened TM3 helices are predicted to work as 'spreader bars' for the structural frame of the open state. The hydrophobic 'sphincter' formed by L105 and L109 rings would tend to constrict the lumen and buckle the helices, whereas external tension is expected to counteract this tendency and keep the helices straight. High flexibility near G121 is required for exit from the open state and upon tension release buckling at G121 brings L105 and L109 closer to occlude the pore. Expulsion of water follows and formation of water/vapor boundaries stabilize the tight conformation (Beckstein and Sansom, 2003; Anishkin and Sukharev, 2004). This closing transition that occurs at intermediate (sub-saturating) tensions clearly relies on conformational freedom of TM3b around G121, and might be facilitated by structural adjustments that bring the ends of the TM3s closer (possibly due to relaxation of the cage), resulting in the observed right shift of the activation curve. The nature of desensitization (mode-shifting) remains unclear and is the subject of current studies.

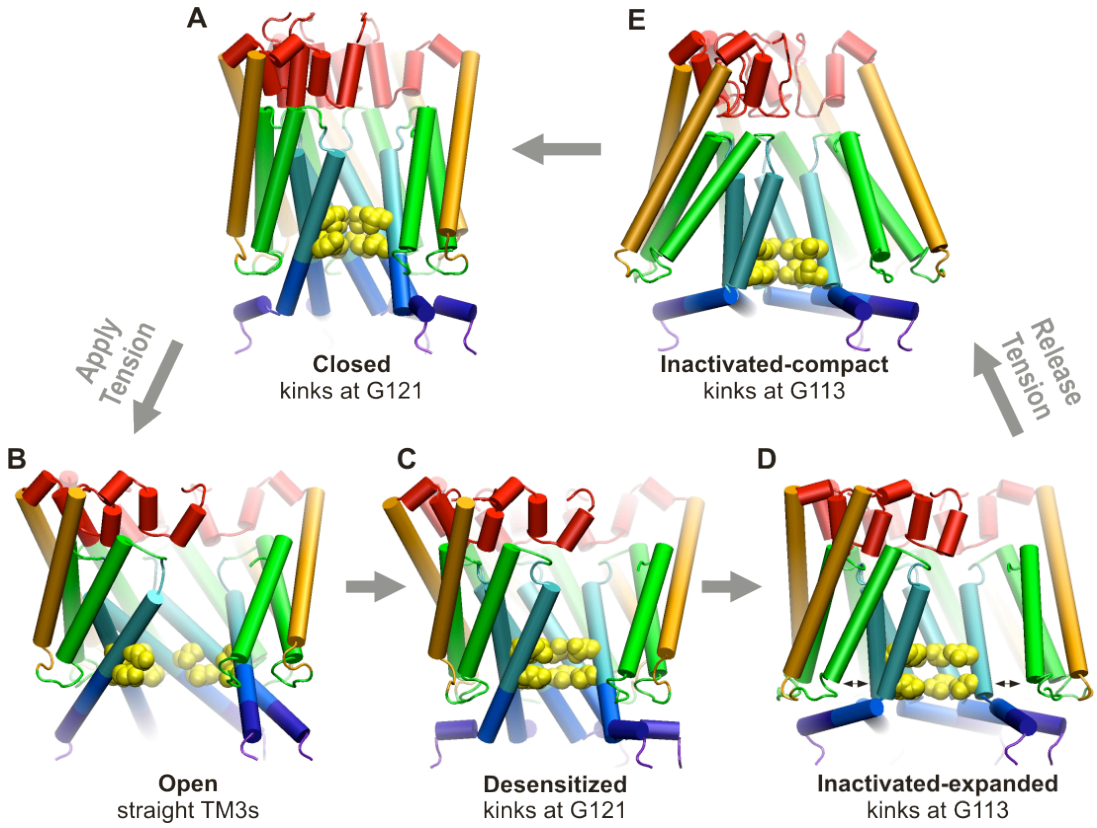

Figure 4-S4. Models representing complete gating cycle of WT MscS.
(A) Channel starts in a compacted resting state with TM3b kinked at G121A. **(B)** Upon application of membrane tension TM1, TM2 and TM3 move outward in a concerted fashion to open the conducting pathway. The TM3 helices straighten and the gate-keeping leucines, L105 and L109 (yellow), swing away from the now hydrated lumen and stabilize the open state. **(C)** At sustained intermediate tensions, the dynamics of TM3s near G121 allows for re-association of the hydrophobic gate, thus the cytoplasmic facing portions of TM1, TM2 and TM3 collapse to expel water from the pore. Since the TM1-TM2 pairs are still associated with TM3a, additional tension can be used to reopen the conducting path. In this model of the desensitized state the kinks in TM3b reform at G121A. **(D)** At intermediate tensions TM3b may buckle at G113. Kink formation at this site favors detachment of TM3a from TM1-TM2 and would decouple the peripheral TM1-TM2 helices from the gate thus rendering it tension-insensitive. In this model of the inactivated state of the channel under tension, the peripheral helices remain in an expanded configuration. **(E)** Upon the release of tension the TM1-TM2 helical pairs are now free to collapse into a 'conical' conformation, which resembles the shape found in the crystal structure. Straightening of TM3 at G113 and reformation of the kink at G121 may limit the rate of recovery for the WT channel back to the resting conformation.

While buckling at G121 takes MscS out of the open state, subsequent helical breaking at G113 leads to channel inactivation. This transition occurs only if membrane tension persists, as lateral forces spreading the helical ends would impose a stronger bending stress near the hydrophobic constriction. The fact that G121A mutation promotes 'silent' inactivation and stabilizes the inactivated state strongly suggests buckling at G121 and G113 is not independent. Imposing stronger helicity at one site increases the probability of buckling at the other and vice versa. Because higher helicity at G121 promotes inactivation, it is likely that buckling at G113 is accompanied by straightening at G121. Higher flexibility at G121 (A120G), on the other hand, promotes fast recovery from the inactivated state (Fig. 4-3F) apparently by facilitating the straightening of TM3b at G113. On a complete release of tension, increased lateral pressure of lipids re-packs the majority of channels into the compact resting state with a characteristic time of ~7 s (Fig. 4-2E). We are currently exploring the possibility of kink propagation during the desensitized-to-inactivated transition where buckling that starts at G121 propagates through TM3b to a new location at G113.

Due to its direct structural connection to TM3b our analysis suggests that the cytoplasmic cage of MscS must be an important regulatory element. In our simulations the cage was not rigid and the equatorial portals, which provide ion passage, could partially constrict. It is yet unclear whether or not these portals can act as a separate gate. Our data show that MscS does not have a separate 'inactivation' gate like many voltage-gated channels. The mutations in TM3 not only changed the characteristics of activation (Edwards et al., 2005) but also enhanced or abolished

closure, desensitization, inactivation and recovery. These results place the structural features that regulate all stages of the gating cycle close to the constriction and suggest that all these functions are fulfilled by the same gate, a conclusion validated by previous study of the bacterial channel NaChBac (Zhao et al., 2004). It is now clear that in the mechanosensitive channel MscS, membrane tension modulates the helical stability of the TM3s to orchestrate its functional cycle.

Acknowledgements

The authors would like to thank Lena Shirinian for generation of some MscS mutants. We also acknowledge Mike Kiyatkin for compiling MscS and MscK homologues and conducting the multiple sequence alignments. The work was supported by NIH grants to Sergei Sukharev.

Chapter 5: General conclusions and future directions

Conclusion 1

The MscS channel has at least four distinct functional states: closed-resting (C), open (O), desensitized (D) and inactivated (I). Normally the channel undergoes sequential transitions between the C, O, D and I states, however, in some mutants we are able to change this sequence and even open new pathways such as inactivation from the closed state.

Characterization of the desensitized and inactivated states

We have yet to make a careful determination of the tension and voltage dependencies for the desensitizing and inactivating transitions. In the initial patch-clamp characterization of WT MscS we were able to observe the time and tension dependent nature of adaptive current decline. We quantified 'inactivation', by fitting with a single exponential, to determine the characteristic time (τ) of current decay. τ was revealed to be dependent on both tension and voltage (Akitake et al., 2005). However, when these experiments were conducted, we did not realize that adaptive current decline in MscS was really the sum of two processes, inactivation and desensitization. By utilizing new pressure protocols and a next generation pressure clamp that can achieve an order of magnitude faster pressure rise times (10 vs 100 ms) we can now separate these two processes in physiology experiments using test-pulses.

I have started these experiments that are aimed at the measurements of both τ_{desens} and τ_{inact} in an extended range of pressures and voltages (-100 to +100 mV). With these data, a tension and voltage dependence landscape can be generated to

visualize how these two physical factors affect the rates of desensitization and inactivation. Early data show that desensitization and inactivation move in opposite directions with respect to their tension sensitivities. This would mean that during the O to D transition MscS shrinks, however the transition from D to I involves expansion in the plane of the membrane. These observations also being to address, mode-shifting, where non-conducting D state channels can reopen at a higher tension. Collection of these data will be critical as they also serve as a basis for comparison in a large number of future experiments targeted at the D and I states such as the effects of mutations, cross-linking, the addition of co-solvents and the replacement of permeant ion species.

Conclusion 2

Opening of the MscS channel is associated with a substantial lateral expansion in the membrane, which is estimated to be between 9 and 18 nm^2. This expansion cannot occur from the crystal structure state therefore packing of the closed-resting channel state must be more compact.

Verifying the closed model of MscS and exploring the role of water in gating

To address this issue we must first seek a better understanding of the nature of MscS gating which is hypothesized to involve 'wetting' and 'dewetting' transitions to either connect or break the aqueous conduction pathway (Anishkin and Sukharev, 2004). This important proposal provides an explanation for the cooperativity of MscS gating (Akitake et al., 2005) and the lack of subconducting states (Shapovalov and Lester,

2004). The involvement of a 'vapor-locking' mechanism to gate MscS contrasts with other channels such as KcsA, which appear to use more tightly associated helices to physically occlude the conduction pathway (Jiang et al., 2002b; Gulbis and Doyle, 2004).

In my experiments of WT MscS I recently observed a strong hysteresis (shift) (Fig. 5-1, black trace) of the midpoint pressure necessary to open versus to close the channel ($\Delta p_{1/2}$ ~20 mmHg) (Akitake, unpublished data). This hysteresis, which was also observed in MscS homologues with a similar pore structure (Nakayama et al., 2007), may be attributable to hydration penalties which need to be overcome in order to wet or dewet the pore. Non-reversibility of the opening and closing transitions has prompted us to look more closely at our original representation of MscS as an equilibrium process (Akitake, 2005). Indeed, it now appears that opening and closing are distinctly non-equilibrium and proceed through different conformational pathways. Although these new observations directly impact our previous calculation of $\Delta A = 18$ nm^2 for MscS opening, they also help to explain the discrepancy of $\Delta A =$ 9 nm^2 measured for MscS closing in liposomes (Sukharev, 2002). To determine a more accurate ΔA for the equilibrium C to O transition I am currently conducting experiments using A98S MscS mutants in which hysteresis is absent (Fig. 5-1, blue trace). A98S is a pore hydration mutant, which shows increased propensity to wet the conduction pathway in MD simulations however its open conductance remains at a WT level. This mutation aims to lower the energetic barriers to wetting and dewetting the MscS pore with the result being more equilibrium behavior.

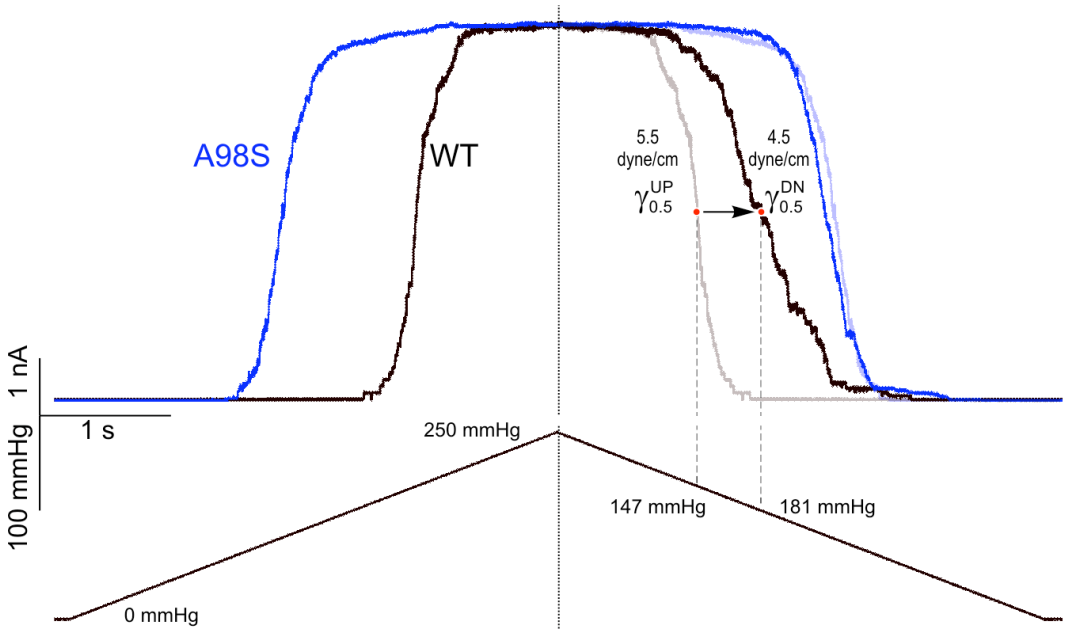

Figure 5-1. Hysteresis of WT MscS and the mutant A98S.

Patch-clamp traces showing the activation of WT MscS (black) and the A98S (blue) mutant with a triangular ramp to saturating pressure. There is strong hysteresis (shift) between the midpoint pressures for the opening and closing in WT MscS. The midpoint difference for WT in this trace is ~Δ30 mmHg. The A98S MscS mutant shows no hysteresis. The shaded grey and light blue traces are symmetric reflections of the opening transitions.

The ΔA's calculated for the opening and closing transitions in A98S were measured to be identically 12 nm^2. Using this and other hydration mutants I hope to clarify the role of hydration in MscS gating and determine if simple capillary dewetting phenomena can define the separation between the forward and backward pathways.

A second experimental aim connected with conclusion 2 is to verify our model of the closed-resting conformation of MscS, which is more compact than the crystal structure. The models of the functional states of MscS, generated by Dr. Anishkin through 'extrapolated motion' of the crystal structure, are by far the most detailed to date. However, the real test of these models lie in the quality of the predictions that they can provide. In a recently completed publication our lab presents the technical details of the 'extrapolated motion' protocol used to generate the closed-resting state model of MscS from the crystal structure and experimental data that supports this conformation (Anishkin et al., 2007).

To test the modeled closed-resting conformation Dr. Anishkin first identified pairs of residues in TM2 and TM3 that when mutated *in silico* to cysteines should be close enough to form disulfide cross-links. These pairs were also selected to be too far from each other, in their crystal conformation, for disulfide bridges to easily form (Table 5-1). Using these predicted residue pairs as a guide (Fig. 5-2A) I generated the corresponding MscS double cysteine mutants. We tested for the presence of cysteine cross-linking in two ways, the first was through western blot analysis of isolated *E. coli* inner membrane expressing the mutant MscS. The analysis, conducted by Dr. Sukharev, under both normal ambient and oxidizing ($+I_2$) conditions showed cross-linking up to the MscS heptamer (Fig. 5-2B).

Table 5-1. Distances between the beta-carbons of the key contact residues in the crystal structure and in the relaxed closed-state models.

Distances were determined after *in-silico* substitutions of these pairs of residues with cysteines. IMXM and 2OAU are the original and revised versions of the crystal structure solved by Rees and coworkers (Bass et al., 2002; Steinbacher et al., 2007).

Structure	L69C-A103C	L69C-A106C	L72C-V99C	L72C-G104C	A106C-G108C	A84C-T93C	V89C-V91C	S95C-I97C
1MXM	15.4	16.9	12.5	12.2	2.9	6.0	5.2	6.4
2OAU	14.1	16.2	10.5	12.9	3.9	12.8	7.6	6.9
Closed model	7.9	7.3	6.6	6.5	2.7	11.5	5.4	6.3

Note: on opening, the distances for the pairs A84C-T93C, V89C-V91C, and S95C-I97C are predicted to increase to 14.4, 9.8 and 16.2 Å respectively.

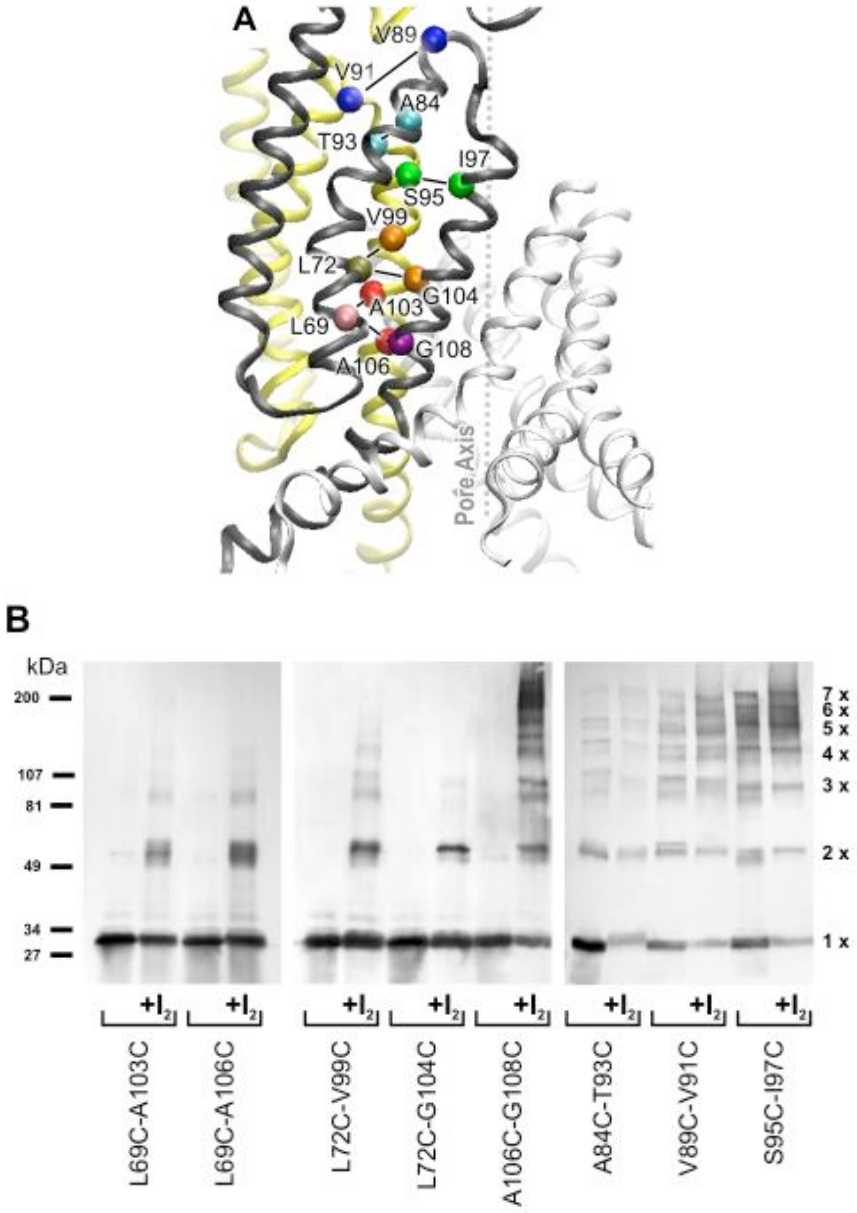

Figure 5-2. Intersubunit contacts in the transmembrane barrel of the MscS close state model. **(A)** Ribbon representation of two adjacent subunits (yellow and black). TM1, TM2 and TM3 helices are in order from left to right. Alpha-carbons of critical residues are shown as spheres. **(B)** Western blots indicating cross-linking products in the double cysteine mutants. Cross-linking was achieved by adding 0.03 mM iodine to native membrane vesicles under isoosmotic conditions (marked $+I_2$). Control lanes (unmarked) represent samples at ambient atmospheric conditions. Protein bands were visualized with anti-His_6 AP-conjugated antibodies. The L69C-A106C and L72C-V99C pairs bridge TM2 to TM3 of the neighbor, whereas A106C-G108C, A84C-T93C, V89C-V91C and S95C-I97C pairs bridge TM3 helices of adjacent subunits.

Control experiments show only dimerization of the single cysteine variant of each mutant (Fig. 5-3). These data strongly suggested that distance predictions from the closed state model were indeed accurate and that the actual resting state of the channel is more compact than the crystal conformation.

I then tested for the functional consequences of cross-linking in these double cysteine mutants through patch clamp analysis (Fig. 5-4). I found initially that many of these double cysteine mutants especially those that showed a strong ability to cross-link in the western blots, were apparently also cross-linked strongly under ambient patching conditions (normal KCl recording buffers). Patches with these mutants like V89C-V91C and A84C-T93C showed little channel activity. Perfusion of 10 mM DTT into the bath, to reduce the disulfide bridges, was observed to restore some activity, however a pre-incubation of these mutant MscS expressing spheroplasts (1 hr in 10mM DTT) was necessary to restore activity to WT levels (Fig. 5-4C, D). In a second type of experiment DTT pre-incubated mutant channels were exposed to I_2 from the pipette (periplasmic) side. In control experiments it was found that the addition of any amount of I_2 to the cytoplasmic face abolished all channel activity even for WT channels. Exposure of the WT channel to I_2 from the pipette showed no effect even for very long experiments (Fig. 5-5A) however patches were unable to seal when I_2 was present at patch formation. For this reason, exposure to I_2 from the pipette side was delayed by diffusion through a small sucrose plug in the pipette tip. For both the L72C-V99C and the A106C-G108C mutants it was observed that channel activity declined over time as higher concentrations of the oxidizing I_2

drove disulfide bridge formation in these mutant channels as compared to controls (Fig. 5-4A, B and 5-5 B).

The patch clamping data show clearly that MscS must move from the positions predicted by the closed state model in order to open and reducing these cross-links restores the ability to open. One mutant in particular, A106C-G108C forms strong cross-links between adjacent TM3-TM3 helices near the channel gate. The location of this pair strongly suggests that the TM3 barrel of resting MscS exists in a near-crystal conformation and must expand in order to conduct. Overall, these experimental data strongly support our proposed model of a more compact closed-resting MscS.

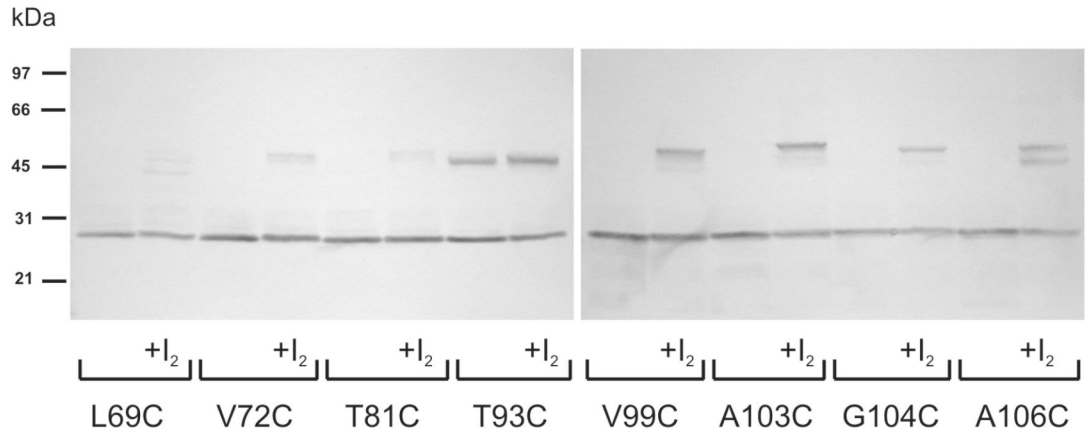

Figure 5-3. Cross-linking controls with single cysteine mutants

Western blot performed with single cysteine mutants under conditions identical to those used for double-cysteine mutants (Fig. 5-2B). Unmarked lanes represent ambient conditions; $+I_2$ indicates the presence of 0.03 mM iodine. It is clear that cysteines inserted in TM3 (residues 93-106) see each other with higher probability that cysteines in TM2 (L69C, L72C) or those in the connecting loop (T81C). None of the cross-links form oligomers higher than 2x thus excluding the possibility of non-specific entrapment of extra subunits. None of these cysteines, except T93C, are close enough to form cross-links under ambient conditions.

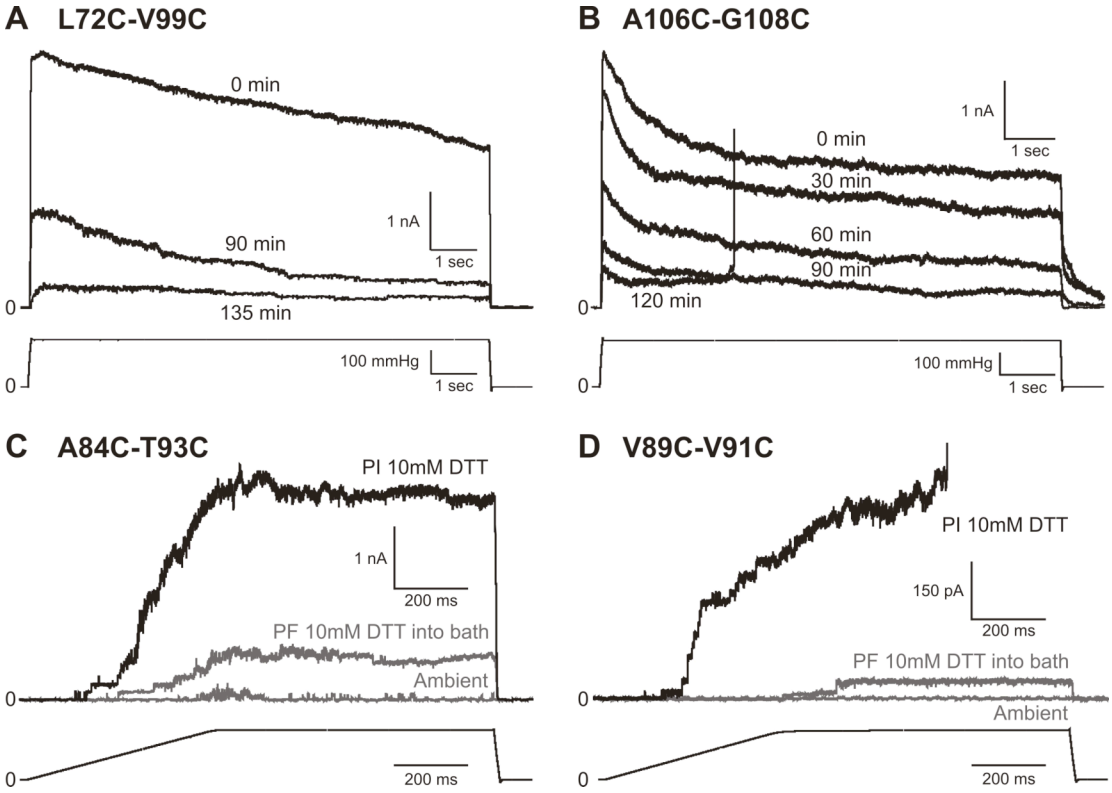

Figure 5-4. A series of traces representing effects of cysteine cross-linking or disulfide reduction on the gating of selected double cysteine mutants.

(A) The effect of adding iodine (0.04 mM) from the pipette (periplasm) on the activity of the L72C-V99C mutant. Spheroplasts were pre-incubated in 5 mM DTT for 1 hr. The data show an obvious decline of channel activity with time as iodine reaches the patch through the sucrose plug. **(B)** A similar experiment displays a reduction in current of the A106C-G108C MscS population. **(C and D)** The A84C-T93C and V89C-V91C pairs located in the upper part of the barrel cross-link spontaneously under ambient conditions, and these channels exhibit very low activity. Perfusion (PF) of 10 mM DTT in the bath restores small fraction of activity, whereas pre-incubation (PI) of spheroplasts with 10 mM DTT for 1 hr restores the population current.

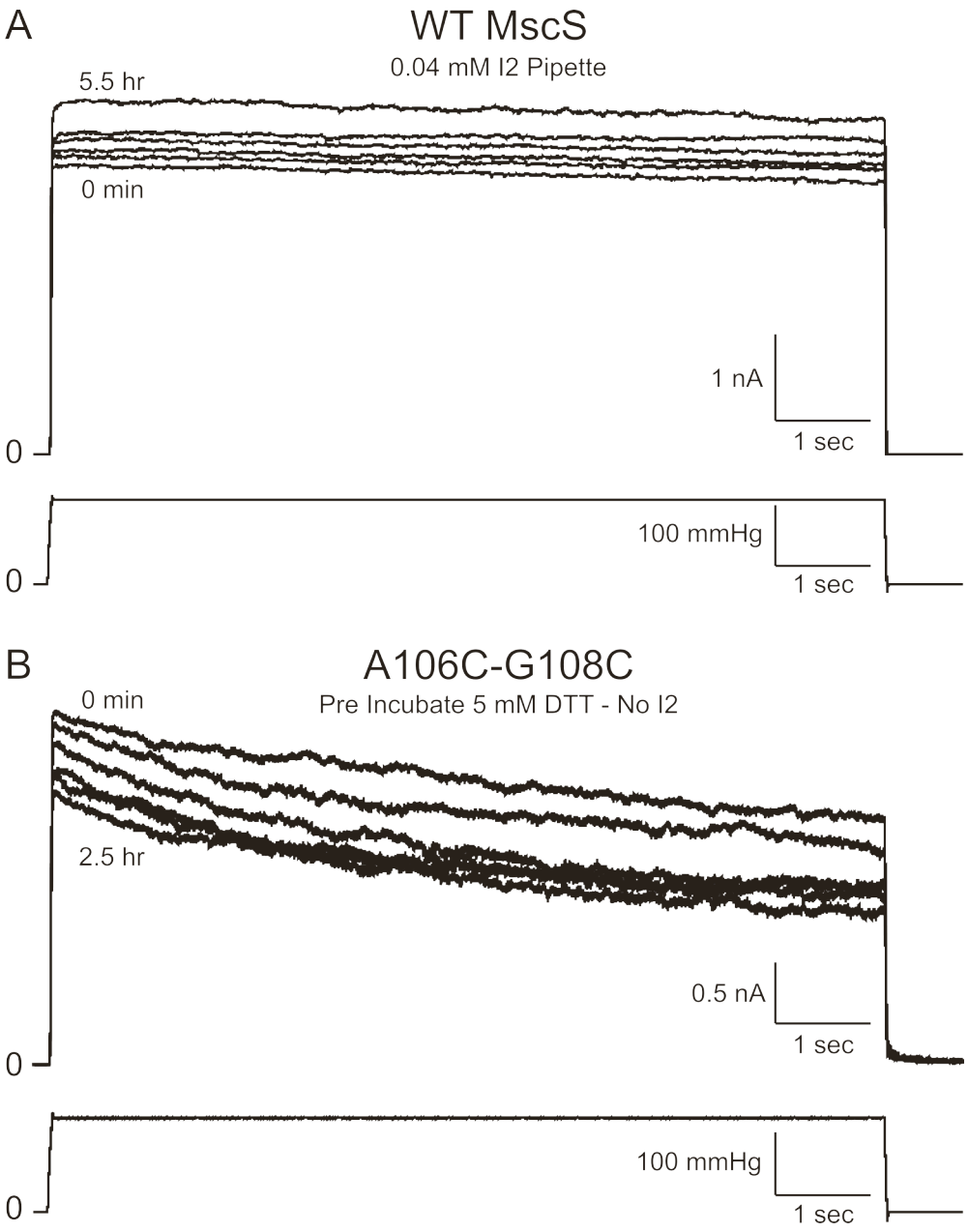

Figure 5-5. A series of control traces representing effects of iodine.
(A) The effect of adding iodine (0.04 mM) from the pipette (periplasm) on the activity of WT MscS. Measure currents were not shown to decline during the course of this 5.5 hr experiment. Currents were actually observed to increase most likely attributable to electrode drift or patch slippage. **(B)** Control experiment showing a time course for DTT pre-incubated A106C-G108C with no I_2 present. Currents are observed to decline slowly as a result of cross-link formation in ambient conditions.

Conclusion 3

We showed in chapter 3 that the effect of TFE incorporation into the cytoplasmic side of the bilayer appears to create extra lateral pressure, which shifts the activation curve of MscS to the right. The addition of TFE also had the effect of accelerating the rate of inactivation. We proposed that this increase in the inactivation rate might be related to partitioning of TFE into the hydrophobic crevices displayed prominently in the crystal structure caused by separation of the peripheral TM1-TM2 helices from TM3. We believe that this helical separation in MscS is a structural feature of the inactivated state.

Exploring the structural features of the inactivated state

The positions of peripheral helices in the inactivated state of MscS are not understood. Modeling and simulations may predict cross-links that stabilize inactivated state. My early attempts to verify the separation of the peripheral TM1-TM2 helices as the mechanism for MscS inactivation proved unsuccessful. The interhelical TM2 to TM3 disulfide mutants L69C-A106C and L72C-V99C were initially designed to prevent this separation and hence stop inactivation. However, cross-link formation of these pairs also prevented channel opening making it impossible to see the effect of these cross-links on inactivation. Pre-treatment of L72C-V99C with DTT to reduce the disulfide bridges did allow for channel opening and it does appear that inactivation is somewhat slowed (Fig. 5-4A). These results however were far from conclusive.

Analyses of the new models and trajectories indicate that there is some tilt and rotation of TM1-TM2 relative to TM3 during opening. Using the models and with the

help of new Tcl script written by Dr. Anishkin, we have also identified a few new pairs of residues between TM2 and TM3 (Table. 5-2) which do not experience as much displacement during the opening transition but are required to separate in the inactivated state. These mutants have not yet been generated. It may, however, still be possible to utilize the current cross-linking mutants L69C-A106C and L72C-V99C to prevent inactivation. I am currently assessing the possible use of bi-functional methanethiosulfonate (MTS) reagents, which have a variable length linked between the functional domains, to allow more conformational freedom for channel opening. MTS reagents react with cysteines to form a disulfide bridges. If an appropriate linker length can be found it may yet be possible to trap the open or desensitized conformations of MscS with these mutants.

Table 5-2. TM2-TM3 cross-linking pairs based on our new models aimed at preventing separation of the peripheral helices during inactivation.

Distances were determined from the beta-carbon positions in models of the MscS closed-resting, open and inactivated states (Akitake et al., 2007). Residue pairs were chosen to minimize movements relative to each other during the closed to open transition and maximize separation in the inactivated state.

Residue Pair	Closed State (Å)	Open State (Å)	Inactivated State (Å)	Subunit Position
T64-S114	4.94	4.54	12.49	Intra-
T64-A110	4.69	7.28	15.18	Intra-
T64-L111	5.19	5.39	16.02	Intra-
F68-A110	5.81	10.52	13.71	Intra-
I57-A103	7.56	7.05	23.89	Inter-

Conclusion 4

Despite early beliefs that MscS was tension and voltage sensitive, we found that its activation was essentially voltage independent. However, inactivation was found to be a voltage dependent process with its rate being observed to increase with the application of higher depolarizing voltages (Akitake et al., 2005). This nature of this voltage-dependence is interesting because it was found to be independent of the static charged residues, the hallmark of traditional voltage sensing, which lie in the transmembrane part of MscS (Nomura et al., 2006b). We hypothesize that it may be the actual ionic current through the channel, which defines the rate of inactivation.

Voltage dependent inactivation and the role of the C-terminal 'cage' domain

Inactivation is one of the most intriguing features of the MscS gating cycle and it is also the least understood. Inactivation appears to underlie the adaptive abilities of MscS, allowing the channel to 'sense' and respond to quickly applied membrane tension while ignoring stimuli that develop more slowly and presumably pose less of a threat (Akitake et al., 2005). Preferential inactivation of MscS also occurs in response to stimuli that are applied quickly but are of too low a magnitude for any risk of lysis. Inactivation has also been demonstrated to be a voltage-dependent process with the rate of inactivation being sped up considerably by depolarizing voltages greater than -40 mV (Akitake et al., 2005).

Our work with the flexibility of TM3, which was presented in chapter 4, highlighted a keen interest in the C-terminal 'cage' domain as a possible regulator of the inactivation process. The involvement of the C-terminal domain of MscS in the

inactivation process is an area of active study for other groups as well. Deletion studies have revealed that almost the entire C-terminal domain is required for proper channel assembly (Miller et al., 2003a). Study of a mild C-terminal truncation mutant (Δ266-286), in which the 7-fold β-barrel forming the base of the cytoplasmic cage was removed, revealed greatly reduced activity and a striking inability to recover from inactivation (Schumann et al., 2004). Cross-linking experiments, targeting multiple lysines concentrated in cage, were demonstrated to affect both MscS inactivation and recovery (Koprowski and Kubalski, 2003). Grajkowski and colleauges noticed that large molecular weight cosolvents, when added from the cytoplasmic face, had a marked effect on MscS inactivation. Data collected with polyethylene glycols (PEGs) of various sizes, showed that smaller molecular weight PEGs, that presumably penetrate the C-terminal cage and make their way to the gate, tended to reduce channel conduction. However, larger PEGs did not affect conduction, rather their presence increased the rate of MscS inactivation.

The structural design of MscS is such that the gate-forming TM3 helix is directly connected the large C-terminal cage domain. I am currently conducting experiments, which aim to decipher the interplay between the opening and inactivation processes with the volume and/or conformation of this hollow domain. Our working hypothesis is that the cage may function as an internal osmosensor that discriminates between the osmotic pressure created by small (permeable) osmolytes from the oncotic pressure created by large macromolecular constituents. If a substance easily penetrates the fenestrations in the cage domain, it will not contribute to a pressure gradient across the cage wall. One example is when the turgor pressure

inside the cell is created primarily by inorganic ions such as potassium during the first stage of the cellular response to hyperosmotic stress. The cage will not experience any extra pressure and the channel will open to release these extra ionic constituents and balance the osmotic gradient. However, larger macromolecules that are cage-impermeable are also too large to be expelled by MscS. If these molecules are responsible for the cellular turgor pressure, their exclusion from the cage will exert a secondary osmotic imbalance on the C-terminal domain, causing its collapse. This mechanism would appear to prevent futile openings that would only destroy the membrane potential and normal ionic gradients. The cage of MscS senses the 'squeezing' action of these high-molecular-weight osmolytes and renders the channel insensitive to membrane tension by driving the gate into an inactivated conformation. Data presented by the Kubalski group (Grajkowski et al., 2005) is highly consistent with this hypothesis.

In a secondary role to being an internal osmosensor, the cage domain of MscS may also act as a voltage or ionic flux sensor. The most recent report by Nomura and coworkers (Nomura et al., 2006b) has demonstrated that the voltage dependence of inactivation remains even when most of the charges in the transmembrane domain are neutralized by mutations. It is important to note that voltage-dependent inactivation is observed to develop only after the channel opens. It appears that high depolarizing potentials are unable to drive the closed channel into the inactivated state. These observations suggest that the ionic flux itself, and/or the accompanying elecroosmotic water flux, drives MscS into the inactivated state.

I am currently working to test both of these hypotheses in patch-clamp experiments of WT MscS. First, in exploring the c-terminal cage domain's role as an osmosensor I have currently designing protocols to characterize the activity of WT MscS in the presence of natural cytoplasmic constituents (spheroplasts attached with membrane permeabilized), high-molecular weight compounds (PEGs) and compatible osmolytes (glutamine, proline and betaine). Preliminary data of MscS inactivation in the presence of 3350 MW PEG, that is reported not to enter the cage, showed a sharp increase in the inactivation rate similar to what was found by the Kubalski group (Grajkowski et al., 2005). However, in my experiments the onset of this faster inactivation occurred at 10 times lower an osmotic differential (adjusted with sorbitol), 30 versus 3 mOsm/kg H_2O, than previously observed (Fig. 5-6). This effect was observed to be more severe as the osmotic differential increased (Fig. 5-6). I am working to verify these results and determine if there is any significance to this discrepancy.

I am just beginning experiments to test the role of the C-terminal cage domain on voltage-dependent inactivation by characterizing the activities of WT MscS in recording solutions where the permeant ion species has been changed or removed. I have so far tried replacing Cl^- with gluconate or glutamate, and K^+ with N-Methyl-D-glucamine (NMDG). My very preliminary data suggest that changing or removing one species of permeant ion can indeed modulate characteristics of MscS inactivation by voltage, though I have yet to reproduce its abolishment.

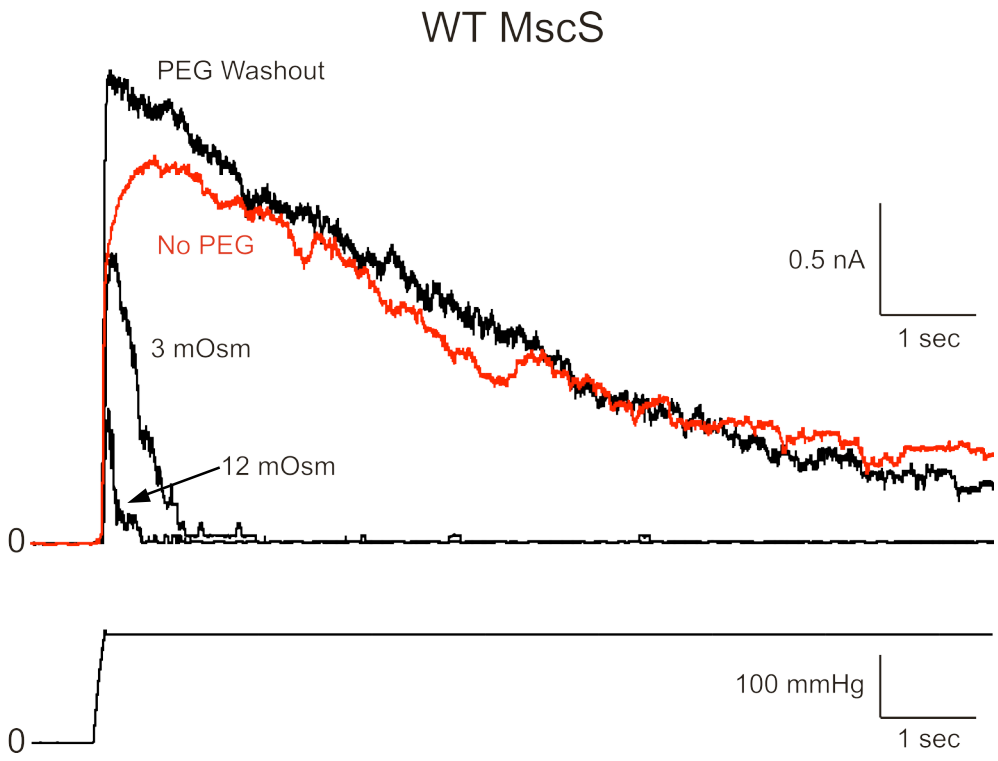

Figure 5-6. Effect of high-molecular weight co-solvent (PEG) on MscS inactivation.
Traces show the effects of adding 3350 MW polyethylene glycol (PEG) to the cytoplasmic (bath) side on WT MscS inactivation. The osmotic pressure of each 4.30% PEG solution was adjusted with sorbitol to 3 and 12 mOsm/kg H_2O. A strong effect is seen at 3 mOsm compared to the wild type response in red. 12 mOsm was made slightly more severe with the 12 mOsm solution. A washout of PEG with regular bath solution restores WT inactivation.

I am currently conducting several control experiments most notably a careful determination of MscS activity in normal KCl recording buffers of different concentrations (low, normal and high salt). These promising data appear consistent with the idea that the voltage sensor in MscS is not located in the membrane where it would perceive static voltage. Rather, it may be that the C-terminal cage domain perceives unbalanced ion fluxes, along with their coupled waters, to change its conformation and by so doing modulates inactivation.

Closing remarks

MscS is undoubtedly a high value system for experimentation and molecular computation that will aid in the discovery of new biophysical principles of ion channel regulation. I am hopeful that the continued study of MscS will eventually link its unique and complex phenomenology to a greater understanding of the mechanisms of cellular/organellar growth, development and flexible adaptation to various environments.

Appendices

Appendix 1 – Variable geometry of membrane patches

The *E. coli* mechanosensitive ion channel MscS is gated directly by tension developed in the lipid bilayer. In their native environment, bacteria can experience this type of stretching force as a result of cell swelling in conditions of osmotic downshock. In my experiments this type of force is emulated by the application of suction (negative pressure) to create a pressure gradient across excised membrane patches containing the MscS channel. In this appendix I will discuss briefly the challenges of quantifying the tension stimuli in patch-clamp experiments and provide some additional justification for our methods of pressure to tension conversion in *E. coli* spheroplasts membranes.

Bubble number: measurement of tip diameter in micropipettes

To determine the tension generated within a membrane patch we employ Laplace's law to relate membrane tension to the applied pressure gradient (Eq. 1).

$$T = (P * r) / 2 \qquad (1)$$

T is tension, P is the pressure and r is the radius of curvature. An explicit radius (r) can be determined by measuring the diameter of the pipette tip, which was done by calculating a bubble number (BN). The methodology for BN measurement is presented in work by Mittman and colleagues (Mittman et al., 1987). The BN relies on the fact that there is a defined transmural pressure (P_b) to produce a stream of air bubbles in a medium with a given surface tension (σ). This pressure is directly related to the diameter (d) of the pipette tip assuming spherical bubble geometry (Eq. 2).

$$P_b = (4 * \sigma) / d \qquad (2)$$

Shown below in Fig. A1-1 is the relationship demonstrated by Mittman and colleagues between the BN, bubble pressure (P_b) and the outer tip diameter of micropipettes (Mittman et al., 1987).

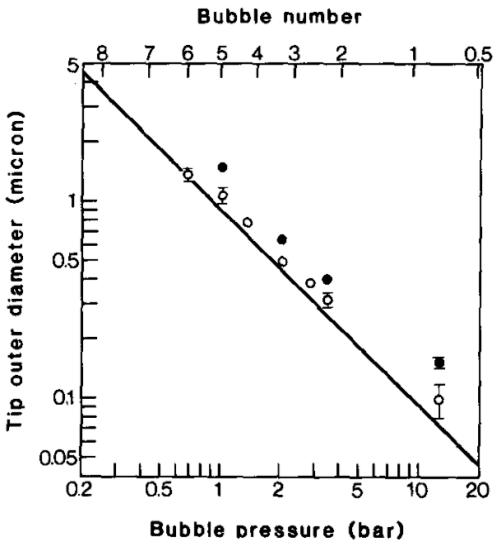

Figure A1-1. Relationship between the bubble number, bubble pressure, and tip outer diameter of micropipettes

Plot of the relationship between the tip outer diameter, the bubble number and bubble pressure in thin-walled (open circles) or thick-walled (closed circles) micropipettes. Bubble number measurements were taken at 20°C in 100% methanol (Mittman et al., 1987).

Modern programmable micropipette pullers such as the Sutter P-97 (Sutter Instruments Co.) that we use, once calibrated, produce highly reproducible tips. After checking 1-2 pulled pipettes by measuring the BN the remainder of the pipettes can generally be trusted.

While the BN is a useful calibrating point, it has been demonstrated through measurement of patch capacitance, that the observed area of the membrane patch is substantially lager than the area corresponding to the pipette tip (Sakmann and Neher, 1995). This occurs because during seal formation the membrane patch is drawn up into the conical tip by ~2-3 μm where the pipette is larger (Sakmann and Neher,

1995). Therefore to accurately measure tension, additional imaging steps are required to determine the curvature in our membrane patches.

Patch shape under pressure

It was found, through imaging of liposome patches in micropipettes, that under an applied pressure gradient excised membrane patches do indeed form spherical caps (Sukharev et al., 1999; Sukharev, 2002; Moe and Blount, 2005). At zero pressure, patches were observed to start out nearly flat with curvature of the patch increasing with pressure. Fortunately, the radius of curvature was shown to saturate near ~4-5 dyne/cm. This implies that after this point the radius of the patch and the applied pressure are independent therefore in this range tension and pressure are proportional (Sukharev et al., 1999; Sukharev, 2002).

Patch curvature in E. coli spheroplasts

In my patch-clamp experiments with MscS a micropipette of BN ~4 was used corresponding to a tip radius of ~0.3 μm. The size of these tips makes difficult the direct observation of membrane patches and currently no experiments have been conducted to measure curvature of spheroplasts patches in micropipettes. Because of this the major question we need to address is: "are the properties spheroplasts patches sufficiently similar to liposomes to allow for Laplace pressure conversion to tension?" The vast majority of the data for MscS activation in *E. coli* spheroplasts seems to indicate that they are as the activities of MscS observed the two environments are essentially indistinguishable (Levina et al., 1999; Sukharev, 2002; Akitake et al., 2005). An analysis of WT MscS traces using Eq. 1, a value of 5.5

dyne/cm as the midpoint activation tension previously determined in liposomes (Sukharev, 2002), and 145 mmHg as the average midpoint activation pressure provides a patch radius of ~0.58 μm. This value is reasonable and consistent given the liposome patch data collected in pipettes with much larger radii (3-5 μm).

Measuring tension in patches of eukaryotic cell membranes

Eukaryotic cells have many features which prokaryotic cells and certainly liposomes lack. In patch-clamp experiments that utilize mechanical stimuli the most notable differences are microvilli or caveolae in the membrane and the presence of an actin cytoskeleton. Though capacitance measurements in *Xenopus* oocytes it was shown that the final area attained by a membrane under pressure was at least 5 times that expected for a smooth sphere despite starting out smooth and flat (Zhang and Hamill, 2000). This extra surface area appears to have come from numerous microvilli or caveolae as they are pulled flat by pressure. It was also observed from imaging mouse myotube patches that the actin cytoskeleton exerts a continuous force on the membrane resulting in a negative curvature of patch at rest (Suchyna and Sachs, 2007). Chemical or physical disruption of the cytoskeleton eliminates this curvature (Suchyna and Sachs 2007). These two experiments clearly demonstrate the difficulties of applying the law of Laplace to convert from pressure to tension in patch-clamp analysis of eukaryotic cells.

References

Akitake, B., A. Anishkin, N. Liu, and S. Sukharev. 2007. Straightening and sequential buckling of the pore-lining helices define the gating cycle of the stretch-activated channel MscS *Manuscript Submitted*.

Akitake, B., A. Anishkin, and S. Sukharev. 2005. The "dashpot" mechanism of stretch-dependent gating in MscS. *The Journal of general physiology*. 125:143-154.

Anishkin, A., B. Akitake, and S. Sukharev. 2007. Characterization of the resting MscS: modeling and analysis of the closed bacterial mechanosensitive channel of small conductance. *Submitted*.

Anishkin, A., C.S. Chiang, and S. Sukharev. 2005. Gain-of-function mutations reveal expanded intermediate states and a sequential action of two gates in MscL. *The Journal of general physiology*. 125:155-170.

Anishkin, A. and S. Sukharev. 2004. Water dynamics and dewetting transitions in the small mechanosensitive channel MscS. *Biophys J*. 86:2883-2895.

Banerjee, T. and N. Kishore. 2005. Does the anesthetic 2,2,2-trifluoroethanol interact with bovine serum albumin by direct binding or by solvent-mediated effects? A calorimetric and spectroscopic investigation. *Biopolymers*. 78:78-86.

Bang, H., Y. Kim, and D. Kim. 2000. TREK-2, a new member of the mechanosensitive tandem-pore K+ channel family. *The Journal of biological chemistry*. 275:17412-17419.

Barrera, F.N., M.L. Renart, M.L. Molina, J.A. Poveda, J.A. Encinar, A.M. Fernandez, J.L. Neira, and J.M. Gonzalez-Ros. 2005. Unfolding and refolding in vitro of a tetrameric, alpha-helical membrane protein: the prokaryotic potassium channel KcsA. *Biochemistry*. 44:14344-14352.

Barry, J.A. and K. Gawrisch. 1994. Direct NMR evidence for ethanol binding to the lipid-water interface of phospholipid bilayers. *Biochemistry*. 33:8082-8088.

Bass, R.B., P. Strop, M. Barclay, and D.C. Rees. 2002. Crystal structure of Escherichia coli MscS, a voltage-modulated and mechanosensitive channel. *Science*. 298:1582-1587.

Beckstein, O. and M.S. Sansom. 2003. Liquid-vapor oscillations of water in hydrophobic nanopores. *Proceedings of the National Academy of Sciences of the United States of America*. 100:7063-7068.

Berrier, C., M. Besnard, B. Ajouz, A. Coulombe, and A. Ghazi. 1996. Multiple mechanosensitive ion channels from Escherichia coli, activated at different thresholds of applied pressure. *The Journal of membrane biology*. 151:175-187.

Besch, S.R., T. Suchyna, and F. Sachs. 2002. High-speed pressure clamp. *Pflugers Arch*. 445:161-166.

Betanzos, M., C.S. Chiang, H.R. Guy, and S. Sukharev. 2002. A large iris-like expansion of a mechanosensitive channel protein induced by membrane tension. *Nature structural biology*. 9:704-710.

Blount, P. and P.C. Moe. 1999. Bacterial mechanosensitive channels: integrating physiology, structure and function. *Trends in microbiology*. 7:420-424.

Bodkin, M.J. and J.M. Goodfellow. 1996. Hydrophobic solvation in aqueous trifluoroethanol solution. *Biopolymers*. 39:43-50.

Booth, I.R. 2003. Bacterial ion channels. *Genetic engineering*. 25:91-111.

Booth, I.R. and P. Louis. 1999. Managing hypoosmotic stress: aquaporins and mechanosensitive channels in Escherichia coli. *Current opinion in microbiology*. 2:166-169.

Britten, R.J. and F.T. McClure. 1962. The amino acid pool in Escherichia coli. *Bacteriological reviews*. 26:292-335.

Cammers-Goodwin, A., T.J. Allen, S.L. Oslick, K.F. McClure, J.H. Lee, and D.S. Kemp. 1996. Mechanism of Stabilization of Helical Conformations of Polypeptides by Water Containing Trifluoroethanol. *J. Am. Chem. Soc.* 118:3082-3090.

Chang, G., R.H. Spencer, A.T. Lee, M.T. Barclay, and D.C. Rees. 1998. Structure of the MscL homolog from Mycobacterium tuberculosis: a gated mechanosensitive ion channel. *Science*. 282:2220-2226.

Chiang, C.S., A. Anishkin, and S. Sukharev. 2004. Gating of the large mechanosensitive channel in situ: estimation of the spatial scale of the transition from channel population responses. *Biophys J*. 86:2846-2861.

Chitra, R. and P.E. Smith. 2001a. A comparison of the properties of 2,2,2-trifluoroethanol and 2,2,2-trifluoroethanol/water mixtures using different force fields. *Journal of Chemical Physics*. 115:5521-5530.

Chitra, R. and P.E. Smith. 2001b. Properties of 2,2,2-trifluoroethanol and water mixtures. *J Chem Phys*. 114:426-435.

Colbert, H.A., T.L. Smith, and C.I. Bargmann. 1997. OSM-9, a novel protein with structural similarity to channels, is required for olfaction, mechanosensation, and olfactory adaptation in Caenorhabditis elegans. *J Neurosci*. 17:8259-8269.

Coraux, C., A. Delplanque, J. Hinnrasky, B. Peault, E. Puchelle, and D. Gaillard. 1998. Distribution of integrins during human fetal lung development. *J Histochem Cytochem*. 46:803-810.

Corey, D.P. 2003. New TRP channels in hearing and mechanosensation. *Neuron*. 39:585-588.

Cortes, D.M. and E. Perozo. 1997. Structural dynamics of the Streptomyces lividans K+ channel (SKC1): oligomeric stoichiometry and stability. *Biochemistry*. 36:10343-10352.

Csonka, L.N. 1989. Physiological and genetic responses of bacteria to osmotic stress. *Microbiological reviews*. 53:121-147.

Csonka, L.N. and A.D. Hanson. 1991. Prokaryotic osmoregulation: genetics and physiology. *Annual review of microbiology*. 45:569-606.

Cui, C. and J. Adler. 1996. Effect of mutation of potassium-efflux system, KefA, on mechanosensitive channels in the cytoplasmic membrane of Escherichia coli. *The Journal of membrane biology*. 150:143-152.

Cui, C., D.O. Smith, and J. Adler. 1995. Characterization of mechanosensitive channels in Escherichia coli cytoplasmic membrane by whole-cell patch clamp recording. *The Journal of membrane biology*. 144:31-42.

Deshusses, J.M., J.A. Burgess, A. Scherl, Y. Wenger, N. Walter, V. Converset, S. Paesano, G.L. Corthals, D.F. Hochstrasser, and J.C. Sanchez. 2003. Exploitation of specific properties of trifluoroethanol for extraction and separation of membrane proteins. *Proteomics*. 3:1418-1424.

Ding, S., L. Ingleby, C.A. Ahern, and R. Horn. 2005. Investigating the putative glycine hinge in Shaker potassium channel. *The Journal of general physiology*. 126:213-226.

Edwards, M.D., I.R. Booth, and S. Miller. 2004. Gating the bacterial mechanosensitive channels: MscS a new paradigm? *Current opinion in microbiology*. 7:163-167.

Edwards, M.D., Y. Li, S. Kim, S. Miller, W. Bartlett, S. Black, S. Dennison, I. Iscla, P. Blount, J.U. Bowie, and I.R. Booth. 2005. Pivotal role of the glycine-rich TM3 helix in gating the MscS mechanosensitive channel. *Nature structural & molecular biology*. 12:113-119.

Eisenberg, D., E. Schwarz, M. Komaromy, and R. Wall. 1984. Analysis of membrane and surface protein sequences with the hydrophobic moment plot. *Journal of molecular biology*. 179:125-142.

Epstein, W. 2003. The roles and regulation of potassium in bacteria. *Progress in nucleic acid research and molecular biology*. 75:293-320.

Ferguson, G.P., J.R. Battista, A.T. Lee, and I.R. Booth. 2000. Protection of the DNA during the exposure of Escherichia coli cells to a toxic metabolite: the role of the KefB and KefC potassium channels. *Molecular microbiology*. 35:113-122.

Fink, M., F. Lesage, F. Duprat, C. Heurteaux, R. Reyes, M. Fosset, and M. Lazdunski. 1998. A neuronal two P domain K+ channel stimulated by arachidonic acid and polyunsaturated fatty acids. *The EMBO journal*. 17:3297-3308.

Grajkowski, W., A. Kubalski, and P. Koprowski. 2005. Surface changes of the mechanosensitive channel MscS upon its activation, inactivation, and closing. *Biophys J*. 88:3050-3059.

Gulbis, J.M. and D.A. Doyle. 2004. Potassium channel structures: do they conform? *Current opinion in structural biology*. 14:440-446.

Gullingsrud, J. and K. Schulten. 2003. Gating of MscL studied by steered molecular dynamics. *Biophys J*. 85:2087-2099.

Hamill, O.P., A. Marty, E. Neher, B. Sakmann, and F.J. Sigworth. 1981. Improved patch-clamp techniques for high-resolution current recording from cells and cell-free membrane patches. *Pflugers Arch*. 391:85-100.

Haswell, E.S. and E.M. Meyerowitz. 2006. MscS-like proteins control plastid size and shape in Arabidopsis thaliana. *Curr Biol*. 16:1-11.

Heerklotz, H. 2001. Membrane stress and permeabilization induced by asymmetric incorporation of compounds. *Biophys J*. 81:184-195.

Hong, D.P., M. Hoshino, R. Kuboi, and Y. Goto. 1999. Clustering of Fluorine-Substituted Alcohols as a Factor Responsible for Their Marked Effects on Proteins and Peptides. *J. Am. Chem. Soc.* 121:8427-8433.

Honore, E., A.J. Patel, J. Chemin, T. Suchyna, and F. Sachs. 2006. Desensitization of mechano-gated K2P channels. *Proceedings of the National Academy of Sciences of the United States of America*. 103:6859-6864.

Humphrey, W., A. Dalke, and K. Schulten. 1996. VMD: visual molecular dynamics. *Journal of molecular graphics*. 14:33-38, 27-38.

Ingber, D.E. 2006. Cellular mechanotransduction: putting all the pieces together again. *Faseb J*. 20:811-827.

Jasanoff, A. and A.R. Fersht. 1994. Quantitative determination of helical propensities from trifluoroethanol titration curves. *Biochemistry*. 33:2129-2135.

Jiang, Y., A. Lee, J. Chen, M. Cadene, B.T. Chait, and R. MacKinnon. 2002a. Crystal structure and mechanism of a calcium-gated potassium channel. *Nature*. 417:515-522.

Jiang, Y., A. Lee, J. Chen, M. Cadene, B.T. Chait, and R. MacKinnon. 2002b. The open pore conformation of potassium channels. *Nature*. 417:523-526.

Jiang, Y., A. Lee, J. Chen, V. Ruta, M. Cadene, B.T. Chait, and R. MacKinnon. 2003a. X-ray structure of a voltage-dependent K+ channel. *Nature*. 423:33-41.

Jiang, Y., V. Ruta, J. Chen, A. Lee, and R. MacKinnon. 2003b. The principle of gating charge movement in a voltage-dependent K+ channel. *Nature*. 423:42-48.

Jorgensen, W.L., J. Chandrasekhar, and J.D. Madura. 1983. Comparison of simple potential functions for simulating liquid water. *J Chem Phys*. 79:926--935.

Kanjilal, S., N. Taulier, J.Y. Le Huerou, M. Gindre, W. Urbach, and M. Waks. 2003. Ultrasonic studies of alcohol-induced transconformation in beta-lactoglobulin: the intermediate state. *Biophys J*. 85:3928-3934.

Kellenberger, S., J.W. West, W.A. Catterall, and T. Scheuer. 1997. Molecular analysis of potential hinge residues in the inactivation gate of brain type IIA Na+ channels. *The Journal of general physiology*. 109:607-617.

Kentsis, A. and T.R. Sosnick. 1998. Trifluoroethanol promotes helix formation by destabilizing backbone exposure: desolvation rather than native hydrogen bonding defines the kinetic pathway of dimeric coiled coil folding. *Biochemistry*. 37:14613-14622.

Kernan, M., D. Cowan, and C. Zuker. 1994. Genetic dissection of mechanosensory transduction: mechanoreception-defective mutations of Drosophila. *Neuron*. 12:1195-1206.

Koch, A.L. and S. Woeste. 1992. Elasticity of the sacculus of Escherichia coli. *Journal of bacteriology*. 174:4811-4819.

Koehl, P. 2006. Electrostatics calculations: latest methodological advances. *Current opinion in structural biology*. 16:142-151.

Koenig, B.W. and K. Gawrisch. 2005. Lipid-ethanol interaction studied by NMR on bicelles. *The journal of physical chemistry*. 109:7540-7547.

Komuro, I. and Y. Yazaki. 1993. Control of cardiac gene expression by mechanical stress. *Annual review of physiology*. 55:55-75.

Koprowski, P. and A. Kubalski. 1998. Voltage-independent adaptation of mechanosensitive channels in Escherichia coli protoplasts. *The Journal of membrane biology*. 164:253-262.

Koprowski, P. and A. Kubalski. 2003. C termini of the Escherichia coli mechanosensitive ion channel (MscS) move apart upon the channel opening. *The Journal of biological chemistry*. 278:11237-11245.

Kumar, Y., S. Muzammil, and S. Tayyab. 2005. Influence of fluoro, chloro and alkyl alcohols on the folding pathway of human serum albumin. *Journal of biochemistry*. 138:335-341.

Lai, C.C., K. Hong, M. Kinnell, M. Chalfie, and M. Driscoll. 1996. Sequence and transmembrane topology of MEC-4, an ion channel subunit required for mechanotransduction in Caenorhabditis elegans. *The Journal of cell biology*. 133:1071-1081.

Lammerding, J., R.D. Kamm, and R.T. Lee. 2004. Mechanotransduction in cardiac myocytes. *Annals of the New York Academy of Sciences*. 1015:53-70.

Lesage, F., E. Guillemare, M. Fink, F. Duprat, M. Lazdunski, G. Romey, and J. Barhanin. 1996a. TWIK-1, a ubiquitous human weakly inward rectifying K+ channel with a novel structure. *The EMBO journal*. 15:1004-1011.

Lesage, F., M. Mattei, M. Fink, J. Barhanin, and M. Lazdunski. 1996b. Assignment of the human weak inward rectifier K+ channel TWIK-1 gene to chromosome 1q42-q43. *Genomics*. 34:153-155.

Levina, N., S. Totemeyer, N.R. Stokes, P. Louis, M.A. Jones, and I.R. Booth. 1999. Protection of Escherichia coli cells against extreme turgor by activation of MscS and MscL mechanosensitive channels: identification of genes required for MscS activity. *The EMBO journal*. 18:1730-1737.

Li, Y., P.C. Moe, S. Chandrasekaran, I.R. Booth, and P. Blount. 2002. Ionic regulation of MscK, a mechanosensitive channel from Escherichia coli. *The EMBO journal*. 21:5323-5330.

Liu, L.P. and C.M. Deber. 1998. Uncoupling hydrophobicity and helicity in transmembrane segments. Alpha-helical propensities of the amino acids in non-polar environments. *The Journal of biological chemistry*. 273:23645-23648.

Lomize, A.L., I.D. Pogozheva, M.A. Lomize, and H.I. Mosberg. 2006. Positioning of proteins in membranes: a computational approach. *Protein Sci*. 15:1318-1333.

Long, S.B., E.B. Campbell, and R. Mackinnon. 2005. Crystal structure of a mammalian voltage-dependent Shaker family K+ channel. *Science*. 309:897-903.

Lu, H., M. Buck, S.E. Radford, and C.M. Dobson. 1997. Acceleration of the folding of hen lysozyme by trifluoroethanol. *Journal of molecular biology*. 265:112-117.

Luo, P. and R.L. Baldwin. 1999. Interaction between water and polar groups of the helix backbone: an important determinant of helix propensities. *Proceedings of the National Academy of Sciences of the United States of America*. 96:4930-4935.

MacKerell, A.D., D. Bashford, M. Bellott, R.L. Dunbrack, J.D. Evanseck, M.J. Field, S. Fischer, J. Gao, H. Guo, S. Ha, D. Joseph-McCarthy, L. Kuchnir, K. Kuczera, F.T.K. Lau, C. Mattos, S. Michnick, T. Ngo, D.T. Nguyen, B. Prodhom, W.E. Reiher, B. Roux, M. Schlenkrich, J.C. Smith, R. Stote, J. Straub, M. Watanabe, J. Wiorkiewicz-Kuczera, D. Yin, and M. Karplus. 1998. All-atom empirical

potential for molecular modeling and dynamics studies of proteins. *J Phys Chem B*. 102:3586-3616.

Magidovich, E. and O. Yifrach. 2004. Conserved gating hinge in ligand- and voltage-dependent K+ channels. *Biochemistry*. 43:13242-13247.

Main, E.R. and S.E. Jackson. 1999. Does trifluoroethanol affect folding pathways and can it be used as a probe of structure in transition states? *Nature structural biology*. 6:831-835.

Maingret, F., M. Fosset, F. Lesage, M. Lazdunski, and E. Honore. 1999. TRAAK is a mammalian neuronal mechano-gated K+ channel. *The Journal of biological chemistry*. 274:1381-1387.

Martinac, B. 2001. Mechanosensitive channels in prokaryotes. *Cell Physiol Biochem*. 11:61-76.

Martinac, B., J. Adler, and C. Kung. 1990. Mechanosensitive ion channels of E. coli activated by amphipaths. *Nature*. 348:261-263.

Martinac, B., M. Buechner, A.H. Delcour, J. Adler, and C. Kung. 1987. Pressure-sensitive ion channel in Escherichia coli. *Proceedings of the National Academy of Sciences of the United States of America*. 84:2297-2301.

McLaggan, D., M.A. Jones, G. Gouesbet, N. Levina, S. Lindey, W. Epstein, and I.R. Booth. 2002. Analysis of the kefA2 mutation suggests that KefA is a cation-specific channel involved in osmotic adaptation in Escherichia coli. *Molecular microbiology*. 43:521-536.

McLaggan, D., J. Naprstek, E.T. Buurman, and W. Epstein. 1994. Interdependence of K+ and glutamate accumulation during osmotic adaptation of Escherichia coli. *The Journal of biological chemistry*. 269:1911-1917.

Miller, S., W. Bartlett, S. Chandrasekaran, S. Simpson, M. Edwards, and I.R. Booth. 2003a. Domain organization of the MscS mechanosensitive channel of Escherichia coli. *The EMBO journal*. 22:36-46.

Miller, S., M.D. Edwards, C. Ozdemir, and I.R. Booth. 2003b. The closed structure of the MscS mechanosensitive channel. Cross-linking of single cysteine mutants. *The Journal of biological chemistry*. 278:32246-32250.

Mittman, S., D.G. Flaming, D.R. Copenhagen, and J.H. Belgum. 1987. Bubble pressure measurement of micropipet tip outer diameter. *Journal of neuroscience methods*. 22:161-166.

Moe, P. and P. Blount. 2005. Assessment of potential stimuli for mechano-dependent gating of MscL: effects of pressure, tension, and lipid headgroups. *Biochemistry*. 44:12239-12244.

Nakayama, Y., K. Fujiu, M. Sokabe, and K. Yoshimura. 2007. Molecular and electrophysiological characterization of a mechanosensitive channel expressed in the chloroplasts of Chlamydomonas. *Proceedings of the National Academy of Sciences of the United States of America*.

Nelson, J.W. and N.R. Kallenbach. 1986. Stabilization of the ribonuclease S-peptide alpha-helix by trifluoroethanol. *Proteins*. 1:211-217.

Nomura, T., M. Sokabe, and K. Yoshimura. 2006a. Lipid-protein interaction of the MscS mechanosensitive channel examined by scanning mutagenesis. *Biophys J*. 91:2874-2881.

Nomura, T., K. Yoshimura, and M. Sokabe. 2006b. Voltage dependence of the adaptation in MscS occurs independent of the charged residues in the transmembrane domain. *Biophys J*. 90A:

O'Neil, R.G. and S. Heller. 2005. The mechanosensitive nature of TRPV channels. *Pflugers Arch*. 451:193-203.

Okada, K., P.C. Moe, and P. Blount. 2002. Functional design of bacterial mechanosensitive channels. Comparisons and contrasts illuminated by random mutagenesis. *The Journal of biological chemistry*. 277:27682-27688.

Ou, X., P. Blount, R.J. Hoffman, and C. Kung. 1998. One face of a transmembrane helix is crucial in mechanosensitive channel gating. *Proceedings of the National Academy of Sciences of the United States of America*. 95:11471-11475.

Ozdirekcan, S., D.T. Rijkers, R.M. Liskamp, and J.A. Killian. 2005. Influence of flanking residues on tilt and rotation angles of transmembrane peptides in lipid bilayers. A solid-state 2H NMR study. *Biochemistry*. 44:1004-1012.

Perozo, E., A. Kloda, D.M. Cortes, and B. Martinac. 2002. Physical principles underlying the transduction of bilayer deformation forces during mechanosensitive channel gating. *Nature structural biology*. 9:696-703.

Phillips, J.C., R. Braun, W. Wang, J. Gumbart, E. Tajkhorshid, E. Villa, C. Chipot, R.D. Skeel, L. Kale, and K. Schulten. 2005. Scalable molecular dynamics with NAMD. *J Comput Chem*. 26:1781-1802.

Pivetti, C.D., M.R. Yen, S. Miller, W. Busch, Y.H. Tseng, I.R. Booth, and M.H. Saier, Jr. 2003. Two families of mechanosensitive channel proteins. *Microbiol Mol Biol Rev*. 67:66-85, table of contents.

Popot, J.L. and D.M. Engelman. 2000. Helical membrane protein folding, stability, and evolution. *Annual review of biochemistry*. 69:881-922.

Qin, Z. and T.C. Squier. 2001. Calcium-dependent stabilization of the central sequence between Met(76) and Ser(81) in vertebrate calmodulin. *Biophys J*. 81:2908-2918.

Rajan, R. and P. Balaram. 1996. A model for the interaction of trifluoroethanol with peptides and proteins. *International journal of peptide and protein research*. 48:328-336.

Reiersen, H. and A.R. Rees. 2000. Trifluoroethanol may form a solvent matrix for assisted hydrophobic interactions between peptide side chains. *Protein engineering*. 13:739-743.

Reyes, R., F. Duprat, F. Lesage, M. Fink, M. Salinas, N. Farman, and M. Lazdunski. 1998. Cloning and expression of a novel pH-sensitive two pore domain K+ channel from human kidney. *The Journal of biological chemistry*. 273:30863-30869.

Robert Fraczkiewicz, W.B. 1998. Exact and efficient analytical calculation of the accessible surface areas and their gradients for macromolecules. *Journal of Computational Chemistry*. 19:319-333.

Roccatano, D., G. Colombo, M. Fioroni, and A.E. Mark. 2002. Mechanism by which 2,2,2-trifluoroethanol/water mixtures stabilize secondary-structure formation in peptides: a molecular dynamics study. *Proceedings of the National Academy of Sciences of the United States of America*. 99:12179-12184.

Ruthe, H.J. and J. Adler. 1985. Fusion of bacterial spheroplasts by electric fields. *Biochimica et biophysica acta*. 819:105-113.

Sachs, F. 1992. Stretch-sensitive ion channels: an update. *Society of General Physiologists series*. 47:241-260.

Sachs, F. and C.E. Morris. 1998. Mechanosensitive ion channels in nonspecialized cells. *Reviews of physiology, biochemistry and pharmacology*. 132:1-77.

Sakmann, B. and E. Neher. 1995. Single-Channel Recording. Vol. 2nd edition. Plenum Press, New York and London.

Sanchez-Esteban, J., Y. Wang, E.J. Filardo, L.P. Rubin, and D.E. Ingber. 2006. Integrins beta1, alpha6, and alpha3 contribute to mechanical strain-induced differentiation of fetal lung type II epithelial cells via distinct mechanisms. *American journal of physiology*. 290:L343-350.

Schleyer, M., R. Schmid, and E.P. Bakker. 1993. Transient, specific and extremely rapid release of osmolytes from growing cells of Escherichia coli K-12 exposed to hypoosmotic shock. *Archives of microbiology*. 160:424-431.

Schober, M., S. Raghavan, M. Nikolova, L. Polak, H.A. Pasolli, H.E. Beggs, L.F. Reichardt, and E. Fuchs. 2007. Focal adhesion kinase modulates tension signaling to control actin and focal adhesion dynamics. *The Journal of cell biology*. 176:667-680.

Schumann, U., M.D. Edwards, C. Li, and I.R. Booth. 2004. The conserved carboxy-terminus of the MscS mechanosensitive channel is not essential but increases stability and activity. *FEBS letters*. 572:233-237.

Serrano, L., J.L. Neira, J. Sancho, and A.R. Fersht. 1992. Effect of alanine versus glycine in alpha-helices on protein stability. *Nature*. 356:453-455.

Shapovalov, G. and H.A. Lester. 2004. Gating transitions in bacterial ion channels measured at 3 microns resolution. *The Journal of general physiology*. 124:151-161.

Shealy, R.T., A.D. Murphy, R. Ramarathnam, E. Jakobsson, and S. Subramaniam. 2003. Sequence-function analysis of the K+-selective family of ion channels using a comprehensive alignment and the KcsA channel structure. *Biophys J*. 84:2929-2942.

Sheetz, M.P. and S.J. Singer. 1974. Biological membranes as bilayer couples. A molecular mechanism of drug-erythrocyte interactions. *Proceedings of the National Academy of Sciences of the United States of America*. 71:4457-4461.

Simons, K.T., R. Bonneau, I. Ruczinski, and D. Baker. 1999. Ab initio protein structure prediction of CASP III targets using ROSETTA. *Proteins*. Suppl 3:171-176.

Simons, K.T., C. Kooperberg, E. Huang, and D. Baker. 1997. Assembly of protein tertiary structures from fragments with similar local sequences using simulated annealing and Bayesian scoring functions. *Journal of molecular biology*. 268:209-225.

Simons, K.T., C. Strauss, and D. Baker. 2001. Prospects for ab initio protein structural genomics. *Journal of molecular biology*. 306:1191-1199.

Sonnichsen, F.D., J.E. Van Eyk, R.S. Hodges, and B.D. Sykes. 1992. Effect of trifluoroethanol on protein secondary structure: an NMR and CD study using a synthetic actin peptide. *Biochemistry*. 31:8790-8798.

Sotomayor, M. and K. Schulten. 2004. Molecular dynamics study of gating in the mechanosensitive channel of small conductance MscS. *Biophys J*. 87:3050-3065.

Sotomayor, M., T.A. van der Straaten, U. Ravaioli, and K. Schulten. 2006a. Electrostatic properties of the mechanosensitive channel of small conductance MscS. *Biophys J*. 90:3496-3510.

Sotomayor, M., V. Vasquez, E. Perozo, and K. Schulten. 2006b. Ion Conduction through MscS as Determined by Electrophysiology and Simulation. *Biophys J*.

Spelbrink, R.E., A. Kolkman, M. Slijper, J.A. Killian, and B. de Kruijff. 2005. Detection and identification of stable oligomeric protein complexes in Escherichi coli inner membranes: a proteomics approach. *The Journal of biological chemistry*. 280:28742-28748.

Spronk, S.A., D.E. Elmore, and D.A. Dougherty. 2006. Voltage-dependent hydration and conduction properties of the hydrophobic pore of the mechanosensitive channel of small conductance. *Biophys J*. 90:3555-3569.

Steinbacher, S., R. Bass, P. Strop, and D.C. Rees. 2007. Structures of the Prokaryotic Mechanosensitive Channels MscL and MscS. *Current Topics in Membranes*. 58:

Stenberg, F., P. Chovanec, S.L. Maslen, C.V. Robinson, L.L. Ilag, G. von Heijne, and D.O. Daley. 2005. Protein complexes of the Escherichia coli cell envelope. *The Journal of biological chemistry*. 280:34409-34419.

Strandberg, E., S. Ozdirekcan, D.T. Rijkers, P.C. van der Wel, R.E. Koeppe, 2nd, R.M. Liskamp, and J.A. Killian. 2004. Tilt angles of transmembrane model peptides in oriented and non-oriented lipid bilayers as determined by 2H solid-state NMR. *Biophys J*. 86:3709-3721.

Suchyna, T.M. and F. Sachs. 2007. Mechanosensitive Channel Properties and Membrane Mechanics in Mouse Dystrophic Myotubes. *The Journal of physiology*.

Sukharev, S. 2002. Purification of the small mechanosensitive channel of Escherichia coli (MscS): the subunit structure, conduction, and gating characteristics in liposomes. *Biophys J*. 83:290-298.

Sukharev, S., B. Akitake, and A. Anishkin. 2007. The Bacterial Mechanosensitive Channel MscS: Emerging Principles of Gating and Modulation. *Current Topics in Membranes*. 58:

Sukharev, S. and D.P. Corey. 2004. Mechanosensitive channels: multiplicity of families and gating paradigms. *Sci STKE*. 2004:re4.

Sukharev, S.I., P. Blount, B. Martinac, F.R. Blattner, and C. Kung. 1994. A large-conductance mechanosensitive channel in E. coli encoded by mscL alone. *Nature*. 368:265-268.

Sukharev, S.I., P. Blount, B. Martinac, and C. Kung. 1997. Mechanosensitive channels of Escherichia coli: the MscL gene, protein, and activities. *Annual review of physiology*. 59:633-657.

Sukharev, S.I., B. Martinac, V.Y. Arshavsky, and C. Kung. 1993. Two types of mechanosensitive channels in the Escherichia coli cell envelope: solubilization and functional reconstitution. *Biophys J*. 65:177-183.

Sukharev, S.I., W.J. Sigurdson, C. Kung, and F. Sachs. 1999. Energetic and spatial parameters for gating of the bacterial large conductance mechanosensitive channel, MscL. *The Journal of general physiology*. 113:525-540.

Suzuki, M., Y. Watanabe, Y. Oyama, A. Mizuno, E. Kusano, A. Hirao, and S. Ookawara. 2003. Localization of mechanosensitive channel TRPV4 in mouse skin. *Neuroscience letters*. 353:189-192.

Tabuchi, K., M. Suzuki, A. Mizuno, and A. Hara. 2005. Hearing impairment in TRPV4 knockout mice. *Neuroscience letters*. 382:304-308.

Tama, F. and C.L. Brooks. 2006. Symmetry, form, and shape: guiding principles for robustness in macromolecular machines. *Annual review of biophysics and biomolecular structure*. 35:115-133.

Tavernarakis, N. and M. Driscoll. 2001. Mechanotransduction in Caenorhabditis elegans: the role of DEG/ENaC ion channels. *Cell biochemistry and biophysics*. 35:1-18.

Toyoshima, C., M. Nakasako, H. Nomura, and H. Ogawa. 2000. Crystal structure of the calcium pump of sarcoplasmic reticulum at 2.6 A resolution. *Nature*. 405:647-655.

Tsapis, A. and A. Kepes. 1977. Transient breakdown of the permeability barrier of the membrane of Escherichia coli upon hypoosmotic shock. *Biochimica et biophysica acta*. 469:1-12.

van den Brink-van der Laan, E., V. Chupin, J.A. Killian, and B. de Kruijff. 2004. Stability of KcsA tetramer depends on membrane lateral pressure. *Biochemistry*. 43:4240-4250.

Vasquez, V. and E. Perozo. 2004. Voltage Dependent Gating in MscS. *Biophys J*. 86:545a.

Virtanen, I., A. Laitinen, T. Tani, P. Paakko, L.A. Laitinen, R.E. Burgeson, and V.P. Lehto. 1996. Differential expression of laminins and their integrin receptors in developing and adult human lung. *American journal of respiratory cell and molecular biology*. 15:184-196.

Walker, R.G., A.T. Willingham, and C.S. Zuker. 2000. A Drosophila mechanosensory transduction channel. *Science*. 287:2229-2234.

Wetzel, C., J. Hu, D. Riethmacher, A. Benckendorff, L. Harder, A. Eilers, R. Moshourab, A. Kozlenkov, D. Labuz, O. Caspani, B. Erdmann, H. Machelska, P.A. Heppenstall, and G.R. Lewin. 2007. A stomatin-domain protein essential for touch sensation in the mouse. *Nature*. 445:206-209.

White, S.H. and W.C. Wimley. 1998. Hydrophobic interactions of peptides with membrane interfaces. *Biochimica et biophysica acta*. 1376:339-352.

White, S.H. and W.C. Wimley. 1999. Membrane protein folding and stability: physical principles. *Annual review of biophysics and biomolecular structure*. 28:319-365.

Wienk, H.L., M. Czisch, and B. de Kruijff. 1999. The structural flexibility of the preferredoxin transit peptide. *FEBS letters*. 453:318-326.

Wood, J.M. 1999. Osmosensing by bacteria: signals and membrane-based sensors. *Microbiol Mol Biol Rev*. 63:230-262.

Wood, J.M., E. Bremer, L.N. Csonka, R. Kraemer, B. Poolman, T. van der Heide, and L.T. Smith. 2001. Osmosensing and osmoregulatory compatible solute accumulation by bacteria. *Comparative biochemistry and physiology*. 130:437-460.

Zhang, Y., F. Gao, V.L. Popov, J.W. Wen, and O.P. Hamill. 2000. Mechanically gated channel activity in cytoskeleton-deficient plasma membrane blebs and vesicles from Xenopus oocytes. *The Journal of physiology*. 523 Pt 1:117-130.

Zhang, Y. and O.P. Hamill. 2000. On the discrepancy between whole-cell and membrane patch mechanosensitivity in Xenopus oocytes. *The Journal of physiology*. 523 Pt 1:101-115.

Zhao, Y., V. Yarov-Yarovoy, T. Scheuer, and W.A. Catterall. 2004. A gating hinge in Na+ channels; a molecular switch for electrical signaling. *Neuron*. 41:859-865.

Zou, Y., H. Akazawa, Y. Qin, M. Sano, H. Takano, T. Minamino, N. Makita, K. Iwanaga, W. Zhu, S. Kudoh, H. Toko, K. Tamura, M. Kihara, T. Nagai, A. Fukamizu, S. Umemura, T. Iiri, T. Fujita, and I. Komuro. 2004. Mechanical stress activates angiotensin II type 1 receptor without the involvement of angiotensin II. *Nature cell biology*. 6:499-506.

Zuobi-Hasona, K., P.J. Crowley, A. Hasona, A.S. Bleiweis, and L.J. Brady. 2005. Solubilization of cellular membrane proteins from Streptococcus mutans for two-dimensional gel electrophoresis. *Electrophoresis*. 26:1200-1205.